A MATHEMATICAL MODEL OF FROST HEAVE

IN GRANULAR MATERIALS

by

David Piper B.Sc.

Thesis submitted to the University of Nottingham for the degree of Doctor of Philosophy, October 1987.

PAGE NUMBERING AS ORIGINAL

For Sallie,

and

for Adam,

with love.

ACKNOWLEDGEMENTS

I would like to thank Prof. A. J. M. Spencer and Prof. P. S. Pell, and the staff and students of the Departments of Theoretical Mechanics and Civil Engineering, for their support during my study at Nottingham.

In particular, I am indebted to Dr. J. T. Holden and Dr. R. H. Jones for their guidance and encouragement throughout the project. I am also grateful to the Science and Engineering Research Council for the award of a research studentship.

In the preparation of this thesis, credit is due to Mrs. Sarah Starsmore for her fast and accurate typing of the manuscript, and to Mr. David Gagg, for his expert binding. I am grateful to both for giving up their time so readily.

Finally, I owe a great debt to my wife Sallie. Without her patience, understanding, encouragement and unstinting support, this thesis would never have been written.

D.P.

September 1987

ABSTRACT

An initial review of the various theories of frost heave indicated that Miller's theory of secondary heave was the most convincing. The crucial area in this is the representation of the behaviour in the partially frozen region, known as the frozen fringe, which exists below the lowest ice lens. However, the computational difficulties of the associated mathematical model were likely to limit its application. A simpler quasi-static approach for a semi-infinite region had therefore been initiated, for a restricted range of conditions, by Holden.

The work described in this thesis traces the development of the quasi-static approach and its application to the unidirectional freezing of a finite soil column. The resulting generalised model successfully predicts the freezing behaviour under a wide range of conditions. In particular, it is applicable to all overburden pressures, including zero. At low overburdens the frozen fringe disappears, but the final phase is nevertheless modelled to its ultimate equilibrium state. The predictions of the model agree with published experimental data from a number of investigators, and thus support the validity of Miller's theory.

Parametric studies with the model have highlighted the importance of the hydraulic conductivity and the relationship between suction, temperature and ice content in the frozen fringe. Simulations are

relatively insensitive to variations in thermal conductivity.

The model has proved to be robust and stable and should form a sound basis for further studies. However, its full application will depend on the development of experimental techniques to determine the hydraulic conductivity in the frozen fringe.

CONTENTS

CONTENTS (continued) Page No.

CONTENTS (continued) Page No.

NOTATION

The notation adopted in this thesis is explained as it is introduced in the text. However, for reference purposes, the most commonly used symbols are defined below.

A number of subscripts are employed, and these refer to the following:

"w" denotes water

"i" denotes ice

"s" denotes the base of the latest ice lens

"f" denotes the freezing front

"ss" denotes the base of the (terminal) lens when no frozen fringe exists.

Any exception to these definitions is clarified below:

Symbol	Quantity	Units
C	Volumetric heat capacity	$J\ m^{-3}\ °C^{-1}$
g	Acceleration due to gravity	$m\ s^{-2}$
H	Heave	m
k	Hydraulic conductivity	$m\ s^{-1}$
k_o	Hydraulic conductivity of saturated unfrozen soil	$m\ s^{-1}$
K	Thermal conductivity	$W\ m^{-1}\ °C^{-1}$
K_s	Thermal conductivity of the solid frozen region	$W\ m^{-1}\ °C^{-1}$

Symbol	Quantity	Units
K_f	Thermal conductivity of the frozen fringe	W m^{-1} $°C^{-1}$
K_u	Thermal conductivity of the unfrozen region	W m^{-1} $°C^{-1}$
L	Latent heat of fusion of water	J kg^{-1}
P	Applied overburden	N m^{-2} (Pa)
r_{iw}	Radius of curvature of ice/water interface	m
R	Soil particle radius	m
t	Time	s
T	Temperature	°C
T_w	Temperature at the base of the soil column (>0)	°C
T_c	Temperature at the surface of the soil column (<0)	°C
T_o	Freezing temperature of bulk water (273.15)	K
u	Pressure (water pressure with s, f or ss subscript)	N m^{-2}
u_n	Neutral stress	N m^{-2}
v	Velocity or volume flux (usually of water)	m s^{-1}
z	Space coordinate	m
z_w	Base of soil column/level of water table	m
θ	Volume fraction	m^3 m^{-3}
θ_o	Porosity	m^3 m^{-3}
σ_{iw}	Ice/water interfacial energy	N m^{-1}
ψ	Suction parameter	m^{-1}
χ	Stress partition factor	-
α	Exponent in water pressure profile approximation	m^{-1}

Symbol	Quantity	Units
ρ	Density	$kg\ m^{-3}$
ρ_s	Density of frozen soil matrix	$kg\ m^{-3}$
μ	Thermal diffusivity	$m^2\ s^{-1}$

CHAPTER 1

INTRODUCTION

1.1 Background and Motivation

When certain types of moist soil are subject to freezing, an uplift or expansion of the soil occurs due to the phenomenon of frost heaving. The main cause of this expansion is the formation of segregated ice, that is distinct layers of more or less pure ice, which force apart the soil matrix. These ice "lenses" develop from the water which is drawn into the freezing zone from elsewhere, as a result of the soil freezing process. The expansion of in-situ pore water upon freezing makes only a very small contribution to the total heave.

For frost heave to occur, three conditions must be present: a frost susceptible material, sub-zero temperatures and a supply of water. A frost susceptible soil is one which has a strong tendency to heave if the other two requirements are fulfilled. In general, the frost susceptibility of a soil is dependent on its permeability and capillarity (or suction characteristic). The permeability is a measure of the resistance of the soil to the flow of water through it, whilst the capillarity indicates the extent to which water can rise through the soil above a water table.

Fine grained soils, such as clays, have high capillarity and adsorption

but a low permeability, which inhibits transport of water to a freezing front. On the other hand, coarse soils, for example sands and gravels, although highly permeable, have a low capillarity which also restricts water movement. Hence, both fine and coarse soils tend not to be frost susceptible. It is those soils with moderate permeability and capillarity, such as silts, silty-sands and silty-clays, which are found to be highly frost susceptible.

Interest in the effects of freezing and thawing of soils has been motivated by the problems associated with both natural and artificial ground freezing.

In many parts of the world, particularly in the northern hemisphere, the climate is such that the temperatures are low enough to cause freezing of the ground. This is only a seasonal occurrence in some areas, but is permanent in others (known as permafrost). Nevertheless, in all these regions, damage to engineering structures, plants and agricultural crops due to frost action (both frost heaving and thaw weakening) is well known. In the past, the cost of repair and reconstruction has been considerable. Nowadays, understanding of the phenomena is such that damage is largely avoidable, but only through application of expensive design procedures. One example of this is the Trans-Alaska oil pipeline, constructed in the 1970s (see Williams, 1979). Another is the design of the Alaska Natural Gas Transportation System, currently being developed in the United States and Canada. It has been estimated that more than $50 million has been spent in five years on establishing field test sites in permafrost areas, to obtain the information on ice segregation and frost heaving required

for the design (National Research Council, 1984).

In the U.K., the main concern over natural freezing has been with regard to road construction, and the current specification demands that materials within 450 mm of the road surface should be non-frost susceptible (see Section 2.9).

The increasing use of artificial ground freezing in construction projects has also stimulated investigations into the behaviour of freezing soils. This technique is used to stabilise weak ground and prevent groundwater intrusion during excavation for shafts, tunnels and other structures. However, refrigeration is expensive and there is a need for accurate predictions of the thickness of freezewalls. In addition, precautions must be taken to reduce the risk of damage to adjacent structures from frost heave and thaw settlement. Another example of "artificial" freezing which has focussed attention in this area is that due to the inground storage of liquefied natural gas, the storage temperature being in the region of -160°C.

Widespread interest has therefore been generated in the phenomena associated with frost action, and reliable predictive methods are required to improve design procedures and mitigate the effects of frost heave and ice lensing. The enormous research effort which has been, and continues to be, expended, is reflected in the number of international meetings which have been held since the early 1970s. These include:

International Symposia on Ground Freezing:

First, 1978, Bochum, West Germany;

Second, 1980, Trondheim, Norway;

Third, 1982, Hanover, New Hampshire, USA;

Fourth, 1985, Sapporo, Japan.

International Conferences on Permafrost:

Second, 1973, Yakutsk, USSR;

Third, 1978, Edmonton, Alberta, Canada;

Fourth, 1983, Fairbanks, Alaska, USA.

Conferences on Soil Water Problems in Cold Regions:

First, 1975, Calgary, Alberta, Canada;

Second, 1976, Edmonton, Alberta, Canada;

Third, 1979, Calgary, Alberta, Canada.

International Symposium on Frost Action in Soils:

1977, Lulea, Sweden.

The published proceedings of these conferences provide comprehensive coverage of all aspects of the subject. References to individual papers are given in full in the usual way at the end of this thesis. Of special significance has been the publication recently of an increasing number of papers from Russia and China. This is important in view of the fact that very little translated material was

previously available (see Miller, 1978, Loch, 1980). Also of particular interest are review articles which appear occasionally giving a state of the art summary at the time (e.g. Anderson and Morgenstern, 1973, Loch, 1980).

1.2 Objectives

The first task was to undertake a review of the literature, in order to provide the necessary background and to establish the state of the art in frost heave research. Particular emphasis was placed on assessing the theories put forward to explain the phenomena, and the mathematical algorithms proposed to model freezing soils.

Having identified current thinking in these areas, the primary aim was to develop a mathematical model for frost heave capable of predicting the observed behaviour, including the initiation and growth of ice lenses, whilst minimising the computing effort required for such a model. Indeed, it was hoped that the resulting program could eventually be run on a microcomputer to provide rapid, inexpensive estimates of frost heave under any applied boundary conditions.

It was also felt that development of the model would inevitably involve examination of the mechanics of frost heaving, in order to isolate the key processes and parameters, and that in the long term, this would aid understanding and improve subsequent modelling of the physics of freezing soils.

CHAPTER 2

RESEARCH INTO FROST HEAVE: A LITERATURE REVIEW

2.1 Introduction

As explained in Chapter 1, the worldwide interest in ground freezing has led to the publication of a vast amount of literature on the subject, with contributions from many disciplines. This chapter however, concentrates on those areas relevant to the work described in this thesis, and hence provides a review of the literature relating to the theory and mathematical modelling of frost heave.

A brief historical introduction to the problem is presented first, followed by a chronological account of the early theoretical and experimental work. Sections 2.4 to 2.7 then trace the development of the various theories proposed to explain the phenomenon. Two other aspects which feature in the literature are subsequently discussed, before, in Section 2.10, the more prominent mathematical models of frost heave are reviewed. Finally, a summary of the recent trends in frost heave research is provided in Section 2.11.

2.2 Historical Background

It appears that the raising of the ground surface as a result of

freezing of soil was well known at least by the middle of the eighteenth century, when an account was given by E. O. Runeberg (1765) (see Beskow, 1935). He wrote: "We can say for certain that earth, stone, or houses, that rest on this (saturated soil that is freezing) must either resist or be displaced." However, it was not until the beginning of this century that the problem was taken seriously, due to the increasing significance of frost damage to roads, foundations and agricultural crops.

The first major works to emerge were those of Taber (1929, 1930) and Beskow (1935). Until this time, it was widely thought that frost heaving was due just to the expansion of water upon freezing, but Taber (1929) found that the heaving of clay samples in the laboratory far exceeded that which could be attributed to the 9% volume expansion. Indeed, he obtained frost heave in a sample in which water was replaced by benzene, which contracts on freezing. Taber published photographs of frozen clay samples containing layers of segregated ice, similar to those found in heaved ground, and explained that the layers of ice were formed as a result of additional water being drawn into the sample. Both Taber and Beskow recognised the significance of the adsorbed film, that is the thin film of water that exists on the surface of a soil particle due to molecular attraction. Taber (1930) pointed out that this provides a mechanism for the growth of segregated ice. A thin film of water between a soil particle and an overlying ice lens will permit water to be drawn up to feed the growth of the lens.

Beskow, on the other hand, related the presence of the adsorbed films to the depression of the freezing point of water in soils. He explained that this bound water needs an "extra force" (lowering of the freezing point) to pull the water molecules away from the surface of the soil particle and permit their formation into ice crystals. The freest water, in the centre of the pore space, freezes first, and hence determines the starting temperature of freezing. However, the greater the proportion of water held in adsorbed films in a soil, the larger the depression of the freezing point, and since the former is a function of the specific surface of the soil, the freezing point depression in, say, clays is greater than in sands. By way of illustration, some typical curves of unfrozen water content against temperature are given in Figure 2.1. A further explanation of the freezing point depression of water in soils, is given later in this chapter.

2.3 Early Theories of Frost Heaving

Among the first researchers to attempt to quantify the effects of freezing was Schofield (1935), who related the suction of the unfrozen water in a soil to the freezing point depression (see Croney and Jacobs, 1967). However, it was not until some years later that the pressures which exist in the water and ice phases during frost heaving were investigated by Penner (1957, 1959) and Gold (1957).

Penner (1957) carried out a number of unidirectional freezing tests on different soil samples blended artificially. First, he obtained suction (or "moisture tension") against moisture content curves for the soils, and then, after freezing, measured the water content of the unfrozen soil in order to estimate the suction induced therein due to freezing. A free water supply was provided at the warm end of the samples, so that when freezing commenced, water could be drawn into the soils (open system freezing). This situation was continued until the maximum rate of frost heave under these conditions was attained. The external source of water was then removed, and heaving continued only as a result of moisture movement from the unfrozen portion to the freezing zone (closed system freezing). The moisture content measurements of the unfrozen soil were carried out once the heave rate approached zero. Penner found that higher moisture tensions were induced in fine-grained soils than in coarse-grained, producing higher moisture flows and higher heaves. He also found that in specimens prepared in layers from two different materials, the moisture tension, or suction, in the unfrozen portion was dependent upon the material in which the freezing plane was located.

Penner's (1959) attempts to explain the heaving mechanism theoretically were based on two equations. The first, given by Sill and Skapski (1956), describes the temperature dependence of the size of a stable spherical crystal in its own melt, thus:

$$\Delta T = \frac{2\, T_o\, \sigma_{iw}}{r\, \rho_i\, L} \qquad \ldots (2.1)$$

where: r = radius of the crystal

ρ_i = density of the ice

σ_{iw} = ice/water interfacial energy

L = latent heat of fusion

T_o = temperature (absolute) of melting at zero curvature of the solid/liquid interface

ΔT = the freezing point depression

The second is a pressure-freezing point depression equation given by Edlefsen and Anderson (1943), namely:

$$\frac{du_t}{dT} = \frac{L}{(V_w - V_i)\ T_o} \qquad \ldots (2.2)$$

where: du_t = total change in pressure (i.e. the total change in pressure on the ice which equals that on the water)

dT = change in freezing point temperature

V_w = specific volume of water

V_i = specific volume of ice

T_o = the absolute temperature at which the phase change occurs

L is as defined in Equation (2.1).

Penner assumed the configuration of the ice/water interface at the freezing plane to be, typically, as shown in Figure 2.2. Here, he claimed, the ice front will be temporarily prevented from propagating down between the soil particles until the temperature has been lowered sufficiently to satisfy Equation (2.1). Before this occurs,

part of the adsorbed water above the particle will freeze, contributing to the growth of the ice lens. As water is being removed from the adsorbed layer into the ice phase, it is replaced from below, and an equilibrium thickness of water is maintained around the soil particle. Equation (2.2) was used to explain the observation that ice lens growth can be stopped by loading the soil. If the soil, and hence the ice lens, is loaded, causing a pressure at the ice/water interface above the soil particle, the freezing point of the water will drop according to Equation (2.2). The limiting pressure to stop ice lens growth will occur when the freezing point of the water above the particle has been lowered to the same temperature as is necessary for ice to propagate through the pore constriction.

Gold (1957) suggested a possible mechanism of frost heaving, starting from the Gibbs thermodynamic potential, or, as it is more commonly called, the Gibbs free energy, g, given by:

$$g = e + uV - Ts \qquad \ldots (2.3)$$

where:
- e = internal energy
- u = pressure
- V = specific volume
- T = absolute temperature
- s = entropy

Assuming a situation at the ice/water interface similar to that given in Figure 2.2, Gold derived the conditions which must be

satisfied if ice and water are to be in equilibrium in a small space, that is local to a soil pore space, for a given temperature depression and water tension. He considered a simple spherical particle arrangement for a soil to illustrate that the theory agreed qualitatively with Penner's observations.

It was research such as this that heralded the beginning of the formulation of the capillary theory of frost heave (so called because moisture movement is attributed to the capillary suction present at a curved ice/water interface), which will now be described more fully. It is worth noting at this point that, in spite of Taber's (1930) observation that ice formed in the soil voids below a growing ice lens, the assumption, central to the capillary theory, that an ice lens forms at the freezing front prevailed for many years, at least until the early 1970s.

2.4 The Capillary Theory of Frost Heaving

In 1961, Everett discussed the problem of frost damage to porous solids from the point of view of equilibrium thermodynamics, and used a simple model to explain the phenomenon in soils. By considering the chemical potential of a small crystal, immersed in and in equilibrium with a fluid subjected to hydrostatic pressure, u_l, Everett derived a generalised form of the Laplace surface tension equation, that is:

$$u_s - u_l = \sigma \frac{dA}{dV} \qquad \ldots (2.4)$$

where: A = area of the interface

V = volume of solid

u_s = pressure within the crystal

σ = interfacial energy between solid and liquid

For a spherical particle of radius r, this equation becomes:

$$u_s - u_l = \frac{2\sigma}{r} \qquad \ldots (2.5)$$

The simple model consisted of two cylinders, each closed by a piston and joined by a capillary tube. Initially, the cylinders are filled with liquid water. The temperature is lowered to 0°C and freezing is nucleated in one of the cylinders (but not the other). Once this cylinder is completely filled with ice, Everett describes the pressure conditions under which preferential growth of bulk ice in the cylinder ("ice lensing") or ice in the capillary ("frost penetration") will take place. It is assumed that the interface adopts a hemispherical shape in the capillary, hence the significance of Equation (2.5) which, in fact, is fundamental to the capillary theory.

This idealised model was thought to be appropriate because it was known that frost heave was associated with materials in which coarser pores were separated from one another by narrow pore

necks. Therefore, an equation such as (2.5) suggested that "for a material of given mechanical strength", or for a given overburden, there might exist a critical pore size which, if present in the material, would lead to frost damage.

It seems relevant at this point to introduce the concept of "heaving pressure". Everett, and several other authors, defined heaving pressure to be the quantity:

$$\Delta u = u_s - u_l \qquad \ldots (2.6)$$

as in Equation (2.5). Penner (1959) had previously defined it as the positive pressure developed at the ice/water interface when vertical displacement is prevented in a frost heaving soil. The latter is, in fact, closer to the definition now in common use, that heaving pressure is the pressure of the ice. That is, the pressure of the ice corresponds to the weight effect, or resistance of the overlying material (Williams, 1979).

Encouraged by the agreement between Penner's (1957) observations and the thermodynamic theory, Everett and Haynes (1965) generalised the treatment of Everett (1961) to include any pore geometry. They considered the pressures existing in ice, solid and water in a "generalised" pore and then applied this theory to a number of simple pore systems. In particular, they looked at a close packed array of spheres of equal radius, and the tetrahedral cavities between the spheres, in the hope that such an arrangement would be amenable to both theory and experiment. Their estimates of heaving

pressure, as a function of particle diameter, were of the right order of magnitude, but no precise experimental data were available at the time to test the theory rigorously.

It was left to Williams (1967) to present the most complete account up to that time of the capillary theory of frost heaving. Both experimental work and theoretical aspects were described in a series of studies, each of which was suggested by the conclusions arising from the preceding one. The last in this collection of papers, however, differed from the others in that it attempted a composite presentation of the soil freezing process, and included therefore a statement of the capillary theory and a description of the rhythmic formation of ice lenses.

Williams explained that the pores of soils can be regarded as a series of interconnected capillaries, so that the pressures in an ice/water interface at a freezing front, such as that shown in Figure 2.2 , can be represented by Equation (2.5). Using the suffices "i" for ice and "w" for water, this becomes:

$$u_i - u_w = \frac{2\sigma_{iw}}{r_{iw}} \qquad \ldots (2.7)$$

where: r_{iw} = radius of (hemispherical) interface.

It can easily be seen from Equation (2.7) that if the ice is under atmospheric pressure (that is, zero gauge pressure), the pore water must have a negative pressure, or suction.

Now, for the frost line or freezing front to advance through a pore of radius r_c, the ice and water pressures must satisfy (following Equation (2.7)):

$$u_i - u_w \geq \frac{2\sigma_{iw}}{r_c} \quad \ldots (2.8)$$

Thus, according to the capillary theory, r_c is an important characteristic for a given soil, since it determines the pore water pressure, relative to that of the ice, occurring at ice/water interfaces at the penetrating frost line. If, on the other hand, the pore pressure is greater, such that:

$$u_i - u_w < \frac{2\sigma_{iw}}{r_c} \quad \ldots (2.9)$$

the radius r_{iw} of the interfaces is greater than r_c and the ice is unable to penetrate through the soil pore. Instead, freezing results in growth of an ice lens. The movement of water to the lens (which occurs as a result of the suction at the interface of radius r_{iw}) results in a decrease in the water pressure to the extent that the conditions of Equation (2.8) are approached. As soon as they are achieved, ice lens growth ceases, and instead the ice advances through the pore.

The pore pressure, however, will usually then begin to rise again (since the removal of water to the ice lens has ceased) until eventually the condition for formation of a lens is once again reached. This explains the alternate layers of ice and frozen

soil in heaving soil, and this process continues until insufficient cooling takes place to permit further frost penetration. The latest ice lens then becomes the final, or terminal lens.

The capillary theory also predicts the depression of the freezing point of pore water. Williams combined Equation (2.7) with one similar to (2.1) to obtain:

$$u_i - u_w = \frac{-(T-T_o)L}{T_o V_w} \qquad \ldots (2.10)$$

where: V_w = specific volume of water

T = freezing temperature (Kelvin)

and confirmed its validity experimentally.

Equation (2.10) is a form of the Clausius-Clapeyron equation which, in its various forms, has received almost universal acceptance in the field of frost heave research. Equations similar to this were quoted by earlier researchers (e.g. Gold, 1957, Penner, 1966). However, Williams appears to have been the first to discuss such an equation explicitly as part of the mechanism behind the capillary theory. If the ice pressure is known, Equation (2.10) provides an expression for the water pressure as a function of temperature.

Throughout this thesis, the following alternative form of the Clausius-Clapeyron equation is used:

$$\frac{u_i}{\rho_i} - \frac{u_w}{\rho_w} = \frac{-LT}{T_o} \qquad \ldots (2.11)$$

where: (defining all symbols for clarity)

u_i, u_w = ice pressure and water pressure

ρ_i, ρ_w = densities of ice and water

T = freezing temperature (°C)

T_o = freezing temperature of bulk water at atmospheric pressure (273.15 K)

L = latent heat of fusion of water

As this equation plays such an important role in the work described herein, a simple derivation from equilibrium thermodynamics is given in Appendix A.

Whilst these theoretical developments were taking place, experimental work continued in an attempt to verify the theory and to establish a criterion for frost susceptibility. That is, experimentalists sought to define a fundamental soil parameter which would provide a measure of a soil's susceptibility or tendency to frost heaving.

Hoekstra et al (1965) carried out a number of constant volume freezing tests, including one on a silt saturated with benzene. A substantial heaving pressure developed, confirming Taber's (1929) observation that such pressures are not due to freezing expansion, since benzene contracts on solidification. In accordance with the capillary theory, Hoekstra et al attributed heaving pressures to the surface energy of the solid/liquid interface, and demonstrated with tests on layered samples that the pressure

originates at the freezing front. They concluded that pore size, and hence heaving pressure, ought to provide a reliable criterion for frost susceptibility.

In contrast, Penner (1967) found that average grain size was a satisfactory basis for assessing frost susceptibility. Heave pressure measurements for various fractions of potter's flint indicated that the smaller pores of the system were responsible for the development of such pressures. To account for this, Penner suggested that at each point on the freezing plane, ice advances through larger pores until, depending on the temperature, further propagation through smaller pores is prevented, according to Equation (2.1). Penner therefore assumed that, on a microscopic scale, the freezing plane appeared as an undulating surface. However, because each fraction contained a large range of pore sizes, heaving pressures were plotted instead against an average particle diameter for each fraction, and the results supported the use of particle size as a criterion for frost susceptibility. The subject of frost susceptibility testing is discussed further in Section 2.9.

2.5 The Concept of Secondary Heaving

Although the capillary theory was apparently capable of explaining the heaving process, and in spite of some encouraging experimental results, by the end of the 1960s there was mounting evidence that the theory was in fact inadequate. Hoekstra (1966) found that

ice lenses in an unsaturated soil form at a considerable distance behind the freezing front and he measured significant moisture flow in the frozen soil. The magnitude of this flow indicated liquid rather than vapour transfer was taking place, and the movement was attributed to the flow of water via the adsorbed films which, as mentioned previously, remain unfrozen at temperatures several degrees below 0°C. Later, in 1969, Hoekstra published a series of photographs showing an ice lens growing behind the freezing front in a saturated clay, and he also photographed an ice lens some distance behind the freezing front in a saturated granular soil (Fairbanks silt). Hoekstra noted that, notwithstanding Penner's (1967) work, attempts to find agreement between calculated and experimental heaving pressures had thus far failed.

It was against this background that Miller (1972) proposed the concept of "secondary heaving" for saturated soil. He supposed that the ice does penetrate the pore system ahead of the latest ice lens and he referred to this region between the ice lens and the unfrozen soil as the "frozen fringe". Miller suggested that under these circumstances, the ice lens can continue to grow and the ice in the frozen fringe will move with it, while the particles remain stationary. This phenomenon was termed "secondary heaving". Heaving according to the capillary model was called "primary heaving" (Figure 2.3). Miller inferred that whenever heaving occurs as the freezing front is descending through the soil, the process must be secondary heaving.

Earlier work by Miller (1970) had suggested a mechanism for the ice in the frozen fringe to move as an integral part of the ice body that includes the ice lens. Ice that fills a large "pore" between two filter papers was found to move readily despite appearing to be stationary. When supercooled water was on opposite sides of the respective filters, an increase in water pressure on one side caused supercooled water to emerge from the opposite side. Concurrent melting and freezing on opposite sides of the ice caused the ice to be in motion between its stationary boundaries. It was therefore thought possible that in the frozen fringe water traverses the ice-filled pores in the ice phase, and moves around the ice and soil particles in the film phase. This bi-modal water movement was later described as "series-parallel" transport (Miller et al, 1975).

Miller (1972) argued that secondary heaving produces larger heaving pressures than primary heaving and explains why previous theories underestimated the maximum heaving pressure of saturated soil. A mathematical expression of secondary heaving however did not appear until later (Miller, 1977, 1978). This aspect is described in full in Chapter 3; further detail therefore is not included here.

In the years following Miller's (1972) original proposal, further evidence emerged supporting the concept of secondary heaving and the existence of the frozen fringe. According to Equation (2.9), the maximum heaving pressure predicted by the capillary theory is:

$$\max u_i = u_w + \frac{2\sigma_{iw}}{r_e} \quad \ldots (2.12)$$

where: r_e = effective radius of pore necks.

Experiments conducted by Sutherland and Gaskin (1973) indicated that the maximum heaving pressure was somewhat larger than predicted by Equation (2.12), with r_e derived from air entry measurements. (Air entry tests measure the pressure at which air replaces water in a material, which is given by:

$$u_a = u_w + \frac{2\sigma_{aw}}{r_e}$$

where: u_a = air pressure

σ_{aw} = air/water interfacial energy).

Similarly, Loch and Miller (1975) found that the limit of heaving pressures developed in a triaxial having test device exceeded that predicted by air entry data using the primary heaving model by factors as large as three to six. They concluded that their results apparently reinforced the concept of secondary heaving, but admitted that there was a need to learn more about transport phenomena in the frozen fringe beneath the ice lens.

The possibility for the rigid pore ice phase and the soil skeleton to move in opposite directions in the presence of a temperature gradient was illustrated by Römkens and Miller (1973). They performed experiments in which a temperature gradient caused particles embedded

in ice to migrate in the direction of increasing temperature. Another requirement of the secondary heaving theory is that water is able to flow through the frozen fringe to feed the growth of the ice lens. Using a "frozen permeameter", Williams and Burt (1974) measured the hydraulic conductivity, due to a hydraulic gradient, of various frozen materials at different temperatures. Significant hydraulic conductivities were measured at temperatures well below 0°C and these were attributed to the unfrozen water remaining in the frozen soil (see Figure 2.1). However, Miller (1978) pointed out that with their apparatus, Williams and Burt must have measured the total flux due to both liquid transport via the unfrozen films and transport of water via the moving ice phase. In other words, they measured the "series-parallel" transport as if all the flux were in the liquid phase.

The secondary heaving concept also received support from a study by Loch and Kay (1978). They measured the location of the growing ice lens relative to the freezing front in columns of saturated silt which were freezing under different overburden pressures and different temperature gradients. These data were then used to evaluate current models of water redistribution in freezing soils. Loch and Kay found that the ice lenses appeared to be located in the frozen soil a distance of 2-4 mm behind the freezing front. As a whole, their results tended to conform to the concept of secondary heaving, but they noted that the theory required a mechanism for predicting the distance of the ice lens behind the freezing front in the presence of an overburden. Such a mechanism was indeed proposed

by Miller (1977, 1978) and is described in the next chapter.

Thus, by the end of the 1970s, considerable experimental evidence supporting the concept of secondary heaving, at least in principle, had been presented. However, around this time, two other theories of frost heaving were proposed, which also sought to explain the recent developments published in the literature. These were the adsorption force theory and the segregation potential theory, both of which will now be briefly discussed. It should first be noted however, that far from receiving universal acceptance, these two theories have attracted a good deal of controversy. Indeed, it is Miller's theory which has been credited most in the literature, perhaps because it is thought to have a firmer physical basis. Moreover, it makes fewer assumptions regarding the soil properties (e.g. thermal and hydraulic conductivity), and unlike the segregation potential theory (Section 2.7), it does not rely upon an empirical parameter. Nevertheless, the controversy remains, and researchers have yet to agree upon a comprehensive theory of frost heave.

2.6 The Adsorption Force Theory

This theory was proposed by Takagi (1980a), based on earlier work by him (e.g. Takagi, 1977), and is centred on the adsorbed film water between the soil particle and the overlying ice lens. Takagi considers that this film has an equilibrium thickness which is

determined by the adsorption forces exerted by the particles and the ice. So, as water molecules become attached to the base of the ice lens, a suction is generated that draws water into the film to maintain its thickness. According to this explanation, the ice lens grows on the soil particle. Takagi refers to the freezing of the film water that generates suction as "segregation freezing". In contrast, the freezing of homogeneous free pore water, called "in-situ freezing", does not generate suction. That is, the in-situ freezing front advances as the in-situ freezing progresses.

The adsorption force theory asserts that the film water, although a liquid, should be treated as a solid, because it can sustain the weight of the overburden. The primary cause of frost heaving is said to be the creation of a solid-like stress in the unfrozen film water between ice and soil surfaces. The freezing point of the film water is referred to as the "segregation freezing temperature", T_S, and this is always less than the in-situ freezing temperature, T_I. A formula for the average segregation freezing temperature, $\overline{T}_S$, is derived from classical thermodynamics, and is written:

$$\overline{T}_S = T_I \left[1 - (w + \rho_i g h)/(\rho_i L)\right] \qquad \ldots (2.13)$$

where: $w + \rho_i g h$ = increase in ice pressure

w = surcharge overlying the ice lens

h = thickness of the ice lens

This equation can, in fact, be obtained from the Clausius-Clapeyron

Equation (2.11) by setting pore water pressure, $u_w = 0$, ice pressure, $u_i = w + \rho_i gh$, temperature $T = \overline{T}_s - T_I$ and $T_o = T_I$.

Takagi has used continuum mechanics to produce a mathematical structure for the theory, but admitted that this was incomplete due to the lack of a description of the mechanics of film water using continuum mechanics. However, Takagi expected that "modern continuum mechanics will, in the future, improve the theory of film water". These expectations appear not to have been fulfilled, as yet, since no further work on the adsorption force theory has been published, apart from Takagi's (1980b) short summary of the essential features.

Finally, it should be mentioned that because reviews of Takagi's (1980a) paper revealed areas of controversy, Miller (1980) was invited by the editor of the publishing journal to submit a commentary, in which he presents an alternative point of view.

2.7 The Segregation Potential Theory

This theory was developed by Konrad and Morgenstern (1980, 1981), as part of a research programme aimed at developing a comprehensive engineering theory of frost heave. They adopted the position that any theory requiring local measurements of high accuracy such as temperature, unfrozen water content, or permeability of frozen soil cannot result in a theory that will yield practical results. They

therefore attempted to demonstrate that unique frost heave characteristics for soils are deducible from controlled laboratory freezing tests.

Konrad and Morgenstern's view of the heaving process was in accord with that of Miller in that they recognised the existence of the frozen fringe and the continuous flow of water through it to feed ice lens growth. However, they postulated a different mechanism for the formation of rhythmic ice lenses. It was argued that a lens is initiated at a given location defined by its particular segregation freezing temperature, T_S. With continued heat extraction, the lens grows and the freezing front advances. This produces a change in the temperature profile across the frozen fringe, and, more specifically, the temperature at the base of the ice lens becomes colder. Consequently, overall permeability of the frozen fringe decreases whilst the suction at the base of the lens increases. Further frost penetration results in a further decrease in the temperature at the base of the latest ice lens until, eventually, the permeability of the upper part of the fringe becomes so small that water flow there is essentially stopped. Water now accumulates somewhere below the base of the former ice lens, at a level governed by the segregation freezing temperature of ice lens formation, T_S. This process is repeated until "steady state" conditions are reached and the final ice lens is formed at a temperature T_{SO}.

Konrad and Morgenstern (1980) initially concentrated on "steady

state" conditions which they defined to be the time when the freezing front becomes stationary (in a freezing test with constant temperature boundary conditions). They added that this coincides with the formation of the final ice lens. This was clearly an approximation since Konrad and Morgenstern's own experiments show that after the final lens has been formed in such a test, the freezing front normally retreats to some degree due to continued heaving. The freezing front then only becomes stationary when heaving ceases.

Nonetheless, this steady state condition was assumed and also the thermal conductivity of the frozen fringe was taken to be the same as that of the unfrozen soil, so that the temperature profile throughout the "active system" (that is, the frozen fringe and the unfrozen soil) was essentially linear. Further assumptions led Konrad and Morgenstern to derive the relation:

$$v_o = SP_o \text{ grad } T_f \qquad \ldots (2.14)$$

where: v_o = water intake flux

grad T_f = temperature gradient in the frozen fringe

SP_o = segregation potential (constant)

The "o" subscript refers to the formation of the final ice lens and SP_o is defined as:

$$SP_o = \left| \frac{h_s - h_u}{T_{so}} \right| \bar{k}_{fo} \qquad \ldots (2.15)$$

where: h_s = suction (head, cm of water) at the ice lens

h_u = suction (head) at the 0°C isotherm

$\bar{k}_{f_o}$ = overall permeability of the frozen fringe

Equation (2.14) was verified experimentally, and it was claimed that SP_o was constant for a soil sample freezing under different cold-side step temperatures but with the same warm-side temperature (and under zero applied load).

Still dealing only with the formation of the final ice lens, Konrad and Morgenstern (1981) went on to show the variation of SP_o with suction at the freezing front. From this study, they concluded that it is possible to characterise any freezing soil at the formation of the final ice lens by a set of straight lines passing through the origin on a v_o versus grad T_f plot. Each line corresponds to a given suction developed at the freezing front, the gradient of the line is the appropriate segregation potential, SP_o, and SP_o decreases with increasing suction.

Konrad and Morgenstern (1982a) then attempted to extend their analysis to conditions of transient freezing, or unsteady heat flow. They suggested that at any given time during transient freezing, the segregation potential, SP, defined by:

$$SP = \frac{v}{\text{grad } T_f} \qquad \ldots (2.16)$$

will be a function of both the suction at the freezing front and the "rate of cooling of the current frozen fringe". The rate of cooling was defined as the change in average temperature of the frozen fringe

per unit time, and was approximated by:

$$\frac{dT_f}{dt} = \text{grad } T_f \frac{dX}{dt} \quad \ldots (2.17)$$

where: $\frac{dX}{dt}$ = rate of advance of the freezing front

It was therefore claimed that a soil freezing under zero applied load, with an advancing freezing front, can be characterised by the segregation potential, the suction at the freezing front and the rate of cooling of the frozen fringe. These three parameters provide a "characteristic frost heave surface" that can be determined from experimental data and used as input to a heaving model. By way of illustration, Konrad and Morgenstern carried out instrumented freezing tests to calculate this surface for Devon silt, and their results were shown in a three-dimensional plot.

The final stage of the analysis was to evaluate the effect of applied pressure (Konrad and Morgenstern, 1982b). For this, steady state conditions were again considered and the variation of SP_o with applied pressure, and with suction under different applied pressures, was obtained from tests on Devon silt. The following empirical relation was deduced:

$$SP_o = ae^{-bP} \quad \ldots (2.18)$$

where: P = applied pressure

a,b = "soil constants easily determinable from laboratory tests"

At the end of this latest study, Konrad and Morgenstern presented a simplified method of frost heave determination, in which they assumed that freezing under field conditions could be approximated by characteristics corresponding to the formation of the final ice lens in a laboratory freezing test. They argued that the use of the segregation potential in such a method was highly advantageous because the SP_o could be calculated from two quantities easily measured in the laboratory, namely water intake flux and frozen fringe temperature gradient. It was thought that the method would provide an upper bound frost heave value in a field situation.

Although the segregation potential theory has received rather more coverage in the literature than the adsorption force theory, there exists some doubt about its validity. Recently, Ishizaki and Nishio (1985) carried out a number of freezing tests in which they concentrated on the behaviour after the formation of the final ice lens. They found that Equation (2.14) certainly did not apply after the formation of the final ice lens in their experiments. Since the segregation potential theory is founded upon this relationship, questions concerning its validity clearly remain.

2.8 The Concept of "Shut-Off" Pressure

As mentioned previously, the maximum heaving pressure of a soil was measured in constant volume freezing tests by a number of researchers (e.g. Hoekstra et al, 1965, Sutherland and Gaskin, 1973). The

existence of a maximum heaving pressure was predicted by the capillary theory (Equation (2.12)) and by the secondary heaving theory (Miller, 1972). It was therefore assumed that for each soil there would exist an equivalent "shut-off" pressure, at which the effective stress at the freezing front would cause neither flow of water into or away from the freezing front, thus preventing frost heave (Hill and Morgenstern, 1977). When the shut-off pressure is exceeded, water is then expelled ahead of the freezing front. Takashi et al (1978) proposed a critical effective stress below which water intake and above which water expulsion takes place. The belief in the existence of a shut-off pressure played an important role in the ultimately abortive design of the Mackenzie Valley chilled gas pipeline in Canada (Williams, 1979). It was thought that a berm of soil placed above the pipe would provide the necessary pressure to prevent frost heaving.

However, experimental evidence has recently suggested that water expulsion is followed by water intake, provided that sufficient time is allowed for the experiment to run. Loch and Miller (1975) and Loch and Kay (1978) observed this flow reversal in their experiments. They attributed the expulsion to the formation of pore ice, reflecting the volume change in the freezing of pore water. Konrad and Morgenstern (1982b) extrapolated their experimental results to suggest a shut-off pressure for Devon silt. They found that the value obtained (in the range 1.0 - 1.2 MPa) was much greater than that under which laboratory tests are normally conducted. Hence, they concluded that although the concept was still valid, laboratory

freezing tests will exhibit water intake provided sufficient freezing time is allowed. Similarly, with surcharges up to 300 kPa, McCabe and Kettle (1983) observed that shut-off pressures were not achieved in their tests on a number of different materials.

It is evident then that increased overburden pressures reduce the amount of heave, but it is now thought that heaving pressure can build up slowly but almost indefinitely as long as the process is given sufficient (geological) time (Penner and Ueda, 1978).

2.9 Frost Susceptibility Testing

Much of the research conducted into frost heaving has been stimulated by a desire to establish a reliable criterion for assessing the frost susceptibility of soils. The literature contains a great many publications on the subject and a thorough review here is both inappropriate and impractical (see Chamberlain, 1981). To summarise, however, amongst the numerous suggested criteria are grain size, pore size, heaving pressure, heave rate and heave. Testing methods have employed variations in sample preparation, water supply, load application, freezing procedure, and so on. Consequently, it has in the past proved difficult to reconcile results from different sources. However, most techniques now in use involve the measurement of heave or heave rate in unrestrained tests. Jones (1980) reviewed a number of these tests and discussed developments and applications of frost susceptibility testing.

In the United Kingdom, the main concern over frost heaving has been with regard to damage to roads. The current specification for major roadworks (Department of Transport, 1976 and 1986) requires that all materials within 450 mm of the road surface shall be non-frost susceptible as defined by the Transport and Road Research Laboratory (TRRL) Test (Roe and Webster, 1984, BSI, 1986).

In the TRRL test, specimens are placed in a self-refrigerated unit so that the air temperature above them can be maintained at -17 ± 1°C. The base of each sample is in contact with water which is maintained at a constant level and at +4 ± 0.5°C. Freezing continues for 96 hours, and heave and water intake are recorded every 24 hours. Thermocouples are used to monitor the boundary and internal temperatures of the specimens. Subject to certain specified limits on the test, the material is classified as non-frost susceptible if the "grand average" heave is less than 12 mm.

Details of the TRRL test, including specimen preparation, are supplied by Jones (1987), who also describes the evolution of the test since the specification of Croney and Jacobs (1967).

2.10 Mathematical Modelling of Frost Heave

In the last ten years or so, a great deal of research effort has been devoted to the development of mathematical models coupling fluxes of heat and water in freezing soil-water systems. This work has

been stimulated by the need for predictive methods for use in the design of structures in and on naturally and artificially frozen ground. As O'Neill (1983) pointed out, it is often difficult to extrapolate beyond the specific conditions under which any given experiment is carried out, so investigators have attempted to develop more general mathematical models of the freezing process. As a result, there has been a proliferation in the number of mathematical models of frost heave, and this has emphasised the necessity of improving existing knowledge of the complex physical, chemical and mechanical processes involved in freezing (and thawing) of soils (Berg, 1984).

A number of numerical simulations were discussed by Loch (1980) and, more recently, O'Neill (1983) presented a thorough state of the art review of mathematical frost heave models. A rather less detailed review is given here, the aim being to discuss those models most prominent in the literature.

Every model in the very least must address the problem of heat transfer with phase change. Lunardini (1981) summarises some of the methods employed in the solution of phase change problems without mass transfer, that is, without heave. These range from the analytical solutions of Stefan and Neumann (see Carslaw and Jaeger, 1959) to approximate methods, including the use of finite differences. In most models, the soil-water system is considered to be a macroscopic continuum. This allows the assumption of Darcian-type moisture flux and the application of equations for conservation of mass and energy.

These equations typically take the following form in one dimension:

Mass: $$\frac{\partial \theta_w}{\partial t} + \frac{\rho_i}{\rho_w} \frac{\partial \theta_i}{\partial t} = \frac{\partial}{\partial z} \left(k \frac{\partial \phi}{\partial z}\right) \quad \ldots (2.19)$$

Energy: $$C \frac{\partial T}{\partial t} - \rho_i L \frac{\partial \theta_i}{\partial t} = \frac{\partial}{\partial z} \left(K \frac{\partial T}{\partial z}\right) - C_w \frac{\partial}{\partial z} (T v_z) \quad \ldots (2.20)$$

where:

z = space coordinate

θ_w, θ_i = volumetric water and ice contents

ϕ = total head

k = hydraulic conductivity

K = thermal conductivity

C_w, C = water and soil volumetric specific heat capacities

v_z = water flux

A derivation of these two equations in three dimensions, and their subsequent reduction to one dimension, is given in Appendix B.

Among the earliest models of simultaneous heat and moisture flow in partially frozen soil were those of Harlan (1973) and Guymon and Luthin (1974). They used equations similar to (2.19) and (2.20) although their methods of solution were different. Harlan used an implicit finite difference scheme whilst Guymon and Luthin employed a finite element method. The main concern of these models was the redistribution of pore water in the frozen and unfrozen ground. No heave characteristics were incorporated into the models and their accuracy was limited by unreliable input data, although good qualitative agreement with both field and laboratory observations was

achieved. This approach to the problem has subsequently been developed further. Heave was included by Guymon et al (1980), who again adopted a finite element method of solution with a Crank-Nicolson approximation for the time domain. Frost heave was defined to occur when the total water and ice content in an element exceeded the soil porosity. Following Guymon and Luthin, volumetric unfrozen water content was estimated by Gardner's (1958) relationship:

$$\theta_w = \frac{\theta_o}{A_w \ |\psi|^n + 1} \quad , \quad \psi < 0 \qquad \ldots (2.21)$$

and hydraulic conductivity was estimated by:

$$k = \frac{k_o}{A_k \ |\psi|^m + 1} \quad , \quad \psi < 0 \qquad \ldots (2.22)$$

where: ψ = pore water pressure head

θ_o = porosity

k_o = saturated hydraulic conductivity

A_w, A_k, n, m = constants for a particular soil

Surcharge effects were modelled by computing the total weight of soil, water and ice above the freezing front, including the overburden. This weight was converted to an equivalent water pressure and added to the water pressure at the freezing front. This effectively reduces the suction at the freezing front which results in less water being drawn into the freezing zone. Simulations compared favourably with laboratory data, and it was noted that

the model was highly sensitive to hydraulic parameters and boundary conditions.

The same model has been subjected to further verification by Guymon et al (1981, 1983) using both laboratory and field data. To improve the accuracy of the predictions, a correction factor, E, was included to account for the decreased hydraulic conductivity in the presence of ice. Hydraulic conductivity was therefore expressed as:

$$k = k(\psi).10^{-E\theta i} \quad , \quad E\theta_i \geq 1 \qquad \ldots (2.23)$$

where $k(\psi)$ is determined from the relation between hydraulic conductivity and pore pressure for unfrozen soil. Heave estimates were in reasonable accord with field data after appropriate calibration of the E factor.

Sheppard et al (1978) presented a similar model, although the convection term in the energy equation (the last term in Equation (2.20)) was neglected. They stated that the influence of the overburden pressure on the water pressure could be described by the expression:

$$u_w = u_o + \alpha P + \beta L \rho_i \frac{T}{T_o} \qquad \ldots (2.24)$$

where: u_o = water pressure in the unfrozen state under unloaded conditions

P = overburden pressure

The coefficients α and β are defined in terms of measurable parameters

which are characteristic of the specific soil system under study. However, since the model was only in fact tested under minimal load conditions, the water pressure was not adjusted according to Equation (2.24). Instead, the ice was considered to be at atmospheric pressure and the Clapeyron equation was used (Equation (2.11)) with the ice pressure set to zero. The hydraulic conductivity versus suction relationship was expressed by an exponential function, and the moisture content versus suction relationship expressed as a logarithmic function. Again, heave was accounted for when the sum of water and ice content exceeded the porosity. An explicit solution scheme was used and testing of the model was attempted with both laboratory and field data.

Unfortunately, only twenty minutes of the laboratory experiment were modelled due to temperature fluctuations which occurred at the bottom of the soil column at later times. The authors stated that the model was being tested with experiments which were run for a much longer time, but no further data were supplied. Comparison with field results included only a check on temperature profiles because of lack of significant change in moisture content in the field.

Taylor and Luthin (1978) simulated the closed system freezing experiments carried out by Jame and Norum (1976). Convection was ignored in the heat transfer equation because the authors had previously found (Taylor and Luthin, 1976) that heat transfer by this method was between 0.1 and 1.0% of that due to conduction. Water content was assumed to be a function of temperature only, based on experimental

relationships similar to those shown in Figure 2.1. Experimental curves were also used to describe soil water diffusivity, D, as a function of water content of ice-free soil. For diffusivity in frozen soil, Taylor and Luthin found it necessary to divide the unfrozen soil water diffusivity by a factor of $10^{10\theta i}$. That is:

$$D \text{ (frozen)} = D \text{ (unfrozen)}/10^{10\theta i} \quad \ldots (2.25)$$

so that for an ice content of 0.3, the "impedance factor" is 1000. When the ice content at any point exceeded 85% pore saturation, the soil matrix was expanded to simulate heaving. Overburden effects were not considered and a finite difference scheme was used to solve the heat and mass transfer equations. Oddly, ice content was not treated as an unknown in the coupled differential equations, but determined at the beginning of each time step by an equation which in differential form is:

$$\frac{\partial \theta_i}{\partial t} + \frac{R}{L}\frac{\partial}{\partial z}\left(K\frac{\partial T}{\partial z}\right) = 0 \quad \ldots (2.26)$$

The parameter R was adjusted between time steps so that the water content calculated by solution of the mass equation agreed with that given by the water content/temperature relation. Holden (1979) has shown however that Equation (2.26) is incorrect.

Nonetheless, agreement between simulated and experimental temperatures and total water contents was reasonable: differences in temperature were less than 0.5°C, while water content differences were less than 5%. The freezing front location was predicted within

1 cm. No heave was recorded in Jame and Norum's experiments, but simulation of some tests by Dirksen and Miller (1966) produced a heave of 2.8 mm as compared with the experimental value of 3.8 mm. Taylor and Luthin concluded that the model was sensitive to the soil water diffusivity and did not predict water movement behind the advancing freezing front.

Recently, Fukuda and Nakagawa (1985) used Taylor and Luthin's approach in a model which was tested against field data obtained from an experimental site in Hokkaido, Japan, during the 1982/3 winter. Included in the model was a method for simulating the variations in ground surface temperature over the four month period. Comparison of calculated and field results indicated good agreement for temperature profiles, similar trends in water content profiles and discrepancies in heave and frost penetration predictions. Specifically, the model underestimated heave and overestimated the depth of frost penetration.

In reviewing a number of mathematical frost heave models, Hopke (1980) pointed out that most fail to incorporate the effects of overburden and none predict the presence of a frozen fringe. He then proposed a model to include both of these features as well as a criterion for lens initiation and growth. The Clapeyron equation, including the ice pressure term, was adopted and the model also used the capillary relationship:

$$u_i - u_w = \beta F(\theta_w) \qquad \ldots (2.27)$$

where: $\beta = \frac{\sigma_{iw}}{\sigma_{aw}}$

and $F(\theta_w)$ is a single-valued function of the volumetric water content. The value of β varies from 0.42 for granular materials up to 1.0 for clays. However, for unsaturated soils, due to assumptions about the ice pressure behaviour, a value of β less than 1.0 led to computational problems. Therefore β was taken to be unity throughout. Ice pressure was assumed to be zero at the freezing front and also within the frozen soil when pores were not completely filled with liquid water and ice. Lensing was allowed to occur whenever the ice pressure was at least equal to the overburden. Hopke solved the conventional mass and energy equations (2.19) and (2.20), using a one-dimensional Galerkin finite element solution with a deforming mesh. The time derivatives were approximated by a backward difference, fully implicit method.

The experimental data of Penner and Ueda (1977) provided a check on the accuracy of the model. Initially, the calculated heave versus time curves did not reproduce the shape of the experimental curves and an empirical variable was introduced to overcome this. Even so, although the reduction in heave rate with applied pressure was predicted, the match to the laboratory data was not good. Calculated frozen fringe thicknesses were apparently too small to give agreement with the experimentally observed heave rates.

A rather simpler model, but one of the first to predict rhythmic ice lensing, was presented by Holden et al (1980). The development

of this model formed part of a larger research effort at Nottingham University, aimed at improving the design procedures for preventing frost heave damage to roads. Hence, overburden effects were not included in the model and the Clapeyron equation was used to express water pressure as a function of the freezing point depression. This was linked with capillary theory to provide a mechanism for heave and frost penetration.

The freezing front, given by $z = \varepsilon(t)$, separated the frozen and unfrozen regions in which simple heat conduction was assumed and described by:

$$\frac{\partial}{\partial t}(CT) = \frac{\partial}{\partial z}\left(K \frac{\partial T}{\partial z}\right) \qquad \ldots (2.28)$$

In practice, the freezing front was taken to be a narrow zone of thickness Δz, in which the suction head, ψ, increased from a small value ψ_o to the value ψ_m given by the Clapeyron equation for a freezing point depression ΔT. Hydraulic gradient was then assumed to be $\psi_m/\Delta z$, and a form proposed by Gardner (1958) was adopted for hydraulic conductivity, namely:

$$k = \begin{cases} k_o & \psi > 0 \\ \dfrac{k_o}{1-A\psi^3} & \psi < 0 \end{cases} \qquad \ldots (2.29)$$

This enabled calculation of the quantity of pore water sucked to the freezing front.

The heat energy balance at the freezing front was written:

$$\Delta Q = -K_f \frac{\partial T_f}{\partial z} + K_u \frac{\partial T_u}{\partial z} = -\theta_w L \rho_w \frac{d\varepsilon}{dt} + \Delta Q' \quad \ldots (2.30)$$

where: $\Delta Q' = -L \rho_w k \frac{\partial \phi}{\partial z}$

and the subscripts f and u refer to frozen and unfrozen regions respectively. Equation (2.30) was used to calculate heave in the following manner. ΔQ was calculated from the heat conduction across the frozen/unfrozen boundary and compared with $\Delta Q'$, the heat released due to freezing of migrating pore water. If $\Delta Q > \Delta Q'$, frost penetration and cooling of the freezing front can occur. If $\Delta Q = \Delta Q'$, the heat extracted is only sufficient to freeze the water sucked to the front, and penetration cannot occur. Finally, if $\Delta Q < \Delta Q'$, the temperature distribution must be re-calculated with the front temperature increased to reduce the suction and bring $\Delta Q = \Delta Q'$.

These decision processes were performed at each time step in a numerical scheme employing implicit Crank-Nicolson finite differences, together with an expanding/contracting mesh. The phenomenon of rhythmic ice lenses was predicted by allowing the pore radius to vary with position. The model was evaluated against laboratory tests on sand/limestone filler mixtures. Computed temperature profiles agreed closely with the measured values, but heave results did not give such good agreement. The authors concluded that this may have been due to uncertainty in the values of the hydraulic conductivity of the material. Further details of the model, the numerical procedure and the experimental verification

are given by Dudek (1980).

At the same time that the early models of Harlan (1973) and Guymon and Luthin (1974) emerged, a different, more complex approach was presented by Frémond (1974). By defining a new unknown, the freezing index:

$$I(z,t) = \int_0^t T(z,\tau)\, d\tau \qquad \ldots (2.31)$$

Frémond introduced a variational formulation, and solution of the Stefan problem. He then coupled the phase change problem with water propagation in the unfrozen region in order to model frost heave. The hydraulic head ϕ was taken to be zero on the frost line and equal to a constant $c > 0$ on the water table boundary. On this occasion a more conventional mathematical formulation was used and the equations solved by a finite difference method with a variable space mesh. Heaving was defined to be proportional to:

$$\int_0^t \text{grad}\ \phi\ (z,\tau)\, d\tau \qquad \ldots (2.32)$$

Some results comparing computed and measured heave and frost penetration for a road pavement were given, but were rather inconclusive.

The variational approach to the coupled problem was developed further by Aguirre-Puente and Frémond (1976). The two unknowns in the system were the freezing index and the head of water. The head was now defined as follows:

$\phi(z,t) = -d$ in the frozen region and on the frost line

and: $\phi(z,t) \geq -d$ in the unfrozen region

($d \geq 0$) where d is a constant. The mathematics of the problem were described in considerable detail but, again, very few numerical results were presented.

In the following year, Aguirre-Puente et al (1977) used a similar model to introduce variable permeability in the partially frozen soil. Here, calculated curves of heave and frost penetration versus time for different values of the freezing point depression were reasonably successful in reproducing laboratory data. Also, in the same paper, a new model was proposed to describe water movement in the frozen soil and its effect on the heave. Energy and mass conservation equations were written down in terms of parameters representing porosity, unfrozen water content and amount of segregated ice; that is, ice not occupying pore space. Unfortunately, no computations based on this model were presented.

Finally, in this series of papers, Menot (1978) suggested another alternative formulation for frost propagation in unsaturated porous media, which led to a system of non-linear partial differential equations with the frost line as a free surface. The unknowns were temperature, water pressure and degree of saturation. Once more though, the absence of any numerical calculations prevented an assessment of the validity of the model.

Thus, it was left to O'Neill and Miller (1980) to produce probably

the most complete numerical model of frost heave to date. The details of this are given in the next chapter and therefore only a brief description follows here. The model is based on the secondary heaving concept and represents an expression of Miller's (1978) earlier work in a form amenable to computation. The Clapeyron equation, a capillary equation and a "freezing characteristic curve" are used to relate temperature, liquid and ice pressures, and phase composition in each of the coupled heat and mass equations throughout a frozen fringe. Mass transfer above the latest ice lens is neglected, but beyond that, heat and mass transfer are simulated throughout a freezing column, with particular emphasis on activity within the frozen fringe. Only saturated granular soil is considered.

The contribution to the overall pore (neutral) stress from water and ice is evaluated by a stress partitioning factor. When this neutral stress surpasses the overburden pressure in the frozen fringe, pore contents alone support the overburden. With continued freezing, a new lens is initiated at this level, which then grows as heave proceeds. The model is therefore capable of predicting the formation of rhythmic ice lenses. O'Neill and Miller considered freezing of a soil column for which soil parameters were estimated or assigned values based on experimental data. A Galerkin finite element scheme was used for solution in space, with finite differences in time. For a fixed value of the overburden, predicted lens spacing in time and space, the expulsion of water and its reversal, and the overall magnitude of the heave were all qualitatively reasonable.

O'Neill and Miller (1985) have subsequently improved parameter representation and computational procedures for the model, and carried out a number of small and large scale simulations with varying overburden pressures. Again, the results reproduced observations in both form and magnitude. However, it is pointed out that efforts at strict verification are impeded by the difficulty of obtaining accurate values of certain key parameters, especially hydraulic conductivity in the frozen fringe.

The other main drawback of the model is that many researchers have found it to be intractably complex. In an attempt then to aid understanding of the theory and mechanisms behind the model, Holden (1983) reformulated the equations using quasi-static approximations for the temperature and pore water pressure profiles. This approach had the advantage of simplifying the mathematics and numerical computations without any serious loss in the ability of the model to predict the observed phenomena. Although Holden only considered a semi-infinite soil region, simulations were sufficiently successful to warrant further investigation and development of the method. It is the subsequent evolution of the model which forms the major part of the work described in this thesis. Therefore, in view of its significance, a detailed account of Holden's formulation is given in the following chapter.

Finally, it should be acknowledged that Holden's quasi-static approach was similar to, although developed quite independently of, the model of Gilpin (1980). He also used quasi-static temperature profiles and

assumed that all water freezes either at the freezing front, or at the base of the warmest ice lens. Gilpin however, derived pressure relationships from his own previous work concerning regelation and behaviour of water in close proximity to a substrate. Unlike O'Neill and Miller, he reasoned that a "separation pressure" was responsible for forcing apart the soil particles as heave occurs. The model computed the initiation and growth of successive lenses and the redistribution of water between lenses. In terms of lens distribution, overburden effect and water expulsion followed by intake, the results were qualitatively good.

The above, then, represents a brief review of mathematical frost heave models and, in conclusion, it seems appropriate to repeat comments made by O'Neill (1983) in the summary of his review. He noted that "no model is completely successful in a strict test of frost heave prediction, or in the unequivocal verification of any physics which has been assumed". This statement still reflects the current situation and was recently echoed by the remarks of Kay (1985), who suggested that there is perhaps a need to devote a greater research effort to understanding the processes involved in frost heaving.

2.11 Recent Research Trends

Despite the vast amount of time and money devoted in the past to research into frost heave, areas of conflict remain, and a great deal of effort continues to be expended on every aspect of the

problem. Evidence of this is provided by the proceedings of recent conferences and symposia (see Chapter 1), which illustrate the worldwide concern over problems associated with ground freezing and permafrost.

As far as those areas of research relevant to the work in this thesis are concerned, recent work has, broadly speaking, tended to fall into one of the following four categories:

(1) Development of mathematical and computational techniques for modelling ice lensing and frost heave;

(2) Laboratory and/or field evaluation of numerical models;

(3) Improving input data to numerical models, e.g. hydraulic conductivity and unfrozen water content measurements.

(4) Improving understanding of the frost heaving process.

The research reported herein falls into the first category, but it does, of course, have to account for results emerging from the other three areas. Reference is therefore made in the following chapters to publications under all four headings, thus providing some measure of the state of the art in frost heave research.

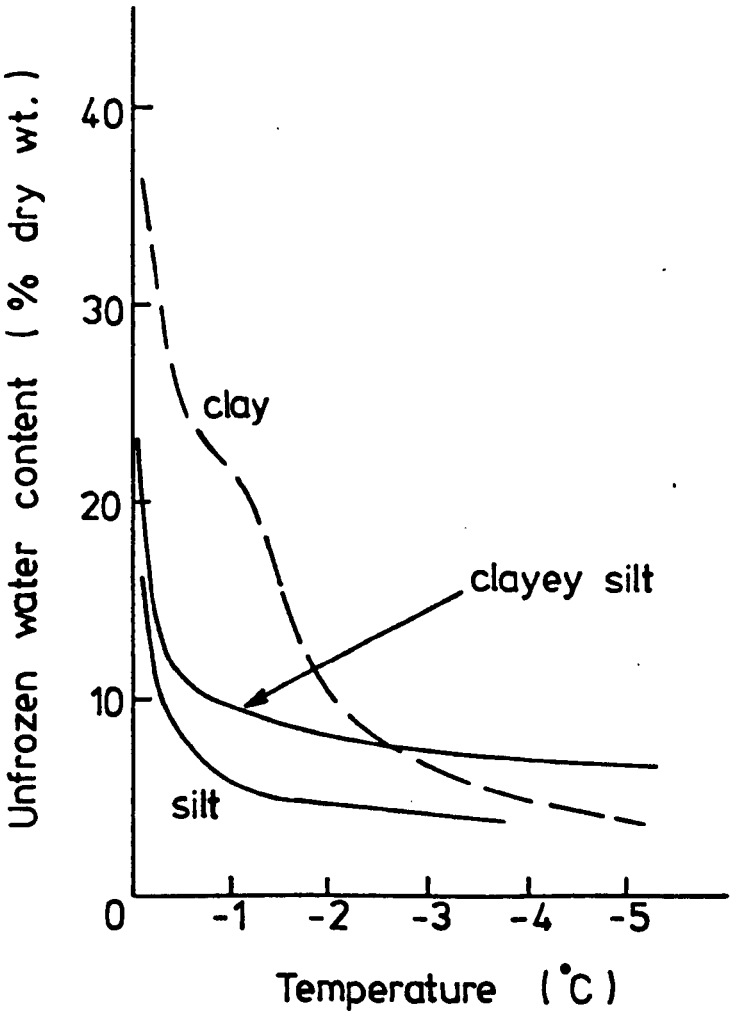

Figure 2.1 Typical curves of unfrozen water content versus temperature (after Burt and Williams, 1976)

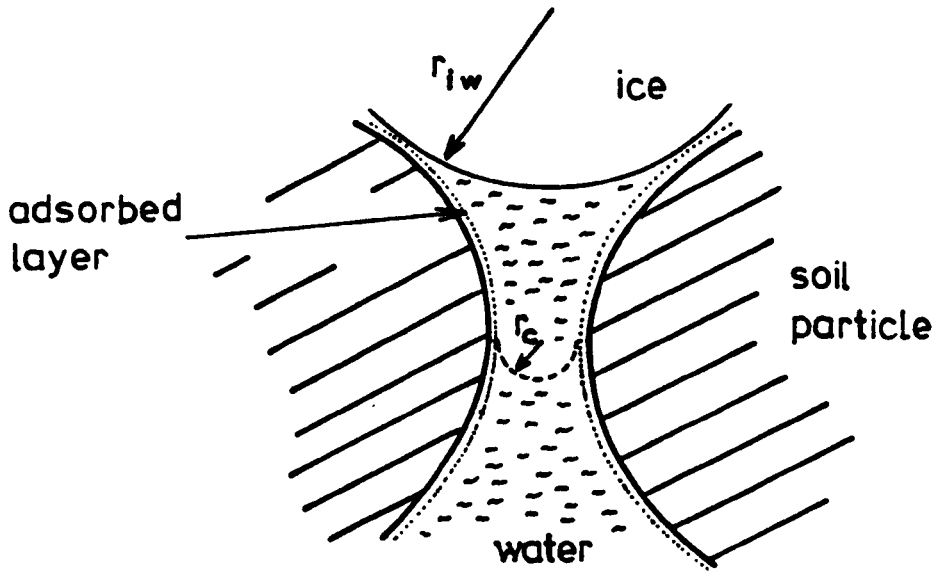

Figure 2.2 Ideal capillary pore (adsorbed layer not to scale)

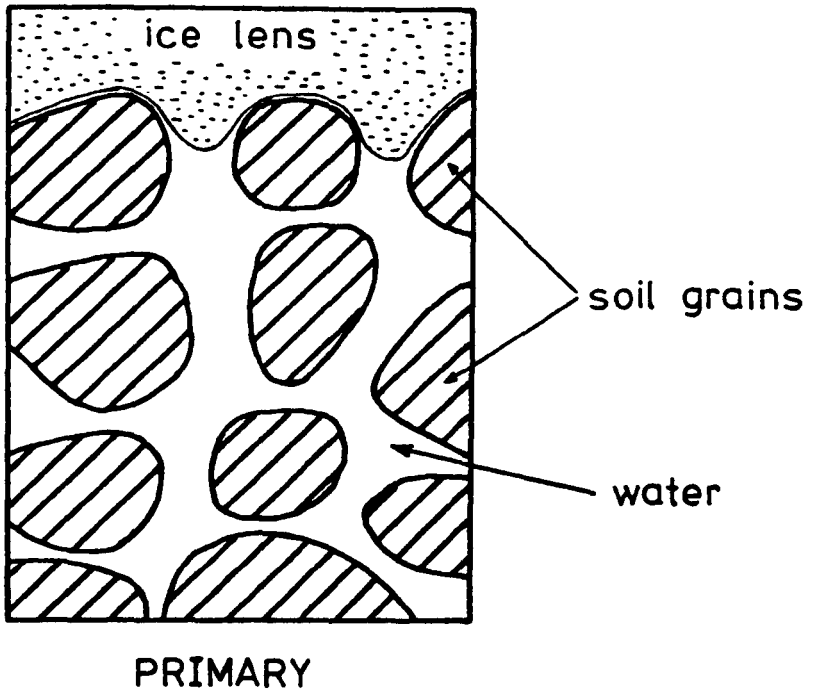

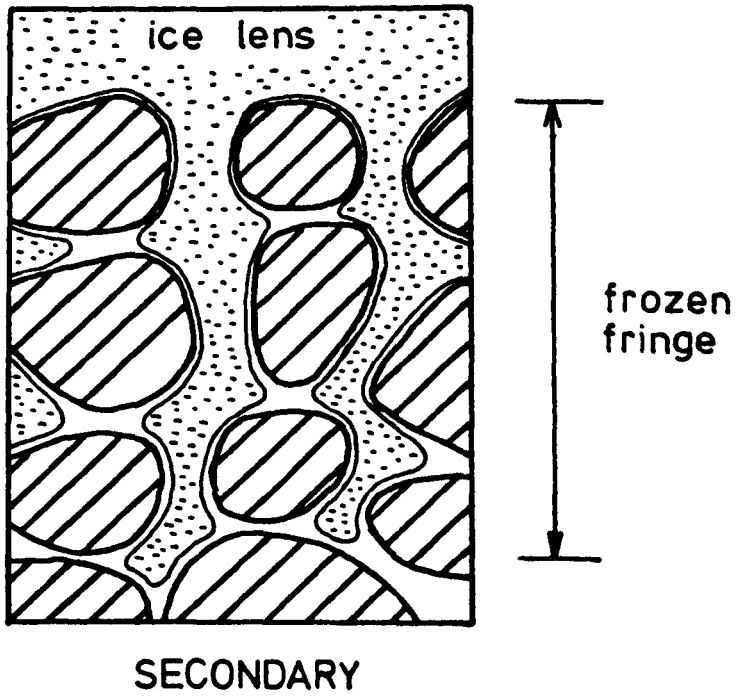

Figure 2.3 Schematic diagrams of primary and secondary heaving

CHAPTER 3

THE THEORY AND MODELLING OF SECONDARY FROST HEAVE

3.1 Introduction

The theory of secondary frost heaving, conceived and developed by Miller (1972, 1977, 1978), forms the basis of much of the work in this thesis and is therefore described in detail in this chapter.

As explained in Chapter 2, Miller (1972) proposed his theory at a time when evidence began to emerge which cast doubt on the ability of the early capillary (or "primary") model to describe fully the heaving process. In the years following, Miller's ideas received increasing support from experimentalists, and it is now generally accepted that the heaving mechanism is most readily explained by the secondary heaving theory.

However, with publication of the many other mathematical models, the computational aspects of the theory have received less coverage in the literature. Nevertheless, the success of computer simulations performed by O'Neill and Miller (1980, 1985, described later in this chapter) illustrates the advantages of this approach over other models such as the adsorption force and segregation potential theories. For example, Miller's theory has shown itself to be amenable to mathematical expression, and to subsequent computation,

without the need for any a priori assumptions concerning material properties. As pointed out by O'Neill (1983) in his review, this has produced perhaps the most detailed current model and in the simulations, predictions of rhythmic ice lensing, of the effects of overburden and the overall magnitude of heave are qualitatively accurate.

It is for these reasons that Miller's view of heaving was adopted as the foundation for the work described herein. It should be said that the main criticism levelled against the O'Neill-Miller model is that it requires accurate experimental data in an area for which measurement is extremely difficult.

In this chapter then, the main features of the secondary heaving theory are first described, including a mathematical formulation of the essential elements of the system. The mathematical model is then made complete with appropriate conservation equations and the results of some computations are briefly assessed. Finally, a simplified approach to the modelling task is presented which provides the introduction to the work subsequently detailed in Chapter 4.

3.2 The Principal Components of the Secondary Heaving Theory

The feature of secondary heaving which renders it fundamentally different to the primary heaving mechanism is the existence of the so-called frozen fringe, whereby ice forms in the pores below

the ice lens proper whilst still permitting growth of the lens. This difference was illustrated in Figure 2.3 of Chapter 2. In addition, the secondary heave model defines where the ice lens will form within this frozen fringe.

In primary heaving, the ice lens rests on films of water adsorbed onto the surface of soil particles. As freezing continues, some of this film water freezes, contributing to growth of the lens. Liquid water is then drawn into the films from below to restore the "equilibrium" thickness, thereby displacing the lens upward whilst simultaneously lowering the local pore water pressure, which in turn induces the necessary flow of ground water towards the growing ice lens. The ice lens is at a pressure determined by the overburden, P, whereas below the lens the load is borne by the soil skeleton and by the pore contents. Thus, the Terzaghi (1936) effective stress equation may be written:

$$P = \sigma' + u_n \qquad \ldots (3.1)$$

or:

$$\sigma' = P - u_n \qquad \ldots (3.2)$$

where: σ' = the effective stress (the portion of the overburden borne by the soil skeleton)

u_n = the neutral stress (the resultant pore pressure)

If the pores contain only water, then:

$$u_n = u_w \qquad \ldots (3.3)$$

and since the pore water pressure, u_w, below the lens is negative, then in primary frost heaving $\sigma' > P$. This means that below the ice lens, the effective stress always exceeds the maximum pressure at which ice could exist there, according to this model. Miller (1977) therefore argued that there was no obvious mechanism for initiating the regular sequence of lenses normally observed when a freezing front penetrates through a soil.

The secondary heaving theory however overcomes this difficulty and the mechanism for the initiation of ice lenses is described later in this section. Miller reasoned that growth of ice into the pores below the ice lens (the frozen fringe) would not prevent the ice phase from moving providing, as in primary heaving, a continuous liquid phase always prevents direct solid-to-solid contact between moving pore ice and stationary soil particles. Instead, the ice phase moves as a continuous rigid body with velocity equal to the rate of heave, and pore ice movement is viewed as a process of microscopic regelation. This movement is driven and accompanied by a parallel transport of unfrozen water, the overall transport being referred to as series-parallel transport (Miller et al, 1975).

The presence of pore or "non-film" water required by the theory explains why it is only applicable, at least in principle, to non-colloidal or granular soils (see Koopmans and Miller, 1966, Miller, 1978). Moreover, only saturated, that is air-free, soils have been considered.

It is worth echoing at this point Miller's (1977, 1978) own remarks

regarding work done along similar lines in the Soviet Union. It appears that as a result of careful observation, Soviet scientists had also concluded that ice lenses appear and grow in soil already containing pore ice, and had undertaken measurement of liquid water movement in frozen soil. However, as far as Miller could ascertain, the Soviet researchers had not proposed any model similar to the secondary heaving theory to explain the phenomenon.

Two essential components of the model (which are also found in the primary heave formulation) are the Laplace surface tension equation:

$$u_i - u_w = \frac{2\sigma_{iw}}{r_{iw}} \qquad \ldots (3.4)$$

and the Clapeyron equation:

$$\frac{u_i}{\rho_i} - \frac{u_w}{\rho_w} = \frac{-LT}{T_o} \qquad \ldots (3.5)$$

in which the effect of solutes has been neglected. Hence, the model strictly only applies to solute-free soils.

In order to provide a mechanism for rhythmic ice lensing, the neutral stress was partitioned in the manner of Bishop (1955) into contributions from the two pore phases, ice and water, thus:

$$u_n = \chi u_w + (1-\chi)\, u_i \qquad \ldots (3.6)$$

where χ, called the stress partition factor, is a function of the

degree of saturation, i.e. the amount of water (as opposed to ice) contained in the pores. Hence, $\chi = 1$ for ice-free soil and tends to zero as the unfrozen water content tends to zero. An explicit form for this function, based on experiment, is given later.

Before explaining the lensing mechanism, a definition of the freezing front is required. Often the 0°C isotherm is taken to mark the extent of freezing or frost penetration. However, to allow for the depression of the freezing point of soil water, the freezing front is defined here as the macroscopic boundary between ice-free soil and soil in which some ice exists (Miller and Koslow, 1980). The frozen fringe is therefore the region lying between the base of the latest ice lens and the freezing front, and although the ice pressure is continuous within the frozen fringe, there is discontinuity at the freezing front as shown in Figure 3.1(A).

The stress profiles of Figure 3.1(A) illustrate the situation in the frozen fringe a moment before a new lens is initiated. The water pressure decreases more or less exponentially across the frozen fringe, due to the corresponding decay of the hydraulic conductivity. It therefore falls from a slightly negative value at the freezing front to a very large negative at the base of the ice lens. The difference between ice and water pressure, $u_i - u_w$, increases with elevation above the freezing front but not as fast as u_w decreases. Thus, the ice pressure increases with elevation at a decreasing rate, and passes through a maximum some distance below the ice lens before falling to the overburden pressure, P, at the

base of the lens.

Hence, the neutral stress, u_n, will also pass through a maximum implying that at the same level the effective stress, σ', passes through a minimum. If the minimum of σ' falls to zero, corresponding to $u_n = P$, the pore contents alone support the overburden and the soil grains are no longer held stationary against their neighbours. They therefore move along with the moving ice and a new lens is initiated at this level. The spacing between successive lenses can then be established since the base of the previous lens lies at the level at which the ice pressure is equal to the overburden.

As soon as the new lens is initiated, the pressure within it cannot exceed P and u_i immediately drops to this value (Figure 3.1(B)). Local adjustments in temperature and water pressure cause the effective stress to rise and lens initiation is therefore prevented for the time being. However, with continued freezing, the new lens grows and the freezing front descends through the soil so that the maximum value of u_n again approaches P, the minimum of σ' approaches zero and the lens initiation cycle repeats at a new, lower level (Figure 3.1(C)).

If this next lens initiates at a time Δt later than the previous lens initiation, then the last lens will have grown to a thickness h given by:

$$h = \dot{H}\Delta t \qquad \ldots (3.7)$$

where: H = heave

$\dot{H} = dH/dt$ = heave rate, assumed here to be constant over the time interval.

Miller thus provided not only a mechanism for rhythmic ice lensing, but also a means of predicting the time and distance between lens formations and their thickness. Undoubtedly, this is one of the great advantages of the model.

3.3 Miller's Mathematical Model

It was in his paper of 1978 that Miller first attempted a complete mathematical expression of the theory, and he began by using the surface tension equation to define a variable, ψ:

$$\psi = \frac{u_i - u_w}{\sigma_{iw}} \qquad \ldots (3.8)$$

ψ is a measure of the suction and is a convenient parameter to use in relating water (or ice) content and hydraulic conductivity to suction in the frozen fringe. It can be interpreted as a mean curvature of the ice/water interface. With the aid of the Clapeyron equation (3.5), the parameter ψ may be written as:

$$\psi = A\, u_w + BT \qquad \ldots (3.9)$$

where A and B are constants, as follows:

$$A = \frac{1}{\sigma_{iw}} \left(\frac{\rho_i}{\rho_w} - 1\right)$$

$$B = \frac{-\rho_i L}{\sigma_{iw} T_o} \qquad \ldots (3.10)$$

Koopmans and Miller (1966) had shown that, by considering the similarity between freezing (and thawing) and drying (and wetting) of a granular soil:

$$\theta_w(\psi) = \theta_w(\psi_a) \qquad \ldots (3.11)$$

that is, for the same water content, θ_w, in the two situations, $\psi = \psi_a$. ψ_a is defined for ice-free unsaturated soil by:

$$\psi_a = \frac{u_a - u_w}{\sigma_{aw}} \qquad \ldots (3.12)$$

where: u_a = pore air pressure

σ_{aw} = air/water interfacial energy

It was therefore possible to obtain relatively easily a relationship between the unfrozen water content and ψ for a saturated soil undergoing freezing. Specific examples used in the computations are given in the next section.

As the soil is considered to be saturated, the liquid phase is continuous from the water table or base of the soil column, through the frozen fringe to the base of the growing ice lens, where it terminates. Liquid volume flux then was assumed to obey Darcy's Law throughout

the region in which the liquid phase is continuous. Writing Darcy's Law with z as space coordinate, positive downward, gives:

$$v_w = \frac{-k}{\rho_w g} \frac{\partial}{\partial z} (u_w - \rho_w g z) \qquad \ldots (3.13)$$

where: v_w = volume flux of water

k = hydraulic conductivity

Since the hydraulic conductivity is a function of the ice content, θ_i, and hence of ψ, it follows that v_w is also a function of ψ. Similarly, pore ice flux, v_i is a function of ψ and is related to the heave rate (or ice velocity), v_I by:

$$v_i = \theta_i v_I \qquad \ldots (3.14)$$

where v_I is variable in time but constant in space, in keeping with the "rigid-ice" assumption.

To construct a governing set of differential equations, conservation of mass and energy were considered. Accounting for flux of both water and ice, the mass conservation equation was written:

$$\frac{\partial}{\partial t} (\rho_w \theta_w + \rho_i \theta_i) + \frac{\partial}{\partial z} (\rho_w v_w + \rho_i v_i) = 0 \qquad \ldots (3.15)$$

and energy conservation was of the form:

$$\sum (\rho c \theta)_n \frac{\partial T}{\partial t} - \frac{\partial}{\partial z} (K \frac{\partial T}{\partial z}) - \rho_i L (\frac{\partial \theta_i}{\partial t} + v_I \frac{\partial \theta_i}{\partial z}) = 0$$

$$\ldots (3.16)$$

where: K = thermal conductivity

c_n = specific heat capacity of the n^{th} component of the soil

where all soil components (particles, unfrozen water and ice) are included in the summation. Equations (3.15) and (3.16) are in a slightly different form, but essentially similar, to those derived in Appendix B and their derivation will not be considered further here.

Miller (1978) concluded that Equations (3.8) to (3.10) and (3.13) to (3.16) formed the basis of a model amenable to computer simulation procedures, but no computations were attempted at this stage. However, Miller anticipated that simulations would provide predictions of rate of heave and rate of frost penetration as functions of overburden pressure and thermal regime. Moreover, with the lens initiation mechanism described in the previous section, information on position, time of origin and ultimate thickness of each ice lens was expected to emerge as part of the solution. This indeed proved to be the case, as the computations outlined in the next section illustrate. It was noted however, that successful simulations of real problems would depend on obtaining realistic data for water content, $\theta_w(\psi)$, hydraulic conductivity, $k(\psi)$ and the stress partition factor, $\chi(\psi)$, for the soil in question.

3.4 Computed Results

Before any simulations were attempted for transient boundary conditions,

Miller and Koslow (1980) presented some illustrative examples of numerical solutions for quasi-steady state freezing conditions. Their aim was to use a simple special case to demonstrate the way in which the rigid-ice model responds to thermal and mechanical boundary conditions. The following conditions were applied to an initially uniform column that had undergone monotonic freezing, to reach a state in which:

(i) The temperature field is stationary in the unfrozen zone. This implies a steady and uniform flux of sensible heat through the unfrozen zone and a uniform temperature gradient there.

(ii) The pore water pressure field is also stationary in the unfrozen zone. In other words, there is a steady and uniform volumetric flux of water through the unfrozen zone and a uniform gradient of pore water pressure. This further implies a steady rate of heave.

The principal equations in Miller and Koslow's numerical scheme were Equation (3.9) relating the parameter ψ to pore water pressure and temperature, Darcy's law (3.13) for the flow of liquid water, and the Fourier heat conduction equation:

$$q = -K \frac{dT}{dz} \qquad \ldots (3.17)$$

where: q = the diffusive flux of sensible heat.

Also, instead of defining a freezing front, in this particular model

a "psi-front" was defined as the boundary at which u_w and T satisfy Equation (3.9) when $\psi \equiv 0$. Hence, if the values of water pressure and temperature at the base of the soil column are specified, along with their respective gradients in the unfrozen zone, then the elevation of the psi-front above the base of the column can be obtained by combination of (3.9), (3.13) and (3.17). This allows an estimate of the water pressure at the psi-front which, in turn, gives a value for the steady heave rate by way of a simple mass balance equation. Miller and Koslow then adopted the following numerical procedure.

First, experimental data was provided for the soil functions $\theta_w(\psi)$ and $k(\psi)$, with the data $\theta_w(\psi)$ then being used in theoretical estimates of the thermal conductivity function, $K(\psi)$ and the stress partition function, $\chi(\psi)$. With this information, values for ΔT and Δu_w are estimated, for a thin layer of soil of thickness Δz (above the psi-front), using (3.13) and (3.17). These values yield an estimate for $\Delta\psi$ via (3.9). This allows estimation of $\theta_w(\psi)$ and hence estimation of changes in water and heat flux, which provide improved estimates of K and k. The original estimates of ΔT and Δu_w are now also improved, and this iteration cycle is repeated for the first layer until no further improvement is achieved. A value for the neutral stress (Equation (3.6)) is then recorded before proceeding to the next layer. Both ice pressure and neutral stress pass through a maximum and the layer-by-layer iterative process is terminated when the post-maximum value of u_i reaches the value of the maximum of u_n (equivalent to $u_i = P$ at the base of the growing ice lens).

Results presented by Miller and Koslow were of illustrative rather than quantitative significance. This was because true stationary states normally attained in laboratory tests are rather different to the conditions imposed here, which are difficult to reproduce in the laboratory. A "true" stationary state implies zero heave rate, zero flux of water and a uniform flux of heat throughout the soil column. Nevertheless, the results showed the relative insensitivity of the model to inaccuracies in thermal conductivity and stress partition functions, and exemplified the response of the model to different thermal and mechanical boundary conditions.

3.4.1 O'Neill and Miller (1980)

A thorough test of the model, however, was presented by O'Neill and Miller (1980), who tackled the more difficult, but more relevant problem of transient freezing conditions. They reported on test case solutions of the equations simulating the frost heave history of a soil column, heaving a specified surface load.

O'Neill and Miller used Equations (3.8), (3.9) and (3.13) to (3.16). In addition, in order to express the governing equations in a form amenable to numerical treatment, the ice content was expressed as:

$$\theta_i = \theta_i(\psi) = \theta_i\,(Au_w + BT) \qquad \ldots (3.18)$$

and hence, its differential with respect to time as:

$$\frac{\partial \theta_i}{\partial t} = \frac{\partial \theta_i}{\partial \psi} \left[A \frac{\partial u_w}{\partial t} + B \frac{\partial T}{\partial t} \right] \quad \ldots (3.19)$$

Since the soil is considered to be saturated and incompressible, the porosity, θ_o, is taken to be constant and can be written:

$$\theta_o = \theta_w + \theta_i \quad \ldots (3.20)$$

It is then possible to write the mass and energy conservation equations (3.15) and (3.16) respectively, as two coupled non-linear partial differential equations in the unknowns u_w and T.

These equations were solved using a finite element scheme in space, with finite differences in time. For the finite element system, the dependent variables were expressed as sums of "basis" or "shape" functions, each multiplied by its time dependent coefficient, as follows:

$$T = \sum_{j=1}^{N} T_j(t)\, W_j(z)$$

$$u_w = \sum_{j=1}^{N} u_j(t)\, W_j(z) \quad \ldots (3.21)$$

where: T_j = temperature at node j

u_j = water pressure at node j

and W_j are the basis functions providing linear interpolation of the unknowns between nodes. The total number of nodes is N. If $\underset{\sim}{V}$ is the vector of unknowns, then time derivatives are expressed using a backward difference as:

$$\dot{\underset{\sim}{y}} = \frac{\underset{\sim}{y}^{k+1} - \underset{\sim}{y}^{k}}{\Delta t} \qquad \ldots (3.22)$$

where: $\underset{\sim}{y}^{k}$ = vector of unknowns evaluated at the k^{th} time level

Δt = time step size

Substitution of (3.21) into the governing partial differential equations and use of Galerkin finite element procedures coupled with (3.22) results in two matrix equations of the form:

$$\underset{\sim}{A}\ \underset{\sim}{y}^{k+1} = \underset{\sim}{R} - \underset{\sim}{B}\ \underset{\sim}{y}^{k} \qquad \ldots (3.23)$$

where $\underset{\sim}{R}$ is a vector of known quantities. The matrices $\underset{\sim}{A}$ and $\underset{\sim}{B}$ are essentially time dependent since they contain terms derived from the dependent variables, such as $\partial\theta_i/\partial\psi$. Thus, in the course of a simulation, they are updated iteratively as time proceeds. The solution cycle can in fact be summarised as follows:

Knowing $\underset{\sim}{y}^{k}$, either from the initial conditions or the solution at the previous time step, $\underset{\sim}{A}$, $\underset{\sim}{B}$ and $\underset{\sim}{R}$ are estimated and (3.23) is solved for the unknowns $\underset{\sim}{y}^{k+1}$. This new solution is then used to recalculate $\underset{\sim}{A}$, $\underset{\sim}{B}$ and $\underset{\sim}{R}$ and the system is solved again for a new, presumably more accurate $\underset{\sim}{y}^{k+1}$. This iterative process is repeated until a satisfactory degree of convergence is achieved, and the solution proceeds to the next time step.

At any point in time, the heave rate is calculated by taking a mass

balance at the base of the latest lens. Throughout the lens, ice is moving upwards, giving a mass flux of $\rho_i v_I$. Just below the lens, pore ice is rigidly connected to the lens ice, and has the same velocity but only occupies a fraction, θ_i, of the cross-sectional area. Thus, the ice flux there is $\rho_i v_I \theta_i$. A liquid mass flux, $\rho_w v_w$, also exists in the soil below the lens, so a mass balance at the lens boundary yields:

$$\rho_i v_I = \rho_i v_I \theta_i + \rho_w v_w \qquad \ldots (3.24)$$

or: $$\rho_i (1-\theta_i)\, v_I = \rho_w v_w$$

When Darcy's law (3.13) is substituted into this equation, an expression for v_I is obtained in terms of the current values of u_w and T.

It is assumed that activity in the zone above the lowest lens is slight, in the sense that heat is conducted through the material, but insignificant additional phase change occurs there. Moreover, it is assumed that the freezing process is slow enough to allow the temperature distribution above the latest lens to be considered linear. A temperature boundary condition for the soil below the warmest lens is then obtained by taking a heat balance across the lens boundary, located at $z = z_s$:

$$K_s \left(\frac{T_s - T_c}{d}\right) = K_f \left(\frac{\partial T}{\partial z}\right)_{z=z_s} - \rho_w L v_s \qquad \ldots (3.25)$$

where: T_C = specified soil surface temperature

T_S = temperature at $z = z_S$

d = the length of the frozen zone between the soil surface and $z = z_S$

K_S = thermal conductivity of the material above the warmest lens

K_f = thermal conductivity below the lens

v_S = liquid flux at $z = z_S$

This equation states that the difference in conductive heat fluxes across z_S is proportional to the rate of freezing there, as liquid flows into the lens.

Finally, a boundary condition in u_W at the base of the latest lens is provided by a pressure balance there. Noting that ice pressure is continuous across the lens boundary and that ice in the lens is subjected to the overburden pressure, P, Equations (3.8) and (3.9) give:

$$P - u_S = \sigma_{iW} (Au_S + BT_S) \qquad \ldots (3.26)$$

where: $u_S = u_W$ at $z = z_S$

The boundary conditions (3.24) to (3.26) were incorporated into the governing set of equations.

O'Neill and Miller performed simulations for a column of soil 153 mm in length, subject to a constant overburden pressure and initially at a uniform temperature of 1°C. During freezing, the warm end temperature

remained at 1°C whilst the soil surface temperature was specified through all time. The pressure at the warm end was held at atmospheric, that is $u_w = 0$.

During the initial stages of freezing, as the surface temperature was lowered at a constant rate, heave was temporarily restrained by the overburden and the formation of pore ice caused liquid to be expelled from the soil column. In time this trend reversed with water being drawn into the column as heave and lens formation began. The equations were solved for the "active" region below the lowest lens with mesh point separations as little as 2.5×10^{-2} mm immediately below the lens, increasing to around 30 mm at the unfrozen end. The position and time of each lens initiation were simulated, according to the procedure described earlier, with the maximum of the neutral stress in the frozen fringe being compared with the overburden at each time step. In these simulations, the cold side temperature was decreased to -0.5°C and then held fixed, so that eventually lens formation ceases and a steady state is approached, with the heave rate tending asymptotically to zero.

Information regarding soil properties is of course required by the model and, as pointed out by Miller and Koslow (1980), for a process that involves progressive downward freezing of a column of initially ice-free soil, hysteretic complications are absent, so that simple monotonic functions are sufficient to describe soil functions.

O'Neill and Miller assumed hydraulic conductivity to be similar to

that in an unsaturated soil at the same liquid water content and used the following (cf. Bresler et al, 1978):

$$k(\theta_i) = k(0)\ (1 - \frac{\theta_i}{\theta_o})^7 \qquad \ldots (3.27)$$

where the porosity θ_o was assumed to be 0.4. A convenient representation for $\theta_i(\psi)$ was suggested by data obtained by Horiguchi and Miller (1980) and is illustrated in Figure 3.2. The stress partition factor, χ, also a function of the ice content, was given by:

$$\chi(\theta_i) = (1 - \frac{\theta_i}{\theta_o})^{1.5} \qquad \ldots (3.28)$$

Finally, soil specific heat capacity and thermal conductivity were given constant values in each of two regions, namely where ice was present and where it was absent.

The success of the simulations was evident from the results presented by O'Neill and Miller for the test case described above. As well as being able to predict the cumulative frost heave, the computations yielded information such as the thickness of each ice lens, the time elapsed between successive lens initiations and the form of the pressure profiles in the frozen fringe. The latter proved to be as expected and as illustrated in Figure 3.1. Indeed, when compared with experiment and general experience with heaving systems, the results were both self-consistent and qualitatively reasonable. Perhaps most interesting was the diagram O'Neill and Miller were able to produce of the soil column, or at least a portion of it,

showing the thickness, time of initiation and location in the soil of each ice lens. This diagram is reproduced in Figure 3.3.

Therefore, although O'Neill and Miller, and others, had some reservations (discussed later in this section), the model merited further exploration.

3.4.2 O'Neill and Miller (1985)

A more recent paper included a comprehensive description of the theoretical basis of the model (O'Neill and Miller, 1985), and attempted to clarify certain concepts. Phase equilibrium and thermally induced regelation were discussed in the context of frost heave in general, and this model in particular. The equations of the model were then restated and a number of modifications introduced.

O'Neill and Miller explained that the overall theory and governing equations remained unchanged, "but the particular computational strategies and parameter representations have evolved in the direction of greater realism, relevance, efficiency and accuracy". Among the changes made was the introduction of an alternative means of calculating the heave rate, v_I. Previously, the mass balance equation at the base of the ice lens (3.24) was used. This was replaced by a mass balance taken over the entire length of lens-free soil, that is the frozen fringe and unfrozen soil. The difference between the mass flux at the base of the lens and the mass flux at the warm end of the

column was equated with the rate of change of the aggregate mass content in between. Thus:

$$\rho_i v_I - \rho_w (v_w)_{z=z_w} = \frac{d}{dt} \int_{z_s}^{z_w} (\rho_w \theta_w + \rho_i \theta_i) \, dz \quad \ldots (3.29)$$

where: z_w = the level of the base of the soil column

In practice, the integral on the right-hand side of (3.29) was evaluated with Simpson's Rule, applied over each element, and its time derivative obtained using simple finite differences.

Another significant modification made by O'Neill and Miller (1985) was the use of a "more realistic" representation for $\theta_i(\psi)$. This new interpretation is shown against the previous one as a broken curve in Figure 3.2. The curve is a regression curve fit to experimental data (not given) in the form:

$$\theta_w = \theta_o - \theta_i = \sum_{k=0}^{5} A_k \, (\log \psi)^k \quad \ldots (3.30)$$

where the A_k are constants determined by the regression. The importance of (3.30) is that it can be differentiated analytically to produce an expression for $d\theta_i/d\psi$, which may be used in turn in the governing equations, and also in an updated formula for the stress partition factor, χ, which is rather more complex than (3.28).

A slight alteration was also made to the function used to calculate hydraulic conductivity. This was simply a matter of changing the

exponent, so that (3.27) now became:

$$k(\theta_i) = k(0)(1 - \frac{\theta_i}{\theta_o})^9 \qquad \ldots (3.31)$$

Finally, O'Neill and Miller added two equations for the calculation of thermal conductivity in the frozen zone and in the frozen fringe. These are not quoted here, but involved the use of representative values for the thermal conductivity of pure water, pure ice, frozen silt and a solid sample of the soil minerals in simple formulae.

These then were the most important modifications made by O'Neill and Miller (1985), along with some minor alterations in computational strategy. However, O'Neill and Miller were keen to point out that although the computed results were changed to some extent, indeed improved, their qualitative nature remained the same and it was the general character of the results, rather than the actual numerical values, which they wished to emphasise.

A series of simulations was undertaken to evaluate the sensitivity of the model to variations in overburden. Heave histories were computed for 100 mm soil columns under step freezing conditions, that is, the cold end of the column, initially uniformly at 1°C, was stepped down to -1°C at time zero. The resulting cumulative heave versus time curves are reproduced in Figure 3.4, and are "believable in relation to laboratory observations", illustrating that "the model evidently responds appropriately to variations in P." Cumulative heave was evaluated by numerical integration of the heave

rate over time. Once again, as observed in laboratory freezing tests (e.g. Penner and Ueda, 1977), water expulsion followed by water intake was modelled, the phenomenon being more pronounced in columns subjected to higher values of overburden. As already mentioned, subject to the variations in P, the general character of the results was as reported previously, and this fact was stressed by the reproduction of some of the earlier (O'Neill and Miller, 1980) findings, for example, Figure 3.3.

As a further test of the capabilities of the model, a number of simulations were run on a much larger scale. A 35 m vertical soil column was considered, at an initial temperature of 3°C throughout. The simulations began with an assumed temperature on the upper surface of -5°C, whilst the warm end temperature at the 35 m depth was held fixed at 3°C. It was further assumed that the top 100 mm of the column was solid frozen material. The initial overburden was taken as 5 kPa and water pressure at the warm end was kept at the initial hydrostatic value. These conditions were intended to bear some similarity to those beneath a buried chilled pipeline, and to provide a framework within which to assess the simulation of a field scale problem. The results of the tests appeared to be reasonable, although no comparison was made with actual field data. The chief difference between these and the small scale tests was the effect of overburden: in the large scale tests, as the depth of freeze increases, the weight of overburden on the frozen fringe increases significantly and hence plays a major role in suppressing heave, unlike the soil self-weight in the small scale tests.

Thus, with both small and large scale simulations, O'Neill and Miller provided further evidence in support of their model and the principles underlying the secondary heave theory. Therefore, to conclude this section, a summary of the so-called rigid ice model is given, with a discussion of its merits and drawbacks.

The model, strictly speaking, is for air-free, solute-free, colloid-free, saturated, incompressible soils, and is based primarily on:
(1) governing equations in terms of temperature and water pressure, developed from basic conservation laws and from fundamental thermodynamics (the Clapyron equation);
(2) concepts relating phase composition of the system, its state and its capillarity, all supported by experimental evidence;
(3) rational mechanisms for pore stress partitioning and the ability of a new ice lens to form.
The other major feature of the model is the rigid ice assumption which postulates that soil ice tends to form on pre-existing ice and hence grows through the pore system as one solid body. Whilst this body may have a very complex microscopic geometry, it moves as a rigid body, with a uniform velocity in space, as ice migrates through the soil. During this migration, the ice accommodates the stationary soil matrix where necessary, by melting on the warm side of soil grains and refreezing on the cold side. This concept of microscopic regelation is thus of fundamental importance to the rigid ice assumption, and it must be said that in the absence of strict proof, this is a physically motivated assumption.

As described earlier, the results obtained mimic observation both in

form and in order of magnitude. For example, the suppression of heave and increased frost penetration with increasing overburden is predicted, as is water expulsion followed by water intake in the higher overburden cases. The model also simulates the rhythmic formation of ice lenses, with microscopic, closely spaced lenses during initial rapid freezing and larger lenses and lens spacings during later, slower freezing.

Against these positive features, a number of disadvantages must be weighed. The model is computationally expensive because the formation and growth of each individual ice lens is simulated. This means that during early time when a great many very thin lenses form, a vast amount of repetitive computation of limited significance must be performed. Furthermore, as a consequence of the finite element analysis, mesh point separations in the region of greatest interest, namely the frozen fringe, are as little as 0.025 mm, which again places a heavy computational burden on the model.

Another problem is that strict verification of the model requires accurate data for certain key parameters, in particular unfrozen water content and hydraulic conductivity in the frozen fringe. Measurement of these quantities is extremely difficult and challenges the limits of current laboratory techniques.

Finally, O'Neill and Miller noted that although their approach provides sufficient equations for a solution to be obtained, it is possible that certain interactions which ought to be included, especially on a microscopic scale, have in fact been omitted. In other

words, it is not clear whether such interactions are implicit in the macroscopic equations or if additional mechanics and thermodynamics must be included to complete the description of the physical processes involved in frost heaving. In any case, generalisation of the theory to cover three phases (liquid water, ice and air) is necessary before the unsaturated case can be analysed.

Bearing in mind the drawbacks discussed above, and recognising that, in spite of these, the model still has much to commend it, it seemed that what was needed now was a modified approach which retained the basic features of the rigid ice model, but embodied them in a simpler mathematical framework. Such an approach is described in the following section.

3.5 Approximate Solutions for the Rigid Ice Model

This simplified version of the model, presented by Holden (1983), in fact appeared prior to the later work of O'Neill and Miller (1985) but was in no way invalidated by the latter. Holden's basic strategy was to use quasi-static approximations for the temperature and pore water pressure profiles, along with energy and mass balance equations, to reduce the problem to that of the solution of two ordinary differential equations. The quasi-static assumption was motivated by the slow nature of the freezing process and avoids the more difficult problem of solving a pair of non-linear coupled partial differential equations. Although developed quite independently, this approach was similar to that adopted by Gilpin (1980). Gilpin's work however was

not based so directly on the rigid ice model and the two therefore differ in their fine detail.

For convenience and to test the usefulness of his model, Holden considered a saturated semi-infinite column of soil, as opposed to a finite column. Following Miller's secondary heaving theory, he envisaged a heaving column of soil to be made up of three distinct regions:

1. a solid frozen region of soil that may contain distinct ice lenses;
2. a partially frozen region of soil (the frozen fringe) containing soil, ice and unfrozen water; and
3. an unfrozen region of saturated soil.

This profile of a freezing soil is illustrated schematically in Figure 3.5. If z, the space coordinate, is measured downward and the cumulative heave is H(t), then the soil surface is $z = -H(t)$. The position of the base of the lowest ice lens is denoted by $z = z_s$, the position of the freezing front by $z = z_f$ and the level of the water table (since a semi-infinite column is being considered) by $z = z_w$. These different levels and their associated temperatures are also shown in Figure 3.5.

The soil was assumed to be initially at a temperature $T_1 > 0$. At time $t = 0$ the surface $z = 0$ is cooled to a temperature $T_c < 0$. The freezing front therefore descends through the soil, ice lenses form and the soil heaves. Due to the slow nature of the freezing process and the relative inactivity in the solid frozen region,

the temperature profile there is close to linear, as shown by a number of experimentalists (e.g. Jame and Norum, 1976, Fukuda, 1980). Accordingly, it may be written as:

$$T = \frac{z_s - z}{z_s + H} T_c + \frac{z + H}{z_s + H} T_s, \quad -H \leq z \leq z_s \qquad \ldots (3.32)$$

O'Neill and Miller (1980) had also argued in favour of this linear profile, to produce a temperature boundary condition at the base of the lowest lens.

Holden assumed further that the temperature profile in the frozen fringe was linear, and of the form:

$$T = \frac{z_f - z}{z_f - z_s} T_s + \frac{z - z_s}{z_f - z_s} T_f, \quad z_s \leq z \leq z_f \qquad \ldots (3.33)$$

In the absence of supporting experimental evidence, this is a rather stronger assumption than the previous one. In the unfrozen region, a linear profile cannot be used because the column is semi-infinite. Holden therefore based the temperature on the classical solution (Carslaw and Jaeger, 1959) which, with appropriate adjustment of the variables, gives:

$$T = T_f + (T_l - T_f) \operatorname{erf} \left(\frac{z - z_f}{2\sqrt{\mu t}}\right), \quad z \geq z_f \qquad \ldots (3.34)$$

where μ is the thermal diffusivity. This profile determines the temperature gradient just ahead of the freezing front.

The other profiles needed were for the water pressure in both the

frozen fringe and the unfrozen region. At the level of the water table, z_w, the water pressure is zero and it then decreases linearly up to the level of the freezing front. In the frozen fringe, the ice content increases rapidly with decreasing temperature, with a corresponding rapid decrease in the unfrozen water content. This produces a rapid decrease in the water pressure, u_w, from the small negative value u_f at the freezing front, z_f, to a large negative value u_s just below the ice lens at z_s. Holden assumed continuity of water pressure gradient at z_f and a quadratic profile in the frozen fringe, which yielded:

$$u_w = \begin{cases} \left[(z_w - z) - \dfrac{(z_f - z)^2}{z_f - z_s}\right] \dfrac{u_f}{z_w - z_f} + \left(\dfrac{z_f - z}{z_f - z_s}\right)^2 (u_s - u_f), \\ \qquad\qquad z_s < z < z_f , \\ \dfrac{z_w - z}{z_w - z_f}\, u_f, \qquad z_f < z < z_w \end{cases} \qquad \ldots (3.35)$$

It was pointed out that the choice of a quadratic served merely as an illustration and that other choices were clearly possible.

The ψ parameter was introduced in the manner of O'Neill and Miller (1980), via Equations (3.8) and (3.9), and the same criterion for the formation of a new lens was adopted, with the use of Equation (3.6) for the neutral stress. Adhering to the input data of O'Neill and Miller (1980) as far as possible, Holden used Equation (3.28) for the stress partition function and approximated the experimental curve for $\theta_i(\psi)$ partly by a quadratic and partly by a hyperbola, as follows:

$$\theta_i = \begin{cases} A + B\psi + C\psi^2 , & \psi_1 < \psi < \psi_2 \\ D - \dfrac{E}{\psi - F} , & \psi > \psi_2 \end{cases} \qquad \ldots (3.36)$$

where: $A = 0.01385$ $\quad B = -6.144 \times 10^{-8}$

$C = 3.143 \times 10^{-14}$ $\quad D = 0.4$ (porosity)

$E = 2.8 \times 10^{5}$ $\quad F = 2.2 \times 10^{6}$

$\psi_1 = 2.6 \times 10^{5}$ $\quad \psi_2 = 3.6 \times 10^{6}$

The equations for the model were derived by applying conservation of heat energy and of mass at the base of the ice lens and at the freezing front. In addition, Darcy's Law and a form of the Clapyron equation were employed to complete the set of equations.

The energy balance equation at $z = z_s$ is:

$$K_f \left.\frac{\partial T}{\partial z}\right|_{z_s^+} - K_s \left.\frac{\partial T}{\partial z}\right|_{z_s^-} = \rho_w L v_s \qquad \ldots (3.37)$$

where: v_s = liquid volume flux at the top of the frozen fringe

K_f = thermal conductivity of the frozen fringe

K_s = thermal conductivity of the solid frozen region

At the freezing front $z = z_f$, the energy balance equation is:

$$K_u \left.\frac{\partial T}{\partial z}\right|_{z_f^+} - K_f \left.\frac{\partial T}{\partial z}\right|_{z_f^-} = -\rho_i L \theta_{if} \frac{dz_f}{dt} \qquad \ldots (3.38)$$

where: K_u = thermal conductivity of the unfrozen soil

θ_{if} = volumetric ice content at $z = z_f$

Substitution of the temperature profiles (3.32), (3.33) and (3.34) into Equations (3.37) and (3.38) yields:

$$K_f \frac{T_f - T_s}{z_f - z_s} - K_s \frac{T_s - T_c}{z_s + H} = \rho_w L v_s \qquad \ldots (3.39)$$

and:

$$K_u \frac{T_l - T_f}{\sqrt{\pi \mu t}} - K_f \frac{T_f - T_s}{z_f - z_s} = -\rho_i L \theta_{if} \frac{dz_f}{dt} \qquad \ldots (3.40)$$

Applying conservation of mass now to the base of the ice lens ($z = z_s$) gives:

$$\rho_i (1 - \theta_{is}) \frac{dH}{dt} = -\rho_w v_s \qquad \ldots (3.41)$$

where: θ_{is} is the volumetric ice content at the top of the frozen fringe.

At the freezing front, Holden assumed there is a jump in the ice content which causes a jump in the value of the hydraulic conductivity. Therefore, employing Darcy's Law for water flow, the mass balance equation at this level was written as:

$$\rho_i \, \theta_{if} \frac{dH}{dt} = \frac{-[k_f]}{g} \frac{u_f}{z_w - z_f} \qquad \ldots (3.42)$$

where: $[k_f]$ denotes the jump in the value of k_f, the hydraulic

conductivity at $z = z_f$. The gravity term normally present in Darcy's equation is missing from (3.42) and it is not clear why this is so.

Darcy's Law is also assumed to hold at the top of the frozen fringe so that, again using (3.35):

$$v_s = \frac{-k_s}{\rho_w g} \left\{ \left[\frac{1}{z_w - z_f} + \frac{2}{z_f - z_s} \right] u_f - \frac{2u_s}{z_f - z_s} - \rho_w g \right\} \quad \ldots (3.43)$$

where: k_s is the hydraulic conductivity at $z = z_s$.

Finally, assuming that the ice pressure is continuous and equal to the overburden pressure P at $z = z_s$, (3.8) and (3.9) combine to give:

$$P - u_s = \sigma_{iw} (Au_s + BT_s) \quad \ldots (3.44)$$

which, in fact, is another form of the Clausius-Clapeyron equation.

Eliminating v_s in the process, the system of Equations (3.39) to (3.44) was then rewritten in the form:

$$\frac{dz_f}{dt} = \frac{1}{\rho_i L \theta_{if}} \left[K_f \frac{T_f - T_s}{z_f - z_s} - Ku \frac{T_l - T_f}{\sqrt{\pi \mu t}} \right] \quad \ldots (3.45)$$

$$\frac{dH}{dt} = \frac{1}{\rho_i L (1 - \theta_{is})} \left[K_s \frac{T_s - T_c}{z_s + H} - K_f \frac{T_f - T_s}{z_f - z_s} \right] \quad \ldots (3.46)$$

$$u_s = \frac{P - B\sigma_{iw} T_s}{1 + A\sigma_{iw}} \quad \ldots (3.47)$$

$$\frac{dH}{dt} = \frac{k_s}{\rho_i g (1 - \theta_{is})} \left\{ \left[\frac{1}{z_w - z_f} + \frac{2}{z_f - z_s} \right] u_f - \frac{2u_s}{z_f - z_s} - \rho_w g \right\} \quad \ldots (3.48)$$

$$\frac{dH}{dt} = \frac{-[k_f]}{\rho_i g\, \theta_{if}} \frac{u_f}{z_w - z_f} \qquad \ldots (3.49)$$

At this stage, Holden found it advantageous to non-dimensionalise Equations (3.45) to (3.49) in order to make a further simplification. This was done using a length scale l_o, time t_o, temperature T_o, thermal conductivity K_o and pressure P. The following values were assigned to these quantities:

$l_o = 10^{-3}$m (1 mm)

$t_o = 10^2$ s

$K_o = 3\ Wm^{-1}\ °C^{-1}$

$T_o = 1°C$

$P = 150$ kPa

The effect of this non-dimensionalising was to show that if the heave rate is of the order $10^{-8}\ ms^{-1}$, as may be expected (Jones and Lomas, 1983), the non-dimensionalised term $u_f/(z_w-z_f)$ will be of the order 10^{-8}. This indicates that the first and third terms on the right-hand side of Equation (3.48) will have negligible influence on the heave rate, and (3.48) becomes:

$$\frac{dH}{dt} = \frac{k_s}{\rho_i g(1-\theta_{is})} \left[\frac{-2u_s}{z_f - z_s}\right] \qquad \ldots (3.50)$$

Equation (3.49) is now no longer required as it serves only to calculate u_f, which is insignificant.

The system of Equations (3.45), (3.46), (3.47) and (3.50) has the form:

$$\frac{dz_f}{dt} = A_1 T_s + B_1 \qquad \ldots (3.51)$$

$$\frac{dH}{dt} = A_2 T_s + B_2 \qquad \ldots (3.52)$$

$$u_s = A_3 T_s + B_3 \qquad \ldots (3.53)$$

$$\frac{dH}{dt} = E u_s \qquad \ldots (3.54)$$

By eliminating T_s and u_s from Equations (3.51) to (3.54), Holden reduced the system to a pair of ordinary differential equations of the form:

$$\frac{dz_f}{dt} = F(z_s, z_f, H, t) \qquad \ldots (3.55)$$

and:

$$\frac{dH}{dt} = G(z_s, z_f, H, t) \qquad \ldots (3.56)$$

where:

$$G = \frac{E(A_3 B_2 - A_2 B_3)}{EA_3 - A_2} \qquad \ldots (3.57)$$

and:

$$F = \frac{A_1 (G - EB_3)}{EA_3} + B_1 \qquad \ldots (3.58)$$

The problem was therefore reduced to the solution of the two coupled non-linear ordinary differential equations (3.55) and (3.56), where z_s is a stepwise constant in time. Holden solved the non-dimensional form of these equations using a standard fourth-order Runge-Kutta formula, and employed a simple search procedure to locate the maximum of the neutral stress in the frozen fringe. It was explained that during the formation of a lens, z_s remains fixed, and the lens

grows at this level until the maximum value of u_n below the lens reaches the overburden and a new lens is initiated. At this time, z_s is set equal to the position of the maximum of u_n for the new lens to form. Hence, z_s is a "stepwise" constant.

For the computations, constant values, intended only to be representative, were chosen for the following quantities: thermal conductivities K_s, K_f and K_u; hydraulic conductivity k_s; temperatures T_c, T_l and T_f; ice contents θ_{is} and θ_{if}. The computations were carried out for one value of the overburden only (P = 150 kPa) to evaluate the general performance of this approach. The results (for example, Figures 3.6 and 3.7) were found to be qualitatively reasonable. Allowing for the different geometries modelled (namely a semi-infinite as opposed to a finite soil column), Holden's results were of the same order as those of O'Neill and Miller (1980) and, equally well, the model was able to trace the formation and growth of each ice lens.

Holden therefore felt that there was considerable merit in this quasi-static approach. Not least of the benefits was the marked saving in computing effort. As O'Neill and Miller found, to solve the full set of partial differential equations for the heat and mass flow in the frozen fringe is difficult and computationally expensive. Adequate modelling of this very narrow region over which dramatic changes take place requires a very small mesh size and a correspondingly small time step. With the exception of the early stages of the simulation, during which a small time step was required to accommodate the frequent ice lenses, Holden used a time step appropriate

for the movement of the freezing front, and no "mesh" as such was necessary.

It was also argued that the simplified approach to the formulation of the equations would aid understanding of the rigid ice model and encourage a critical evaluation of the assumptions on which it is based. Finally, because the computer program Holden wrote was relatively short and inexpensive to run, parametric investigations could be performed readily. This would enable straightforward determination of the sensitivity of the heave to the various parameters, and hence their relative importance as elements of the theory.

Clearly then, as a model embodying the essential features of the rigid ice model in a mathematically and computationally simple framework, the quasi-static approach demonstrated sufficient potential to warrant further investigation. Holden (1983) in fact suggested a number of obvious refinements to improve the model immediately, thereby providing a platform from which to begin further development.

3.6 Conclusions

In this chapter, an account has been given of the theory of secondary frost heave, as conceived by Miller (1972, 1977, 1978), along with detail of its mathematical interpretation and attempts at numerical solution.

The model of O'Neill and Miller (1980, 1985), perhaps the most complete model of frost heave to date, has also been described. The model has been shown to be capable of predicting heave behaviour in a one-dimensional soil column, providing information such as heave as a function of overburden, and the time, location and thickness of each ice lens. The main disadvantage of the model is its mathematical complexity; the computations are time-consuming and susceptible to numerical problems, particularly when a "steady-state" solution is approached.

Against this background, Holden (1983) took the so-called rigid ice model and made a number of physically reasonable assumptions, in an attempt to simplify the modelling and reduce the computing effort required. This he achieved without loss of the predictive capability of the model. Holden, however, only went as far as testing the feasibility of his quasi-static approach and it was felt that further work on the model was warranted.

Hence, the development of Holden's model in the direction of greater realism, accuracy and flexibility is the subject of the following chapter.

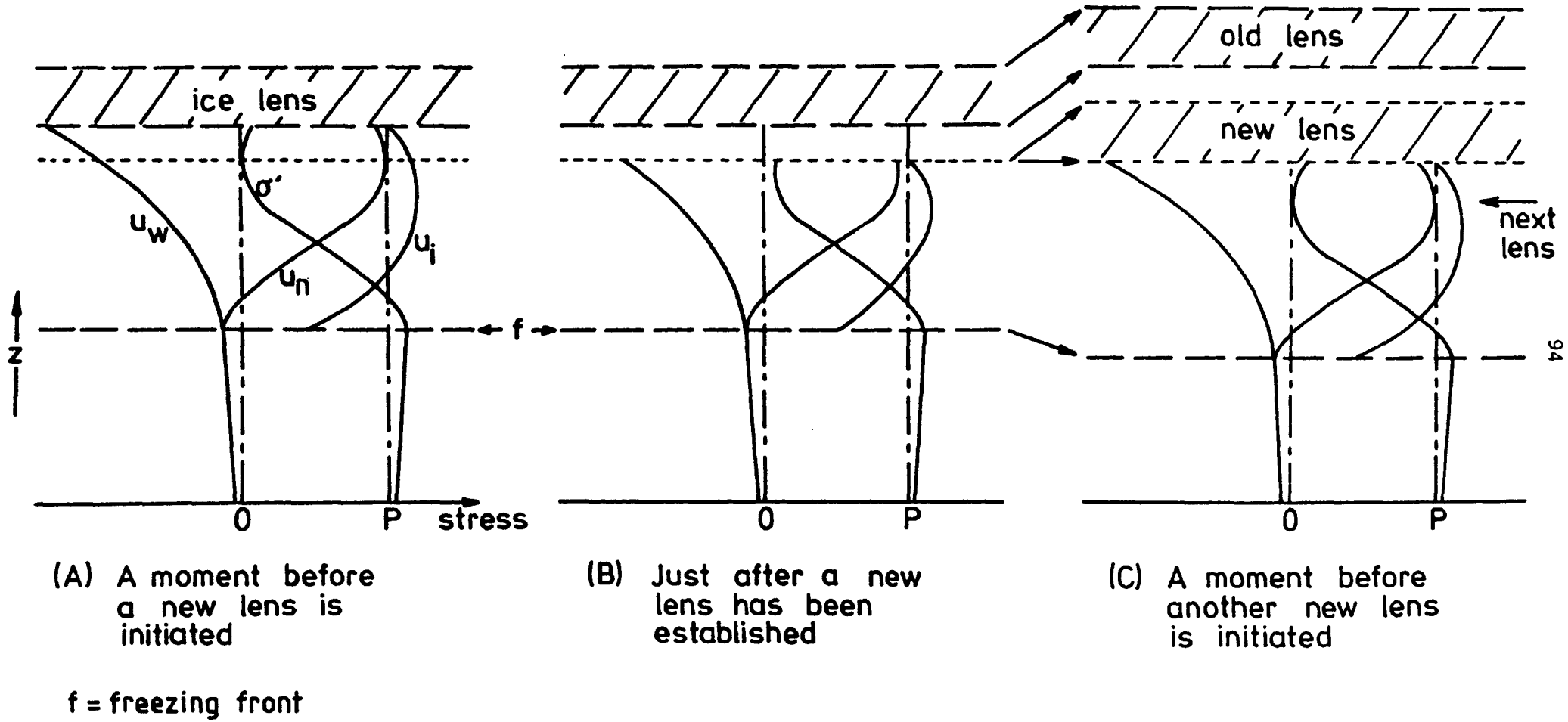

Figure 3.1 Stress profiles in a freezing soil (after Miller, 1978)

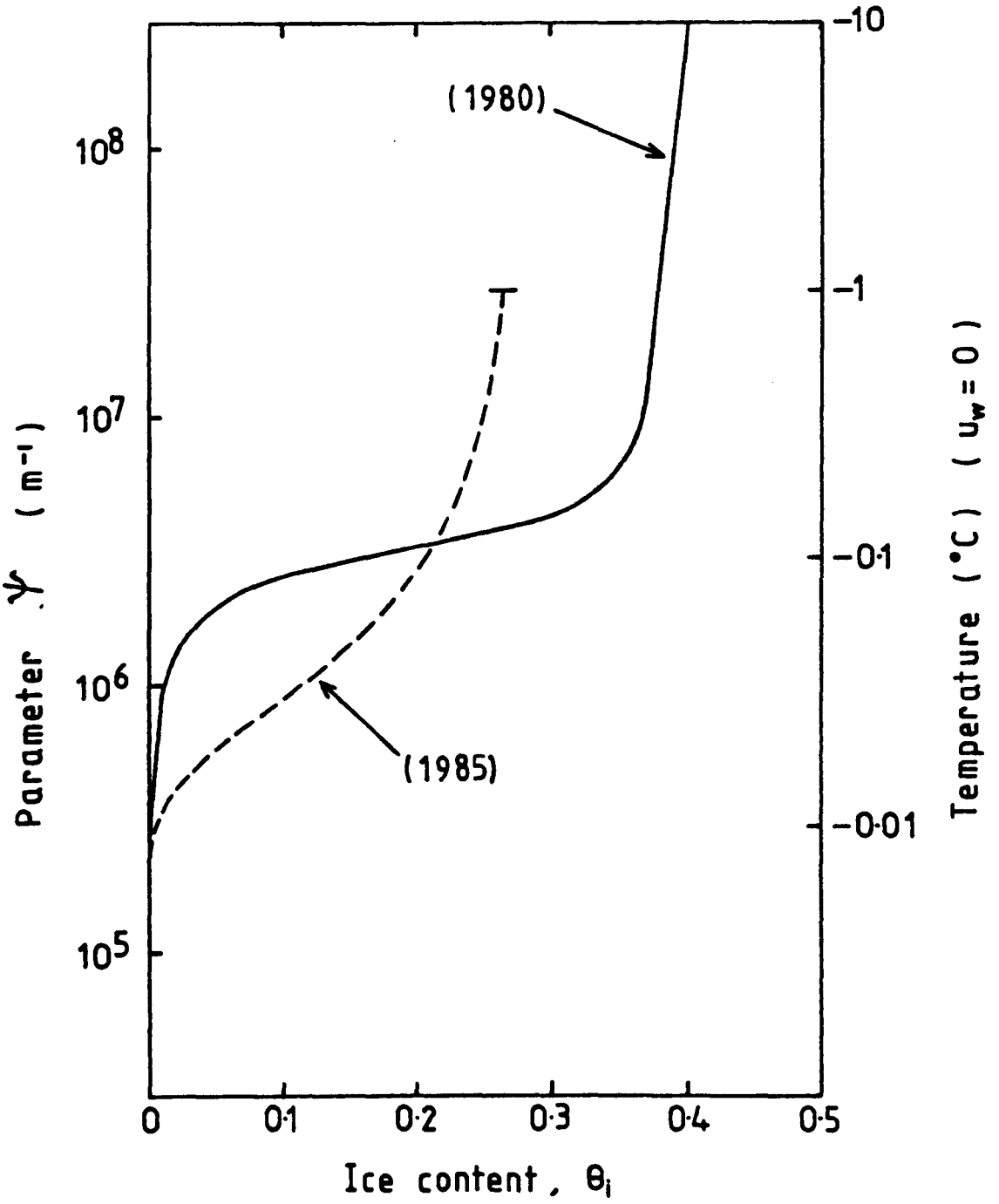

Figure 3.2 Ice content as a function of ψ, and of temperature when $u_w = 0$ (after O'Neill and Miller, 1980, 1985)

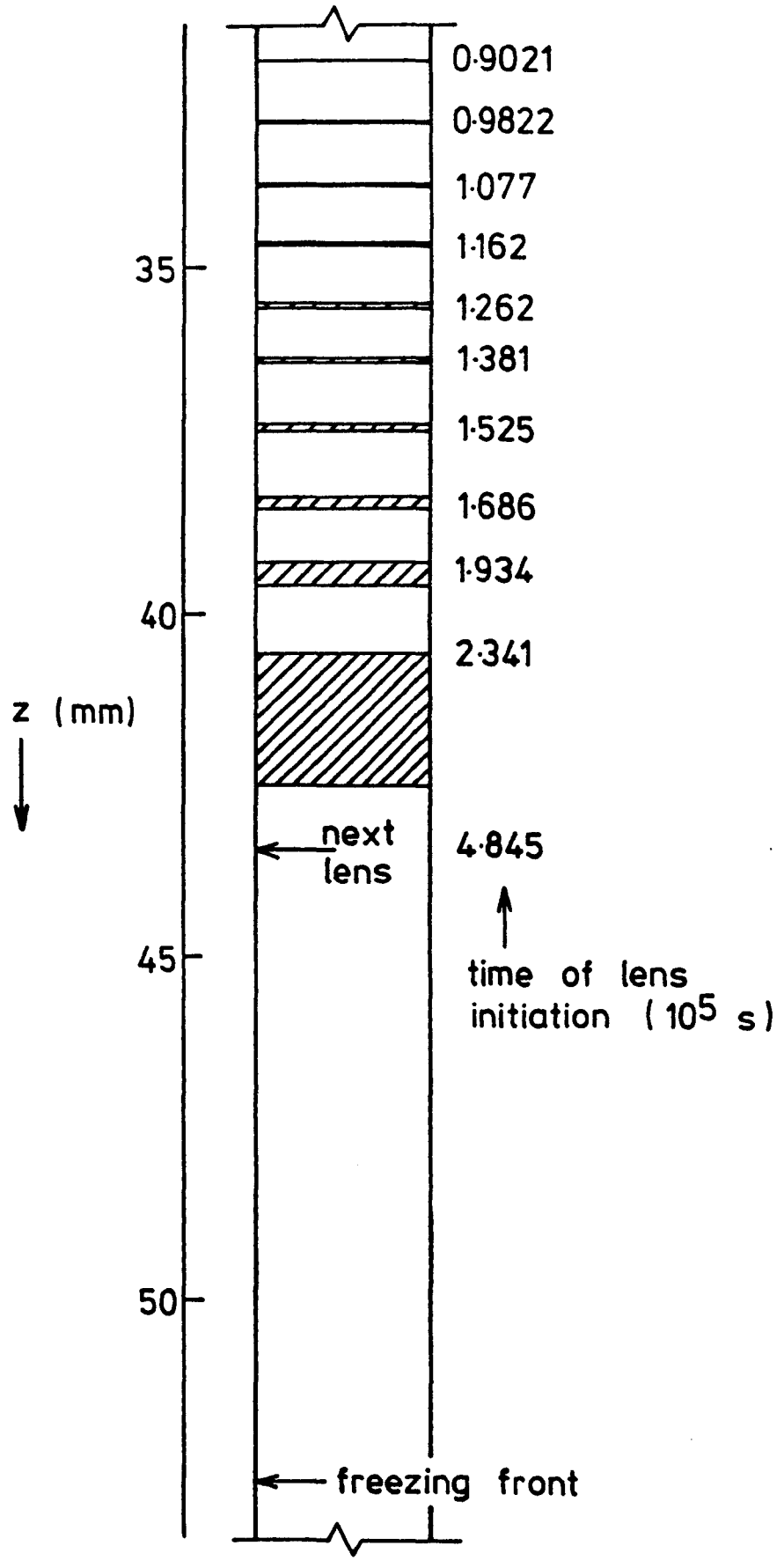

Figure 3.3 Location and thickness of ice lenses in a soil column, from a simulation of O'Neill and Miller (1980, 1985)

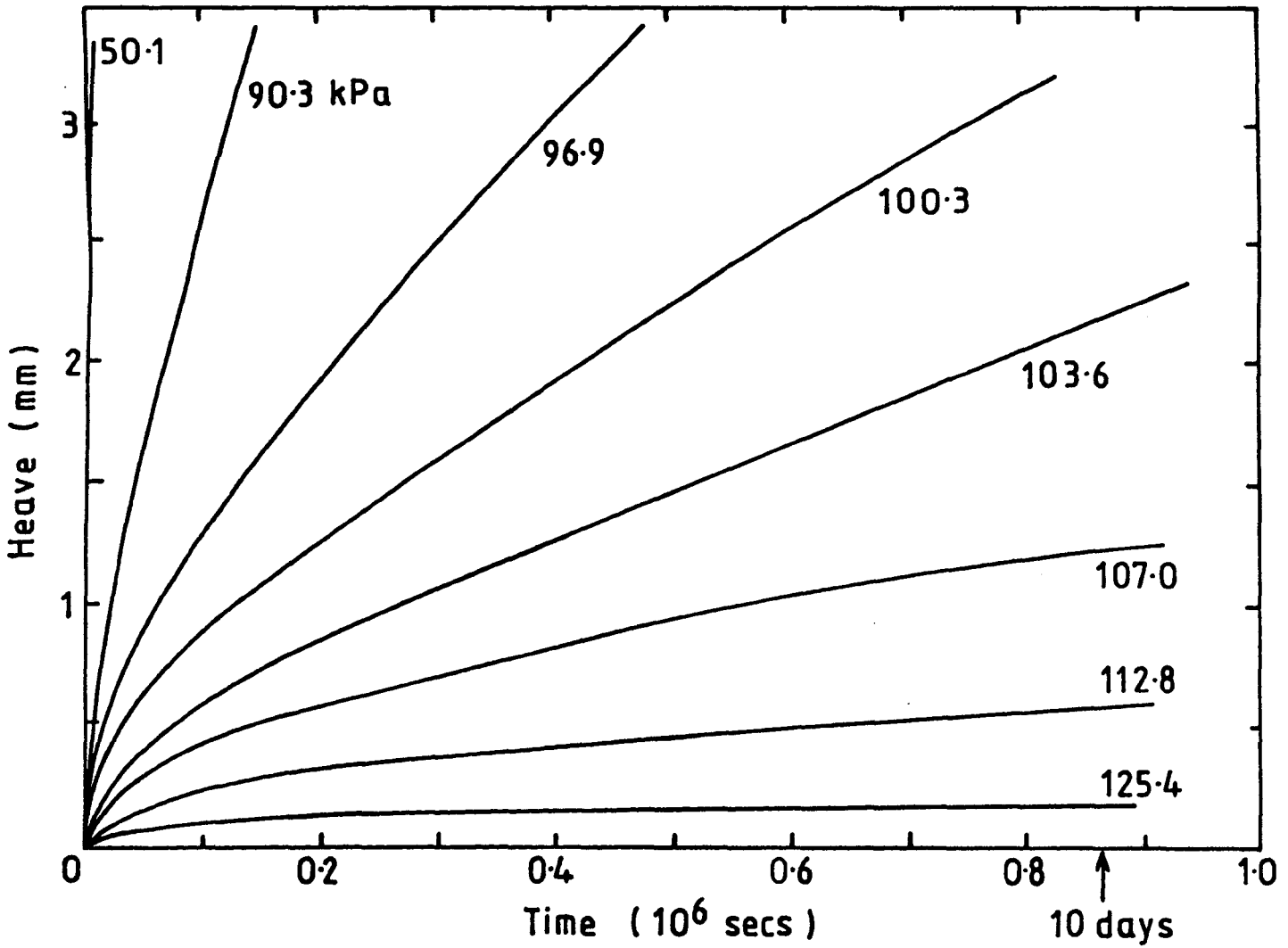

Figure 3.4 Heave versus time curves for different values of the overburden (after O'Neill and Miller, 1985)

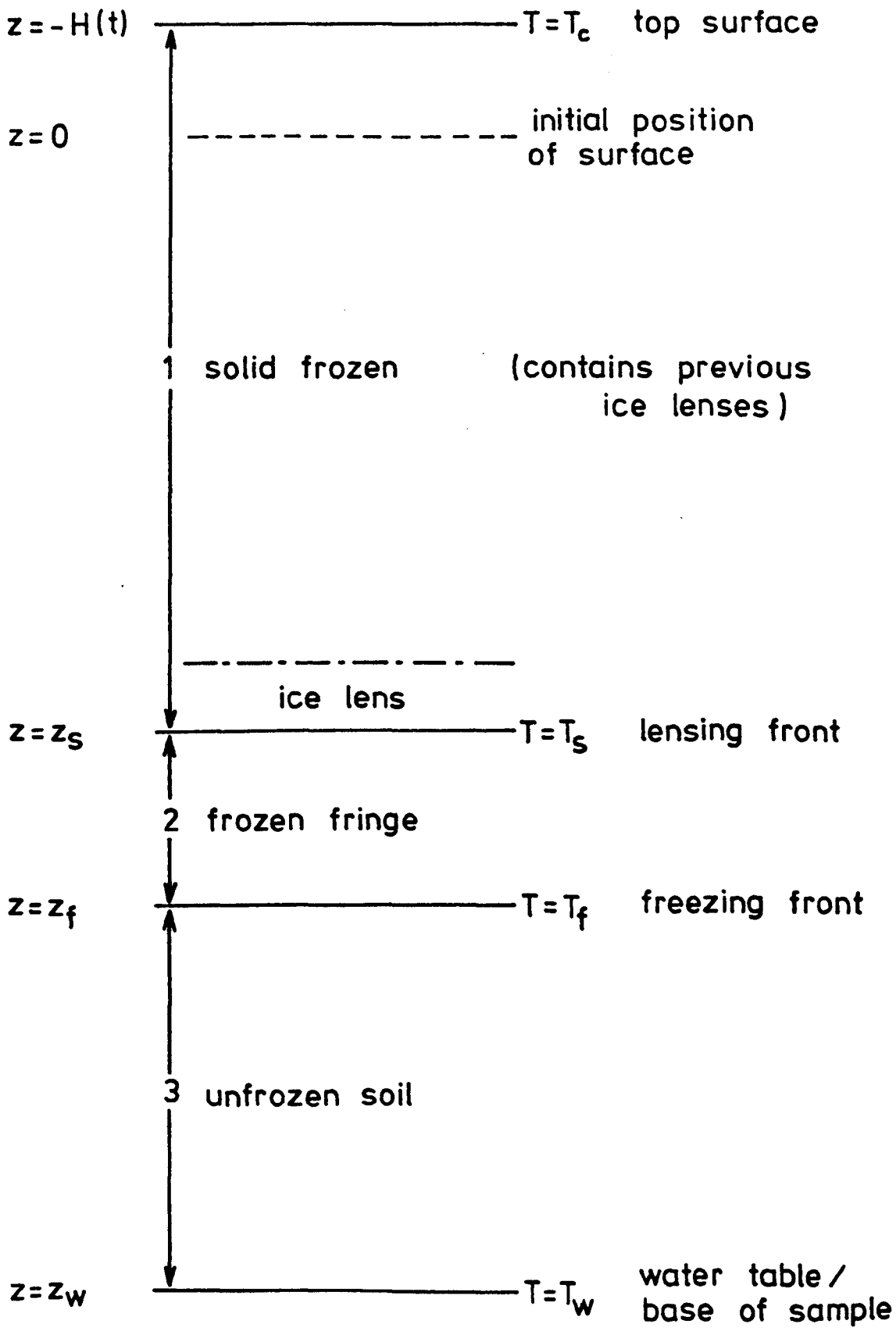

Figure 3.5 Schematic section through a freezing soil sample

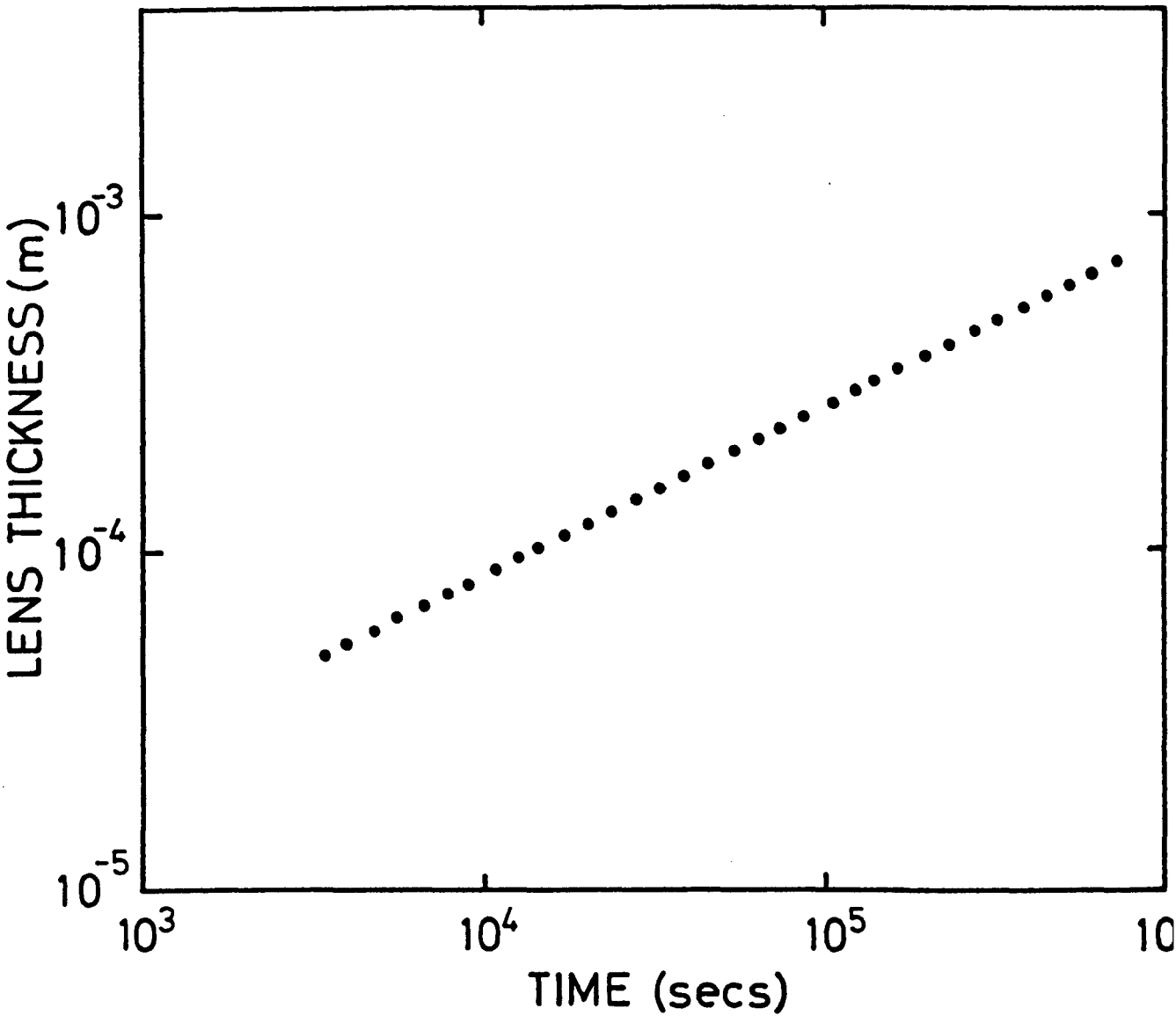

Figure 3.6 Lens thickness versus time (after Holden, 1983)

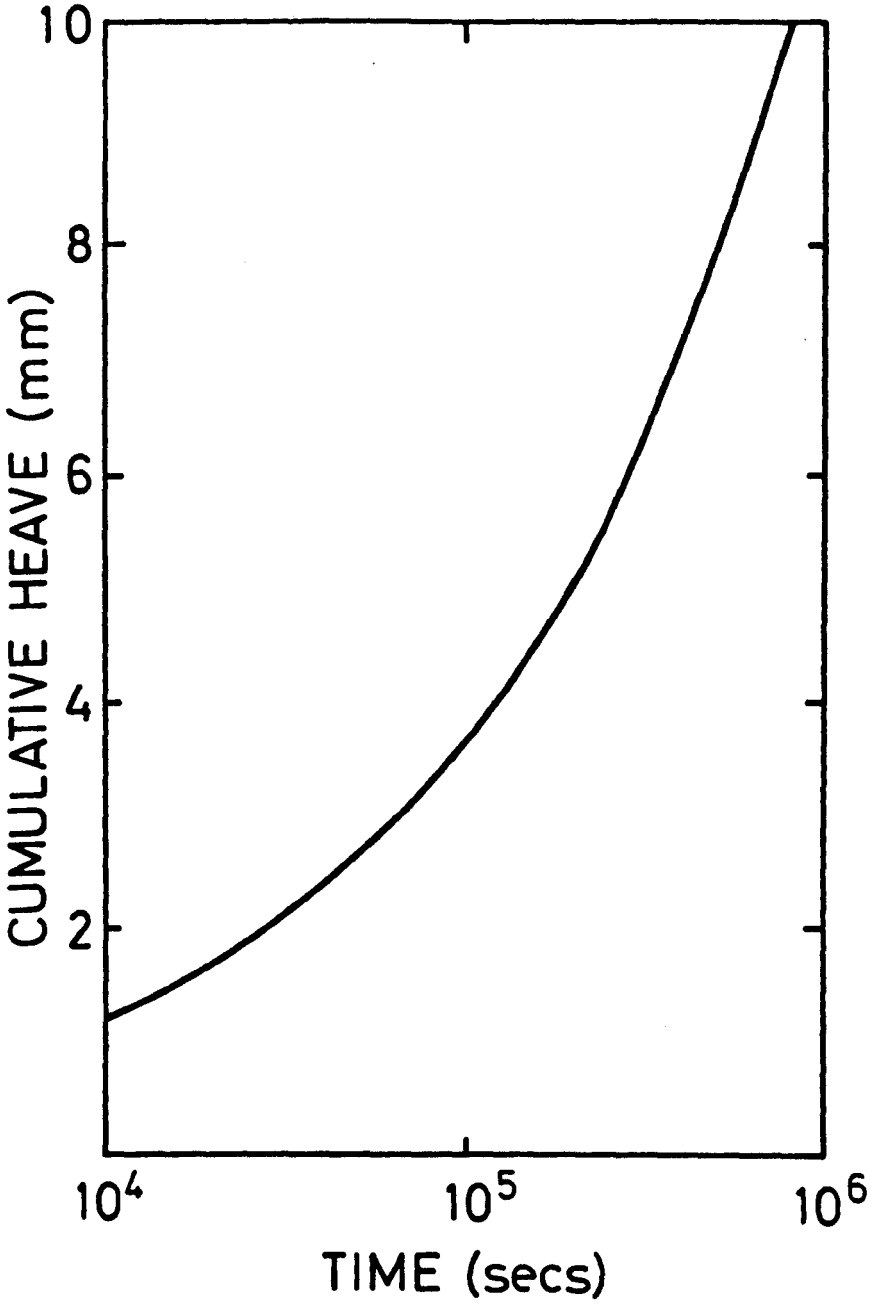

Figure 3.7 Cumulative heave versus time (after Holden, 1983)

CHAPTER 4

DEVELOPMENT OF A ONE-DIMENSIONAL MODEL FOR HEAVE AND ICE LENSING

4.1 Introduction

This chapter describes the development of a model for frost heave which uses Holden's (1983) approach as its basis. Holden's approximate solutions for Miller's theory of secondary heave were detailed in the previous chapter and their success provided the incentive to develop the model further. The primary aim was to produce a relatively simple model, and computer program, capable of simulating the mechanism and magnitude of frost heave in a soil column subjected to any applied temperature and pressure boundary conditions.

The first step was to adjust Holden's formulation so that a finite soil column could be modelled. This was considered necessary to allow comparison with laboratory freezing experiments, which would be important for the verification of the model. Such comparisons would also require the model to cope with any applied temperature boundary conditions, and to predict the initial cooling of a soil sample prior to freezing. Attention was therefore given to these aspects in the early stages of development.

Another critical area in frost heave modelling is the effect of

variations in overburden pressure. Whereas Holden dealt only with one value of the overburden, it was felt that the model would only gain credibility if it was able to simulate the behaviour of the soil under a range of overburden pressures, and, in particular, under zero overburden, when the soil self-weight plays a major role. Much effort was devoted to producing a model with this capability.

Finally, improvement in the representation of certain parameters was sought. Holden had assumed constant values for key parameters in order to test the feasibility of his approach. However, greater variability was now essential to permit parametric studies to establish the relative importance of the parameters.

All these developments were carried out in the context of the overall objective of mathematical and computational simplicity. Thus, whilst some increase in complexity has been inevitable, the final model described towards the end of this chapter still retains the basic elements of Holden's quasi-static approach.

In the following sections, the changes made to Holden's original model are presented in detail and, for the most part, these are given in chronological order. This strategy was adopted because the model indeed evolved over a period of time, and a chronological account provides greater insight into how the final model was attained. The intermediate stages of development are therefore included and it should be emphasised that certain parts of the model were updated on more than one occasion. Hence, for clarity, a statement of the final model is given in Section 4.9.

Since this chapter concentrates largely on the evolution of the model, the results of computer simulations and parametric investigations based on the final model are the subject of Chapter 5.

4.2 Modelling a Finite Soil Column

The reader's attention is drawn to the idealisation of a freezing soil sample given in Figure 3.5 of the previous chapter, which is used again here. For a finite column of soil, the level $z = z_w$ refers to the base of the column as well as the level of the water table.

Holden (1983) considered only a semi-infinite column of soil and, in anticipation of comparison of computer predictions with the results of laboratory experiments, it was necessary to adapt the model to cope with a finite soil sample. This involved reassessment of the temperature profile ahead of the freezing front. Holden used an error function approximation for the temperature in this region, but this is inappropriate for a finite sample and an alternative approach had to be found.

The temperature profile in the unfrozen region is required primarily to calculate the temperature gradient just ahead of the freezing front. This information is needed for the energy balance equation at the freezing front $z = z_f$, which is, recalling (3.38):

$$K_u \frac{\partial T}{\partial z}\bigg|_{z_f^+} - K_f \frac{\partial T}{\partial z}\bigg|_{z_f^-} = -\rho_i L \theta_{if} \frac{dz_f}{dt} \qquad \ldots (4.1)$$

The temperature gradient just behind the freezing front ($z = z_f^-$) is provided by the linear profile approximation in the frozen fringe, but for the finite sample it was decided not to use an approximating profile in the unfrozen region. Instead, the temperature profile was computed by solving the one-dimensional heat equation:

$$\frac{\partial T}{\partial t} = \mu \frac{\partial^2 T}{\partial z^2} \qquad \ldots (4.2)$$

where: μ is the thermal diffusivity, as before.

The solution of (4.2) was achieved using a Crank-Nicolson finite difference approximation, based on a convected finite difference mesh. That is, a fixed number of mesh points was defined in the unfrozen region so that, as the freezing front advances and the length of the unfrozen region decreases, accordingly the finite difference mesh contracts. This solution technique followed that of Murray and Landis (1959) and is described in detail in Appendix C.

The method used to calculate the temperature gradient just ahead of the freezing front was also adapted from Murray and Landis (1959). A parabola was fitted through the first three mesh points and an expression for the slope of the parabola at $z = z_f$ was obtained. Hence:

$$\left.\frac{\partial T}{\partial z}\right|_{z_f^+} = \frac{4T_{1,j} - T_{2,j} - 3T_f}{2\delta z_j} \qquad \ldots (4.3)$$

where: δz_j = mesh point spacing at j^{th} time step, and

$T_{i,j}$ = temperature (j^{th} time step) at point ($z_f + i\delta z_j$)

The derivation of Equation (4.3) is also given in Appendix C.

In practice, the temperature at the base of the sample is held constant at the initial temperature ($T_1 > 0$), and the unfrozen region temperature profile is evaluated at each time step. Equation (4.3) is then used to calculate the temperature gradient ahead of the freezing front and this is substituted into (4.1). This allows the system of equations to be solved as before and the new position of the front to be found. In other words, Holden's original solution procedure in essence remained unchanged. Indeed, by confining the calculation of the unfrozen region temperature profile to a separate subroutine in the computer program, the need for other programming changes was minimal.

Having made the alterations necessary for the modelling of a finite column of soil, further modifications were needed to permit more accurate representation of laboratory temperature boundary conditions, and these are described in the next section.

4.3 Represention of Laboratory Freezing Conditions

In his simulations, Holden (1983) applied a step freezing condition to the surface of his soil column, that is, at zero time, the surface temperature was stepped down to a sub-zero temperature and then held

fixed. This condition is, of course, very easily written into a computer program but does not adequately reproduce the environment normally found in freezing experiments or in nature.

In the laboratory, a sample, initially at a uniform temperature throughout, has its surface cooled at some finite rate, whilst the base of the sample is held at the initial temperature by means of, say, circulating fluid. Upon reaching the desired sub-zero value, the surface temperature is then usually kept constant for the duration of the experiment. Under these conditions, when freezing is initiated in a soil sample, the temperature profile in the sample is not only non-uniform, but probably also non-linear and this may have an effect on the rate of freezing, particularly in the early stages.

It was therefore decided to build into the model the capability to predict the effect of any cooling "curve" applied at the surface of the sample. This meant generalising the application of thermal conditions so that either temperatures or heat fluxes could be specified at the surface. The resulting temperature profile in the soil was computed simultaneously.

Once again, the favoured approach was that of solving the one-dimensional heat equation (4.2), subject to a fixed temperature at the base of the sample and a varying condition at the surface. Crank-Nicolson finite differences were used to approximate the derivatives in (4.2), producing a system of equations of the form:

$$\underset{\sim}{A}\ \underset{\sim}{T}_{j+1} = \underset{\sim}{B}_j \qquad \ldots (4.4)$$

where: $\underset{\sim}{T}_{j+1}$ = vector of unknown temperatures at $(j+1)^{th}$ time step

$\underset{\sim}{B}_j$ = vector of known quantities from previous (j^{th}) time step

$\underset{\sim}{A}$ = matrix of coefficients

Further details of the solution are not given here, since the procedure is essentially similar to that described in Appendix C. The problem is simpler on this occasion because the finite difference mesh is fixed. The result is that matrix $\underset{\sim}{A}$ in (4.4) is both tri-diagonal and symmetric, and the system is easily solved using standard Gaussian elimination and back substitution.

This modelling of the initial cooling of the soil was appended to the program as a separate subroutine, in the same way as the unfrozen region temperature profile calculation. Generally, a simple ramped temperature decrease was applied (see Chapter 5), that is a linear decrease of temperature with time down to the desired value. However, any form of cooling curve can be handled without difficulty, or, if preferred, the heat flux at the surface can be specified via a simple modification.

The temperature profile in the cooling sample is computed at specified time intervals until freezing begins at the surface. This is detected when the surface temperature drops marginally below 0°C. At this instant, the temperature profile is transferred into the main segment of the program and becomes the first unfrozen region temperature profile.

Hence, at this stage, Holden's basic solution strategy has remained largely unaltered, whilst the program has become equipped to model the temperature conditions typically imposed in the laboratory freezing of soil samples.

4.4 Improvement in Parameter Representation

Among the refinements that Holden (1983) suggested could be made to the model, was an improvement in the representation of certain parameters, notably ice content and hydraulic conductivity. Holden used constants for the hydraulic conductivity at the top of the frozen fringe, k_s, and for ice content at both top and bottom of the fringe, θ_{is} and θ_{if} respectively. The values he chose were apparently reasonable, in view of the magnitude of the results. Nevertheless, it was desirable to allow these quantities to vary with the suction parameter ψ to achieve greater generality.

The implementation of these changes was in fact prompted by a study of the behaviour of the model under varying overburden pressures. This revealed a serious flaw in prescribing a constant value for k_s, which Holden had inevitably failed to detect because he considered only one value of the overburden. The study showed that above a certain value of the overburden pressure, the amount of frost heave increased with increasing overburden, contrary to all experimental evidence, and indeed common sense.

Fortunately, the anomaly was easily explained. Under an increased

overburden, ice pressure and therefore ice content, would be expected to increase at the top of the frozen fringe, implying a corresponding decrease in permeability there. Thus, with a fixed value of the permeability, k_s, a point was obviously reached beyond which the chosen value was unrealistically high, producing unreasonably high heaves.

Clearly, the hydraulic conductivity needed to be expressed as some function of ice content, and the relationship used by O'Neill and Miller (1980, 1985) was adopted here, viz:

$$k(\theta_i) = k(0)\ (1 - \frac{\theta_i}{\theta_o})^m \qquad \ldots (4.5)$$

where: θ_o = porosity (taken to be 0.4).
The exponent m was initially taken to be 7, after O'Neill and Miller (1980), but subsequently a value of m = 9 was used (O'Neill and Miller, 1985). Details of parametric studies on (4.5) are contained in Chapter 5.

In addition, calculation of the ice content as a function of ψ was necessary, not only for (4.5) but also to provide reliable values at the top and bottom of the frozen fringe. Ironically, this operation was already part of the program, since $\theta_i(\psi)$ had to be calculated throughout the fringe in order to evaluate the stress partition function, $\chi(\theta_i)$, and hence the neutral stress, u_n.

The above changes were therefore introduced into the model in a

straightforward manner. In the process, a minor alteration was made to the formula for computing the ice content. Holden had expressed O'Neill and Miller's (1980) experimental curve of θ_i versus ψ partly by a hyperbola and partly by a parabola (Chapter 3, Equation (3.36)). However, checks had revealed that the parabolic portion was inaccurate and, although in practice this is not the most important half of the formula, the error was accordingly corrected.

Whilst not a problem of parametric representation, a further improvement was made in the program's rigour at this stage and is included here for convenience. It concerns the numerical algorithm for locating the position of the maximum of the neutral stress in the frozen fringe, a crucial step in the lens initiation procedure. Holden had used a simple search method employing divided differences, which was based on finding a stationary point rather than a strict maximum. Normally, the correct location was found without difficulty, but occasionally the freezing front was returned as the required position, as the routine searched for the minimum value of the neutral stress. Thus, to optimise the reliability of this part of the program, an alternative algorithm was chosen which proceeds as follows: the frozen fringe is divided into ten step lengths:

$$dz = \frac{z_f - z_s}{10} \qquad \ldots (4.6)$$

and, starting at z_s, the neutral stress, u_n, is evaluated at successive points $z_0 = z_s$, $z_1 = z_0 + dz$, $z_2 = z_1 + dz$ etc. Each value of u_n is compared with the previous one until u_n at z_{r+1} is found to be less

than u_n at z_r, that is when the maximum has just been passed. The maximum is then known to lie in the range (z_{r-1}, z_{r+1}), length 2dz. The test is then restarted within this range with a reduced step size of dz/10. This procedure is repeated until the position of the maximum of u_n is located, within the required tolerance limits. Both the position and value of the maximum are passed (via a common block) back to the main segment of the program, for testing against the lens initiation criterion.

4.5 Modelling the Water Pressure

As explained in Chapter 3, part of Holden's quasi-static approach was to use an approximating profile to describe the water pressure in the frozen fringe. This profile did not prescribe a priori values to the water pressure, but determined the shape of the profile in the frozen fringe once the values at the top and bottom of the fringe had been calculated by the model. To illustrate the method, Holden (1983) chose a quadratic profile, but pointed out that other choices were possible.

In practice, Holden needed only to calculate the water pressure at the top of the frozen fringe, u_s. Non-dimensionalisation of the governing equations had inferred that the value at the freezing front, u_f, was negligibly small. As a result, Holden was able to ignore the mass balance equation at the freezing front (Equation (3.49)) with the effect that u_f was taken to be zero.

For the sake of completeness, it was decided to re-introduce the mass balance equation at z_f in order to allow a more precise assessment of the magnitude and hence significance of u_f. This decision was also prompted by the fact that Holden had omitted the gravity term from his equation. With the gravity term, the mass balance becomes:

$$\rho_i \theta_{if} \frac{dH}{dt} = -\left[\frac{k_f}{g}\right]\left(\frac{u_f}{z_w - z_f} + \rho_w g\right) \qquad \ldots (4.7)$$

(cf. Equation (3.49)), which can be written in the form:

$$\frac{dH}{dt} = C_2 u_f + B_5 \qquad \ldots (4.8)$$

In addition to Equation (4.8), an alternative approximating profile for the water pressure in the frozen fringe was incorporated into the model at this time. To some extent, this was done simply to see what effect a different profile would have on the overall behaviour. However, the results of O'Neill and Miller (1980, 1985) had suggested that a quadratic profile might not be appropriate, and instead a quartic approximation was chosen. Thus, the water pressure was defined as:

$$u_w = \left[(z_w - z) - \frac{(z_f - z)^4}{(z_f - z_s)^3}\right] \frac{u_f}{z_w - z_f} + \left(\frac{z_f - z}{z_f - z_s}\right)^4 (u_s - u_f), \qquad z_s < z < z_f$$

$$u_w = \frac{z_w - z}{z_w - z_f} u_f \qquad z_f < z < z_w \qquad \ldots (4.9)$$

Continuity of the water pressure gradient at the freezing front, z_f, was still assumed, and the water flux at the top of the frozen fringe became:

$$v_s = \frac{-k_s}{\rho_w g}\left[\left(\frac{3}{z_w - z_f} + \frac{4}{z_f - z_s}\right) u_f - \frac{4u_s}{z_f - z_s} - \rho_w g\right] \qquad \ldots (4.10)$$

The above changes of course meant the introduction of another equation and another unknown (u_f) into the model. Nevertheless, the solution procedure remained the same, as follows: the system of equations (now five) was written:

$$\frac{dz_f}{dt} = A_1 T_s + B_1 \qquad \ldots (4.11)$$

$$\frac{dH}{dt} = A_2 T_s + B_2 \qquad \ldots (4.12)$$

$$u_s = A_3 T_s + B_3 \qquad \ldots (4.13)$$

$$\frac{dH}{dt} = E u_s + C_1 u_f + B_4 \qquad \ldots (4.14)$$

$$\frac{dH}{dt} = C_2 u_f + B_5 \qquad \ldots (4.15)$$

As before, elimination between (4.11) to (4.15) led to the two ordinary differential equations:

$$\frac{dz_f}{dt} = F \qquad \ldots (4.16)$$

and:

$$\frac{dH}{dt} = G \qquad \ldots (4.17)$$

where now:

$$G = \frac{E(A_2B_3 - A_3B_2) + A_2B_4 - C_1/C_2\ A_2B_5}{A_2(1 - C_1/C_2) - EA_3} \qquad \ldots (4.18)$$

and:

$$F = \frac{A_1}{A_2}(G - B_2) + B_1 \qquad \ldots (4.19)$$

Hence, computational simplicity was retained whilst augmenting the model's overall capability and accuracy.

4.6 Ice Content in the Frozen Fringe

Simulations performed at this stage in the development of the model produced qualitatively good predictions for relatively high overburden pressures, which would have been encouraging were it not for the problems experienced at lower overburdens. For no apparent reason, attempts to compute the behaviour below say 125 kPa yielded unrealistically, and indeed unreasonably, high values for the heave (Piper and Holden, 1984). Even reducing the value of the saturated unfrozen permeability (k(o) in Equation (4.5)), to a level which would in practice have eliminated the heave, served only to lower the overburden threshold below which the "instability" remained.

In an effort to locate the source of the difficulty, thorough checks of all areas of the model and, in particular, the computer program, were carried out. After some considerable time, the problem was traced to the representation of ice content as a function of the suction parameter ψ, which is used to calculate ice content in the frozen fringe. It became clear that the curve given by O'Neill and Miller (1980), and formulated algebraically in the current model, was unrepresentative of real soil behaviour. Comparison with suction-water content curves for a number of soils (Thompson, 1981) highlighted the anomaly.

(Koopmans and Miller (1966) demonstrated the similarity between water content versus suction curves, the "soil water characteristic", and ice content versus ψ curves, the "soil freezing characteristic". The two are related through the equation:

$$u_a - u_w = \frac{\sigma_{aw}}{\sigma_{iw}} (u_i - u_w) \qquad \ldots (4.20)$$

for appropriate soil types and saturation conditions. See also Chapter 3, Section 3.3.)

O'Neill and Miller (1980) and Holden (1983) considered only one (relatively high) value of the overburden and understandably failed to detect such behaviour. In any case, Holden imposed constant values for the ice content at the top and bottom of the frozen fringe, which would have effectively suppressed any potential problem in this area. It was then discovered that later, when evaluating their model over

a range of overburden pressures, O'Neill and Miller (1985) had used a θ_i versus ψ relationship substantially different to their previous one. The two curves are shown together in Chapter 3, Figure 3.2. No explanation was given for the change, but it seems reasonable to suppose that O'Neill and Miller experienced difficulties similar to those described above.

To rectify the situation, a more realistic expression for the ice content as a function of ψ was used. This was derived from the data of Thompson (1981) for Attenborough silt. For the purposes of the model, a bilinear approximation to the experimental data was made, based on linear regression. This produced the following relations for the determination of the ice content:

$$\theta_i = 0.1179\ (\log_{10} \psi) - 0.5583, \quad \psi < 4.25 \times 10^7$$

$$\theta_i = 0.0198\ (\log_{10} \psi) + 0.19, \quad \psi \geq 4.25 \times 10^7 \quad \ldots (4.21)$$

Thompson's (1981) data, together with the straight line fits to it, are given in Figure 4.1.

As expected, the introduction of (4.21) into the model removed the "instability" and allowed the heave to be successfully computed for overburden pressures down to around 5 kPa. Curves of heave against overburden were now qualitatively reasonable, as illustrated in Figure 4.2.

This marked an important point in the development of the model. Having

adapted Holden's original formulation to cope with laboratory freezing conditions, and eliminated the inconsistencies which subsequently arose, the model as it now stood was presented in the Proceedings of the Fourth International Symposium on Ground Freezing (Holden et al, 1985). Further developments however were still necessary to improve the quantitative accuracy of the model, and these are now described.

4.7 The Water Pressure Profile

The curves of Figure 4.2 demonstrate that whilst the model produced qualitatively reasonable results, the magnitude of the predicted heave was still higher than expected, especially at lower overburden pressures. Since the amount of frost heave is dependent on the water flux to the ice lens, it was decided to re-examine the mass balance equations and the validity of the water pressure profile approximation in the frozen fringe, in an attempt to establish the cause of the overestimated heave.

The mass balance at the top of the frozen fringe ($z = z_s$) is, recalling Equation (3.41):

$$\rho_i(1 - \theta_{is}) \frac{dH}{dt} = -\rho_w v_s \qquad \ldots (4.22)$$

whilst at the freezing front, the mass balance was updated earlier (Equation (4.7)) to:

$$\rho_i \theta_{if} \frac{dH}{dt} = -[k_f] \left(\frac{u_f}{z_w - z_f} + \rho_w g\right) \quad \ldots (4.7)$$

It was found that from a simple analysis of these two equations (given below), an expression for the ratio v_s/v_w could be derived, providing an estimate of the relative magnitudes of the two quantities.

According to Darcy's Law, the water flux just ahead of the freezing front, v_w, is given by:

$$v_w = \frac{-k(o)}{\rho_w g} \left(\frac{-u_f}{z_w - z_f} - \rho_w g\right) \quad \ldots (4.23)$$

where k(o) is the hydraulic conductivity of the saturated unfrozen region, and the pressure gradient is obtained from (4.9). Equation (4.7) can therefore be rewritten as:

$$\rho_i \theta_{if} \frac{dH}{dt} = -[k_f] \frac{\rho_w v_w}{k(o)} \quad \ldots (4.24)$$

Eliminating dH/dt between (4.24) and (4.22) yields:

$$\frac{\theta_{if} v_s}{1-\theta_{is}} = [k_f] \frac{v_w}{k(o)} \quad \ldots (4.25)$$

Now: $[k_f] = k_{f+} - k_{f-}$

$$= k(o) - k(o) \left(1 - \frac{\theta_{if}}{\theta_o}\right)^m \quad \ldots (4.26)$$

according to (4.5). Hence, (4.25) can now be written:

$$\frac{v_s}{v_w} = \frac{1-\theta_{is}}{\theta_{if}} \left[1 - \left(1 - \frac{\theta_{if}}{\theta_o}\right)^m\right] \quad \ldots (4.27)$$

For integer m, the minimum (non-zero) value of the term in square brackets is given by m = 1, so that:

$$\frac{v_s}{v_w} > \frac{1 - \theta_{is}}{\theta_o} \quad \ldots (4.28)$$

and, in the extreme case of $\theta_{is} = \theta_o = 0.4$:

$$\frac{v_s}{v_w} > 1.5 \quad \ldots (4.29)$$

Alternatively, using typical values of m = 7, $\theta_{is} = 0.3$ and $\theta_{if} = 0.1$ in (4.27) leads to:

$$\frac{v_s}{v_w} \simeq 6.0 \quad \ldots (4.30)$$

In practice of course, neither (4.30) nor (4.29) can be true, and an inconsistency evidently existed in the mass balance equations (4.7) and (4.22). One of the assumptions made in formulating both (4.7) and the water pressure profile in the frozen fringe was that the water pressure gradient was continuous at the freezing front. It now appeared that this assumption was too "strong" and might be responsible for artificially forcing too much water to the ice lens.

Without the gradient continuity assumption, an alternative means of determining the water pressure profile in the frozen fringe was

required. One option that was considered was to calculate the water pressure by imposing a pointwise steady state continuity within the frozen fringe using:

$$\nabla \cdot v = 0 \qquad \ldots (4.31)$$

where v is the water flux. However, even if the steady state assumption had been sufficiently accurate, it was felt that the amount of extra calculation necessary to incorporate this into the program would have seriously compromised one of the overall aims of the model, namely that of computational simplicity.

Therefore the preferred approach was still to use an approximating profile. Since the water pressure was known to decay more or less exponentially in the frozen fringe (Miller, 1977), an exponential profile was chosen, as follows:

$$u_w = A + Be^{-\alpha(z-z_s)} \qquad \alpha > 0 \qquad \ldots (4.32)$$

The constants A and B are easily found as $u_w = u_s$ at $z = z_s$ and $u_w = u_f$ at $z = z_f$, so that:

$$A = \frac{u_f - u_s e^{-\alpha(z_f - z_s)}}{1 - e^{-\alpha(z_f - z_s)}} \qquad \ldots (4.33)$$

and:

$$B = \frac{u_s - u_f}{1 - e^{-\alpha(z_f - z_s)}}$$

The exponent α has dimensions of the reciprocal of length.

The water pressure profile in the unfrozen region remained as defined in (4.9), but the assumption that the pressure gradient was continuous at the freezing front was now removed. From (4.32), the gradients at the top and bottom of the frozen fringe were now respectively:

$$\left.\frac{du_w}{dz}\right|_{z=z_s} = -\alpha B$$

and:
$$\left.\frac{du_w}{dz}\right|_{z=z_f} = -\alpha B\, e^{-\alpha(z_f-z_s)} \qquad \ldots (4.34)$$

Clearly, the exponent α in (4.32) represented a new unknown in the system of equations and this aspect is dealt with shortly.

The choice of a new water pressure profile also meant reformulation of the mass balance equation at the freezing front, and whilst this was being done it was found that the equation in its present form had a term missing from it. The equation (4.7) had previously been based on the simple balance:

$$\rho_i \theta_{if} \frac{dH}{dt} = \rho_w (v_f - v_w) \qquad \ldots (4.35)$$

where v_f is the water flux just behind the freezing front and, as before, v_w is the water flux ahead of the freezing front. Equation (4.35) however omitted the term accounting for the advancing freezing front. As the freezing front progresses, a small amount of water (θ_{if}) freezes and, due to the volume expansion, this affects the

mass balance. The correct equation is therefore written:

$$\rho_i \, \theta_{if} \frac{dH}{dt} = \rho_w(v_f - v_w) + (\rho_w - \rho_i) \, \theta_{if} \frac{dz_f}{dt} \qquad \ldots (4.36)$$

Using Darcy's law for the water flux terms, and (4.34) for the new water pressure gradient just behind the freezing front, (4.36) can be expressed in the form:

$$\frac{dH}{dt} = E_2 u_s + C_2 u_f + E_3 \frac{dz_f}{dt} + B_5 \qquad \ldots (4.37)$$

which replaces (4.15).

Of the two "final" ordinary differential equations (4.16) and (4.17), the right-hand side of one, given in (4.18), has of course to be amended with the introduction of (4.37). That apart, the solution procedure remained the same and the new water pressure profile in the frozen fringe (4.32) merely replaced the old one.

The problem remained of how to handle the exponent α. This new unknown, which ultimately determined the precise form of the water pressure profile, had been introduced into the model without the introduction of another equation or condition which would allow its evaluation.

At this stage therefore it had to be specified a priori. Of course, this made it possible to select an appropriate value for α, for a given overburden, which yielded accurate results in terms of the

magnitude of the predicted heave etc. However, it could then have been argued that this was a means of "tuning" the predictions to the experimental data, without proper physical motivation.

The next section describes how this obstacle was overcome.

4.8 Conservation of Mass Across the Frozen Fringe

Although an approximating profile was being used for the water pressure in the frozen fringe, it was realised that it should nevertheless satisfy conservation of mass. It was therefore felt that if an equation governing mass continuity over the entire frozen fringe could be written down, as opposed to just mass balances at the boundaries, then this would provide physical justification for the value of the exponent α in the water pressure profile.

Proceeding along these lines, a "control" volume which spanned the frozen fringe was considered, as shown in Figure 4.3.

The total mass M of water and ice (per unit area) within the control volume is given by:

$$M = \int_{z_o}^{z_s} \rho_i \, dz + \int_{z_s}^{z_f(t)} (\rho_i \theta_i + \rho_w \theta_w) \, dz$$

$$+ \int_{z_f(t)}^{z_1} \rho_w \theta_o \, dz \qquad \ldots (4.38)$$

By the conservation of mass law, the rate of change of M is equal to the rate at which mass enters the region. Hence:

$$\frac{dM}{dt} = -\rho_i \frac{dH}{dt} - \rho_w v_w \qquad \ldots (4.39)$$

Now:

$$\frac{dM}{dt} = \frac{d}{dt}\int_{z_s}^{z_f} (\rho_i\theta_i + \rho_w\theta_w)\, dz + \frac{d}{dt}\int_{z_f}^{z_1} \rho_w\theta_o\, dz$$

$$= \int_{z_s}^{z_f} (\rho_i \frac{d\theta_i}{dt} + \rho_w \frac{d\theta_w}{dt})\, dz$$

$$+ (\rho_i\theta_{if} + \rho_w\theta_{wf}) \frac{dz_f}{dt} - \rho_w\theta_o \frac{dz_f}{dt} \qquad \ldots (4.40)$$

But $\theta_o = \theta_w + \theta_i$ = constant, so that:

$$\theta_{wf} = \theta_o - \theta_{if} \quad \text{and} \quad \frac{d\theta_w}{dt} = \frac{-d\theta_i}{dt}$$

Therefore, with this and (4.40), (4.39) becomes:

$$-\rho_w v_w - \rho_i \frac{dH}{dt} = \int_{z_s}^{z_f} (\rho_i - \rho_w) \frac{d\theta_i}{dt}\, dz$$

$$+ (\rho_i - \rho_w)\, \theta_{if} \frac{dz_f}{dt} \qquad \ldots (4.41)$$

It should be noted that this equation does not represent the sum of the mass balance equations at the top and bottom of the frozen fringe, due to the variation in (and rate of change of) the ice content within the region.

The drawback with Equation (4.41) was the presence of the integral term, which threatened the mathematical simplicity which was sought in the governing equations of the model. However, by considering the behaviour of the ice content in the frozen fringe, a simple expression was found which closely approximated the integral term.

Let: $$I = \int_{z_s}^{z_f} \frac{d\theta_i}{dt}\, dz \qquad \ldots (4.42)$$

Using the finite difference approximation:

$$\frac{d\theta_i}{dt} = \frac{\theta_i(z,t+dt) - \theta_i(z,t)}{dt} \qquad \ldots (4.43)$$

(4.42) can be written as:

$$I = \frac{1}{dt} \left[\int_{z_s}^{z_f} \theta_i(z,t+dt)\, dz - \int_{z_s}^{z_f} \theta_i(z,t)\, dz\right] \qquad \ldots (4.44)$$

Figure 4.4 illustrates two typical ice content profiles separated by a time interval dt. It can be seen from this that the term in square brackets in (4.44) is represented by the area of the strip between the two curves. What was needed was some estimate of this area and,

as a first approximation, it was assumed that the ice content profile at time t + dt is obtained simply by moving the profile at time t down a distance dz_f, where:

$$dz_f = z_f(t+dt) - z_f(t) \qquad \ldots (4.45)$$

The area of the strip created at the top of the frozen fringe by this movement is then equivalent to the area of the strip between the two profiles, and is given by:

$$\text{area} \simeq (\theta_{is} - \theta_{if})\, dz_f \qquad \ldots (4.46)$$

Substituting (4.46) into (4.44) yields an approximation to the integral term, viz.:

$$I = (\theta_{is} - \theta_{if}) \frac{dz_f}{dt} \qquad \ldots (4.47)$$

Independent studies of the accuracy of (4.47) in representing (4.42) showed an error of less than 5%. It was therefore felt that (4.47) provided a sufficiently good approximation for the purposes of the model, and the mass conservation equation (4.41) was now written as:

$$-\rho_w v_w - \rho_i \frac{dH}{dt} = (\rho_i - \rho_w)\, \theta_{is} \frac{dz_f}{dt}$$

or:
$$\frac{dH}{dt} = \frac{-\rho_w}{\rho_i} v_w + \left(\frac{\rho_w}{\rho_i} - 1\right) \theta_{is} \frac{dz_f}{dt} \qquad \ldots (4.48)$$

The conservation of mass equation across the frozen fringe was thus

obtained in a convenient form, and it was now used to determine the component α in the water pressure profile.

First, the heave rate term was eliminated by solving (4.48) with the mass balance at z_s (4.22) to give:

$$v_s = (1-\theta_{is})v_w - (1-\frac{\rho_i}{\rho_w})(1-\theta_{is})\theta_{is}\frac{dz_f}{dt} \qquad \ldots (4.49)$$

Using once again Darcy's law for the water flux terms yields:

$$\frac{\alpha(u_s-u_f)}{1-E} + \rho_w g = \frac{k_o}{k_s}(1-\theta_{is})(\frac{u_f}{z_w-z_f} + \rho_w g)$$

$$-\frac{\rho_w g}{k_s}(1-\frac{\rho_i}{\rho_w})(1-\theta_{is})\theta_{is}\frac{dz_f}{dt} \qquad \ldots (4.50)$$

where: $k_o = k(o)$

$$E = e^{-\alpha(z_f-z_s)}$$

This can be rearranged to:

$$\alpha = \frac{1-E}{u_s-u_f}[\frac{k_o}{k_s}(1-\theta_{is})(\frac{u_f}{z_w-z_f} + \rho_w g) - \rho_w g$$

$$-\frac{\rho_w g}{k_s}(1-\frac{\rho_i}{\rho_w})(1-\theta_{is})\theta_{is}\frac{dz_f}{dt}] \qquad \ldots (4.51)$$

or, in short:

$$\alpha = f(\alpha) \qquad \ldots (4.52)$$

The solution to (4.52) was found by simple iteration, that is by computing:

$$\alpha_{r+1} = f(\alpha_r) \qquad \ldots (4.53)$$

successively until convergence was achieved.

Hence, the "correct" value of α was obtained, so that the exact form of the exponential water pressure profile (4.32) was established by the model itself.

In both this section and the previous one, a number of major developments have been described, with the change in the water pressure profile in the frozen fringe, the amendment to the mass balance equation at the freezing front and the introduction of the equation for mass conservation across the frozen fringe. In contrast, the impact of these developments on the computer program was relatively small, with the addition of only one subroutine to perform the iteration scheme of Equation (4.53).

This section in fact completes the description of the most important steps in the development of the model, and it is gratifying to note that throughout, the basic structure of the model has remained the same as that created by Holden (1983), thereby upholding the aims mentioned in the introduction to this chapter. The only area still to be discussed is that concerned with the prediction of the heave under zero overburden pressure, wherein the self-weight of the soil plays a prominent role. This aspect is closely linked with a

particular phenomenon which can occur when frost heave takes place under very low overburden pressures. Since accounting for this behaviour requires an extension to the model, it is treated as a special case and dealt with separately in Section 4.10.

The frost heave model is otherwise complete and a summary is therefore provided in the following section.

4.9 Statement of the Final Model

The approximating profiles and governing equations of the final version of the model are all repeated here for clarity, but no derivations or explanations are supplied, since these appear elsewhere. The aim is to provide a concise summary of the components of the completed frost heave model within one section, as a point of reference. The reader once again is referred to the schematic section of a soil column undergoing unidirectional freezing in Figure 3.5. It is emphasised that the model stated here is valid provided a frozen fringe exists and an overburden is applied to the soil (cf. Section 4.10).

In both the solid frozen region and the frozen fringe, the temperature profiles are assumed to be linear and, recalling (3.32) and (3.33), are written, respectively, as:

$$T = \frac{z_s - z}{z_s + H} T_c + \frac{z + H}{z_s + H} T_s, \qquad -H \leqslant z \leqslant z_s \qquad \ldots (4.54)$$

and: $$T = \frac{z_f - z}{z_f - z_s} T_s + \frac{z - z_s}{z_f - z_s} T_f, \qquad z_s \leq z \leq z_f \qquad \ldots (4.55)$$

In the unfrozen region, the temperature profile is computed by solving directly the one-dimensional heat equation:

$$\frac{\partial T}{\partial t} = \mu \frac{\partial^2 T}{\partial z^2} \qquad \ldots (4.2)$$

using a finite difference formulation (Appendix C). In addition, (4.2) is also used to compute the temperature profile within the unfrozen soil column as the surface is cooled, prior to the onset of freezing.

At the base of the sample z_w, the water pressure is zero and decreases linearly up to the freezing front. In the frozen fringe, in accordance with the expected behaviour, an exponential profile is assumed.

The water pressure is therefore expressed as:

$$u_w = A + Be^{-\alpha(z - z_s)}, \qquad z_s < z < z_f$$

$$u_w = \frac{z_w - z}{z_w - z_f} u_f, \qquad z_f < z < z_w \qquad \ldots (4.56)$$

The constants A and B are given in (4.33).

The governing equations of the model are obtained by writing down

mass and energy balances at the top and bottom of the frozen fringe. Darcy's law for water flux is also employed and the application of the Clausius-Clapeyron equation at the base of the ice lens completes the system of equations.

The energy balance equation at $z = z_s$ is, (from (3.37)):

$$K_f \left.\frac{\partial T}{\partial z}\right|_{z_s^+} - K_s \left.\frac{\partial T}{\partial z}\right|_{z_s^-} = \rho_w L v_s, \qquad \ldots (4.57)$$

and at $z = z_f$,

$$K_u \left.\frac{\partial T}{\partial z}\right|_{z_f^+} - K_f \left.\frac{\partial T}{\partial z}\right|_{z_f^-} = -\rho_i L \theta_{if} \frac{dz_f}{dt} \qquad \ldots (4.1)$$

Substitution of the temperature profiles (4.54) and (4.55) into (4.57) and (4.1) yields:

$$K_f \frac{T_f - T_s}{z_f - z_s} - K_s \frac{T_s - T_c}{z_s + H} = \rho_w L v_s \qquad \ldots (4.58)$$

and:

$$K_u \left.\frac{\partial T}{\partial z}\right|_{z_f^+} - K_f \frac{T_f - T_s}{z_f - z_s} = -\rho_i L \theta_{if} \frac{dz_f}{dt} \qquad \ldots (4.59)$$

The temperature gradient $\partial T/\partial z$ at z_f^+ is evaluated within the procedure for computing the temperature profile ahead of the freezing front.

The mass balance at $z = z_s$ is:

$$\rho_i(1 - \theta_{is}) \frac{dH}{dt} = -\rho_w v_s \qquad \ldots (4.22)$$

whilst at $z = z_f$, mass balance is given by:

$$\rho_i \theta_{if} \frac{dH}{dt} = \rho_w(v_f - v_w) + (\rho_w - \rho_i)\theta_{if} \frac{dz_f}{dt} \qquad \ldots (4.36)$$

Each of the water flux terms v_s, v_f and v_w is rewritten using Darcy's law. In general, this is expressed as:

$$v = \frac{-k}{\rho_w g} \left(\frac{du_w}{dz} - \rho_w g\right) \qquad \ldots (4.60)$$

and the water pressure gradients are obtained from (4.56).

Finally, the Clapeyron equation applied at the top of the frozen fringe yields:

$$u_s = \frac{\rho_w}{\rho_i} P + \frac{\rho_w L}{T_o} T_s \qquad \ldots (4.61)$$

With some rearrangement, Equations (4.22), (4.36) and (4.58) to (4.61) can be written as a system of five equations, in the following form:

$$\frac{dz_f}{dt} = A_1 T_s + B_1 \qquad \ldots (4.11)$$

$$\frac{dH}{dt} = A_2 T_s + B_2 \qquad \ldots (4.12)$$

$$u_s = A_3 T_s + B_3 \qquad \ldots (4.13)$$

$$\frac{dH}{dt} = E_1 u_s + C_1 u_f + B_4 \qquad \ldots (4.14)$$

$$\frac{dH}{dt} = E_2 u_s + C_2 u_f + E_3 \frac{dz_f}{dt} + B_5 \qquad \ldots (4.37)$$

By elimination, this system is reduced to two coupled non-linear ordinary differential equations:

$$\frac{dz_f}{dt} = F(z_f, H, t) \qquad \ldots (4.62)$$

and:
$$\frac{dH}{dt} = G(z_f, H, t) \qquad \ldots (4.63)$$

where:

$$G = \frac{(E_1 - E_2\frac{C_1}{C_2})G_1 + A_2 B_4 - A_2 B_5 \frac{C_1}{C_2} + E_3 \frac{C_1}{C_2} G_2}{A_2(1 - \frac{C_1}{C_2}) - E_1 A_3 + \frac{C_1}{C_2} G_3} \qquad \ldots (4.64)$$

$$G_1 = A_2 B_3 - A_3 B_2$$

$$G_2 = A_1 B_2 - A_2 B_1$$

$$G_3 = E_2 A_3 + E_3 A_1$$

and:

$$F = \frac{A_1}{A_2}(G - B_2) + B_1 \qquad \ldots (4.65)$$

The two ordinary differential equations (4.62) and (4.63) are solved using the standard fourth order Runge-Kutta formulae.

One other equation is included in the model, namely the conservation of mass across the frozen fringe. After some simplification, this is given by:

$$\frac{dH}{dt} = -\frac{\rho_w}{\rho_i} v_w + \left(\frac{\rho_w}{\rho_i} - 1\right) \theta_{is} \frac{dz_f}{dt} \qquad \ldots (4.48)$$

This is used in conjunction with (4.22) to determine the value of the exponent α in the water pressure profile (4.56). In fact, an equation of the form:

$$\alpha = f(\alpha) \qquad \ldots (4.52)$$

is obtained (see Equation (4.51)), and this is solved by simple iteration. During the course of a simulation, α is assumed to change only very slowly so that the equations (4.62) and (4.63) are solved using the value of α calculated at the previous time step. Iteration of (4.52) is then performed, with the new values of the relevant variables, to find the value of α to be used in the next time step.

A number of soil parameters are represented in the model. Based on soil suction data for Attenborough silt (Figure 4.1), the ice content as a function of the suction parameter ψ is written as:

$$\theta_i = 0.1179 \, (\log_{10} \psi) - 0.5583, \quad \psi < 4.25 \times 10^7$$

$$\theta_i = 0.0198 \, (\log_{10} \psi) + 0.19 \quad \psi \geq 4.25 \times 10^7 \qquad \ldots (4.21)$$

The hydraulic conductivity is then expressed as:

$$k(\theta_i) = k_o \left(1 - \frac{\theta_i}{\theta_o}\right)^m \qquad \ldots (4.5)$$

where: $k_o = k(0)$

$m = 7$ or 9

$\theta_o = 0.4$

(θ_o is the soil porosity; a constant, since the soil is assumed to be incompressible).

The criterion for the formation of a new ice lens depends upon the value of the neutral stress which, recalling (3.6), is calculated by the formula:

$$u_n = \chi u_w + (1-\chi)\, u_i \qquad \ldots (4.66)$$

where (from Equation (3.28)) the stress partition function χ is given by:

$$\chi(\theta_i) = \left(1 - \frac{\theta_i}{\theta_o}\right)^{1.5} \qquad \ldots (4.67)$$

Finally, in each of the three regions of the freezing soil column, the thermal conductivity is taken to be constant, that is K_s, K_f and K_u are each assigned a fixed value.

That concludes the summary of the mathematical model in its final

form. The next section describes the additional steps necessary to account for the application of zero overburden, and to cope with a special case which can arise under low overburden pressures. Chapter 5 then follows, which examines the results of the computer simulations performed with the model just described, and contains further details and discussion of the values of constants used in the computations.

4.10 The Self-Weight and the Absence of the Frozen Fringe

This section deals with the inclusion of the soil self-weight in the model, to enable simulations to be performed under zero overburden, and also addresses a particular situation which arises under relatively low overburden pressures, namely the disappearance of the frozen fringe. Although this phenomenon can be expected, the model at present is unable to cope with it, since it assumes the existence at all times of a frozen fringe. It will however be shown that the problem can be handled in a straightforward manner.

A saturated column of soil 150 mm in height, typically the size of a specimen in a laboratory freezing test, represents an overburden pressure of around 3 kPa. Therefore, for a sample undergoing freezing under an applied load of, say, 30 kPa, the contribution of the self-weight of the soil to the overburden is relatively small and becomes increasingly so with increasing overburden. The self-weight has thus been neglected up to this point. However, if the applied load is of the same order of magnitude as the self-weight,

then the latter should be included in the model. Moreover, if no overburden is applied, the self-weight must be included for the model to function at all. Recalling that, according to the secondary heave theory, a lens is initiated when the maximum of the neutral stress in the frozen fringe reaches the overburden, clearly accounting for the self-weight in the overburden is essential to allow the observed sequence of ice lenses to be modelled.

The adjustment to the model to accommodate the self-weight was very easily made. The total pressure P' at the base of the latest ice lens is the sum of the applied overburden P, the pressure due to the ice in the lenses (i.e. the total heave) and that due to the frozen soil between the lenses. Hence:

$$P' = P + \rho_i g H + \rho_s g z_s \qquad \ldots (4.68)$$

where ρ_s is the density of the frozen soil between the individual ice lenses. The Clapeyron equation at the base of the lens therefore became:

$$u_s = \frac{\rho_w}{\rho_i} P' + \frac{\rho_w L}{T_o} T_s \qquad \ldots (4.69)$$

(cf. Equation (4.61)).

The criterion for the formation of a new ice lens remained essentially the same except that now a lens was initiated when the maximum of the neutral stress in the frozen fringe became equal to P', rather than

just the overburden P. To be strictly accurate, the gradient of pressure due to the self-weight in the frozen fringe should also have been considered, but it was felt that this could reasonably be neglected to a first approximation. Indeed, it was found that the absence of this term did not impair the performance of the model.

Computer simulations performed at this time demonstrated that, under low applied overburden pressures (less than around 25 kPa), it was possible for the frozen fringe to disappear, due to the retreat of the freezing front towards the base of the ice lens. That is, dz_f/dt became negative and eventually z_f became equal to z_s, indicating that a frozen fringe no longer existed. This always occurred after the formation of the terminal ice lens when a steady state condition was approached in the soil column. Here, "steady state" refers to the situation wherein the heat flux throughout the column is constant, the temperature profile in each region is therefore linear, and the heave rate has decreased to zero. If a frozen fringe is present under these conditions, the freezing front is stationary.

The lack of a frozen fringe under these circumstances does not contradict experimental evidence, as is explained fully in Chapter 6. However, the simulations were unable to proceed past this point, since the model contained no mechanism for coping with the loss of the frozen fringe.

In order that all simulations could be run until a true stationary state was achieved, it was decided that the model should be capable of handling this contingency. Fortunately, this was found to be

simply a matter of solving a reduced system of equations.

In the absence of the frozen fringe, the base of the (terminal) ice lens is also the extent of freezing, and this level is referred to in the following by the subscript "ss". The freezing column now contains only two distinct regions: the solid frozen and the unfrozen, the boundary between the two being given by $z = z_{ss}$. Since a near steady state exists, the temperature profile in the unfrozen region is now assumed to be linear, so the energy balance at z_{ss} is given by:

$$K_u \frac{T_w - T_{ss}}{z_w - z_{ss}} - K_s \frac{T_{ss} - T_c}{z_{ss} + H} = \rho_w L v_{ss} \qquad \ldots (4.70)$$

(cf. Equation (4.58)) where, clearly, T_{ss} and v_{ss} are the temperature and the water flux respectively at z_{ss}.

With no frozen fringe, no ice exists just below the lens and the mass balance equation is a simplified form of Equation (4.22), that is:

$$\rho_i \frac{dH}{dt} = -\rho_w v_{ss} \qquad \ldots (4.71)$$

The water flux to the ice lens is still described by Darcy's law and, recalling that the water pressure profile in the unfrozen region is linear, is written:

$$v_{ss} = \frac{-k_\Omega}{\rho_w g} \left(\frac{-u_{ss}}{z_w - z_{ss}} - \rho_w g \right) \qquad \ldots (4.72)$$

where u_{ss} is the water pressure just below the ice lens.

Finally, the Clapeyron equation at $z = z_{ss}$ is unchanged from (4.69), thus:

$$u_{ss} = \frac{\rho_w}{\rho_i} p' + \frac{\rho_w L}{T_o} T_{ss} \qquad \ldots (4.69)$$

The equations (4.69) and (4.70) to (4.72) represent a system of four equations in the four unknowns T_{ss}, v_{ss}, u_{ss} and H. Substitution of (4.72) and (4.69) first into (4.70) and then into (4.71) gives two equations in T_{ss} and H, and subsequent elimination of T_{ss} yields a non-linear ordinary differential equation of the form:

$$\frac{dH}{dt} = g(H) \qquad \ldots (4.73)$$

The solution to (4.73) was obtained numerically using, as before, the standard fourth-order Runge-Kutta scheme.

Prediction of the heave after the disappearance of the frozen fringe was therefore a relatively simple operation, in view of the reduced computational effort required. It did however mean the introduction of three new subroutines into the existing computer program.

In the main segment of the program, a statement was added to check for the presence of the fringe at each time step. The moment that the fringe disappeared (that is, $z_f = z_s$), control was passed to

a new subroutine ("NOFRINGE") from where the remainder of the simulation was directed. Two other new subroutines respectively calculated the function g on the right-hand side of (4.73) and performed the Runge-Kutta solution of (4.73). The capability of the program was therefore augmented at the expense of an increase in its length. These additions nevertheless proved to be justified because it was now possible to run simulations successfully, under any applied overburden pressure, for any length of time and certainly until the heaving effectively ceased.

Full details of the simulations performed and their results are given in the next chapter. The computer predictions are then discussed in Chapter 6, which includes an explanation of the loss of the frozen fringe under the circumstances described above.

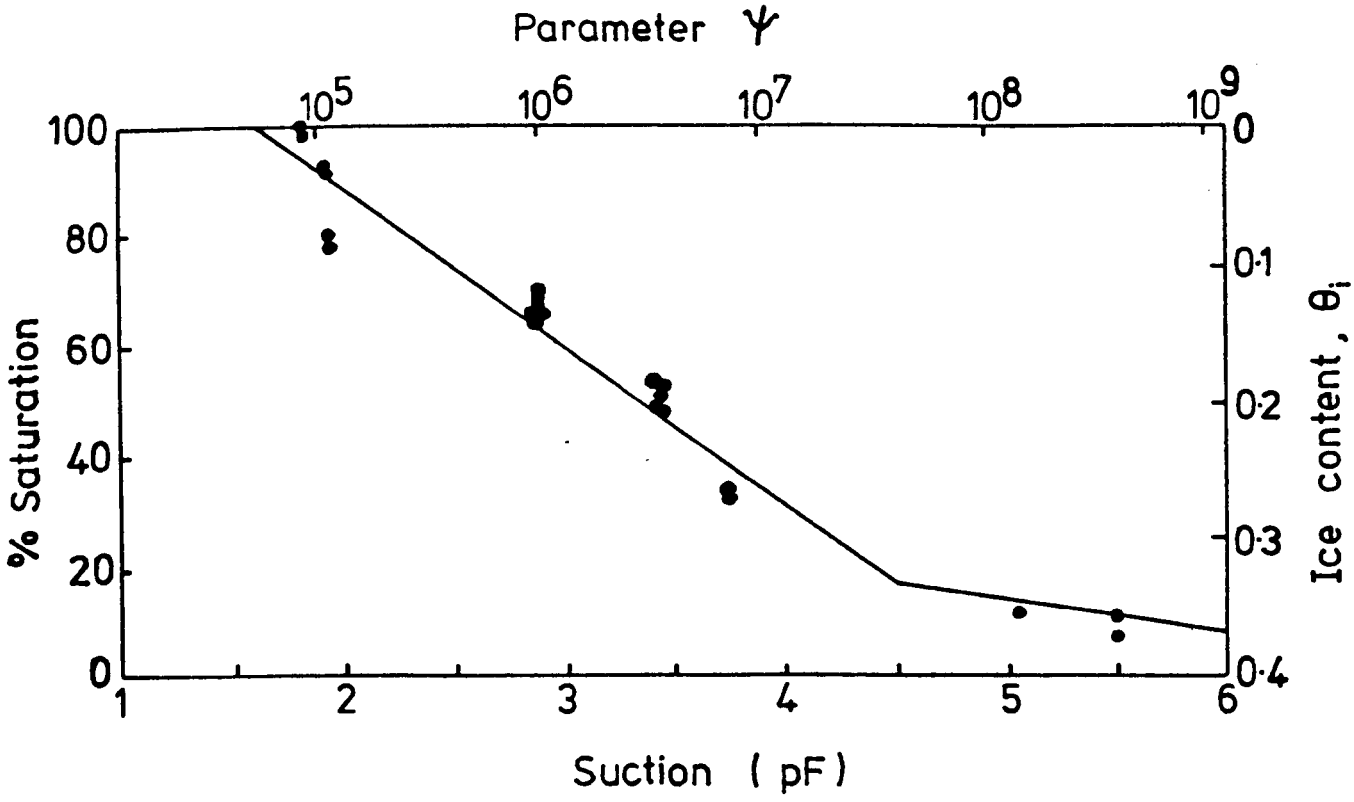

Figure 4.1 Straight line fits to soil suction data for Attenborough silt (data from Thompson, 1981)

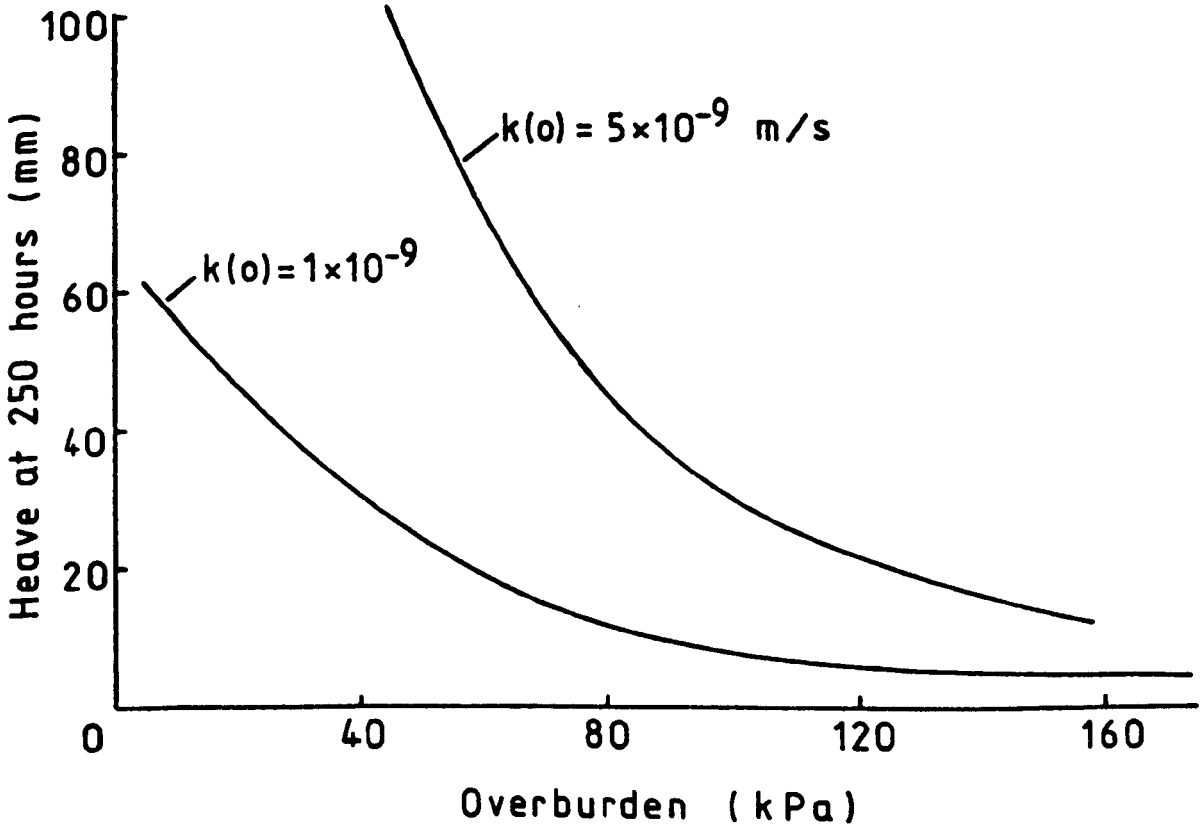

Figure 4.2 Heave after 250 hours versus overburden (after Holden et al, 1985)

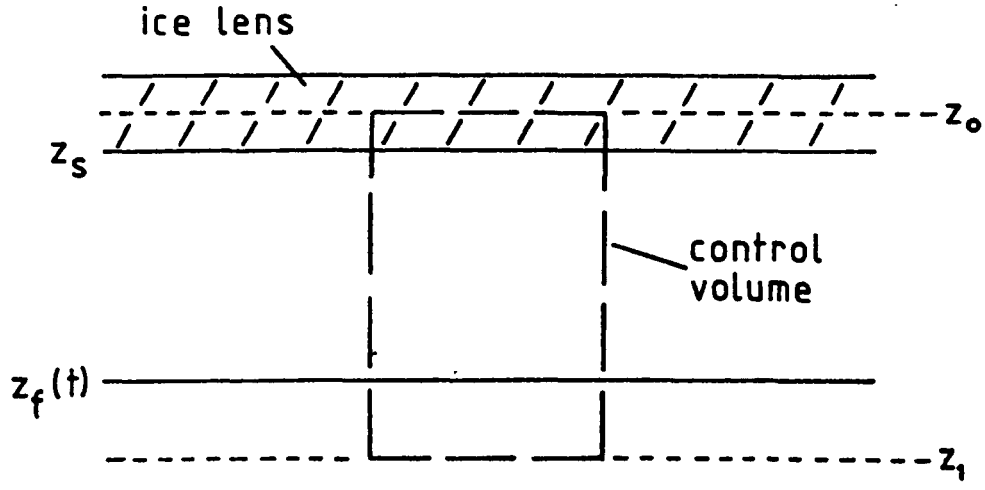

Figure 4.3 Control volume for determination of the conservation of mass equation across the frozen fringe

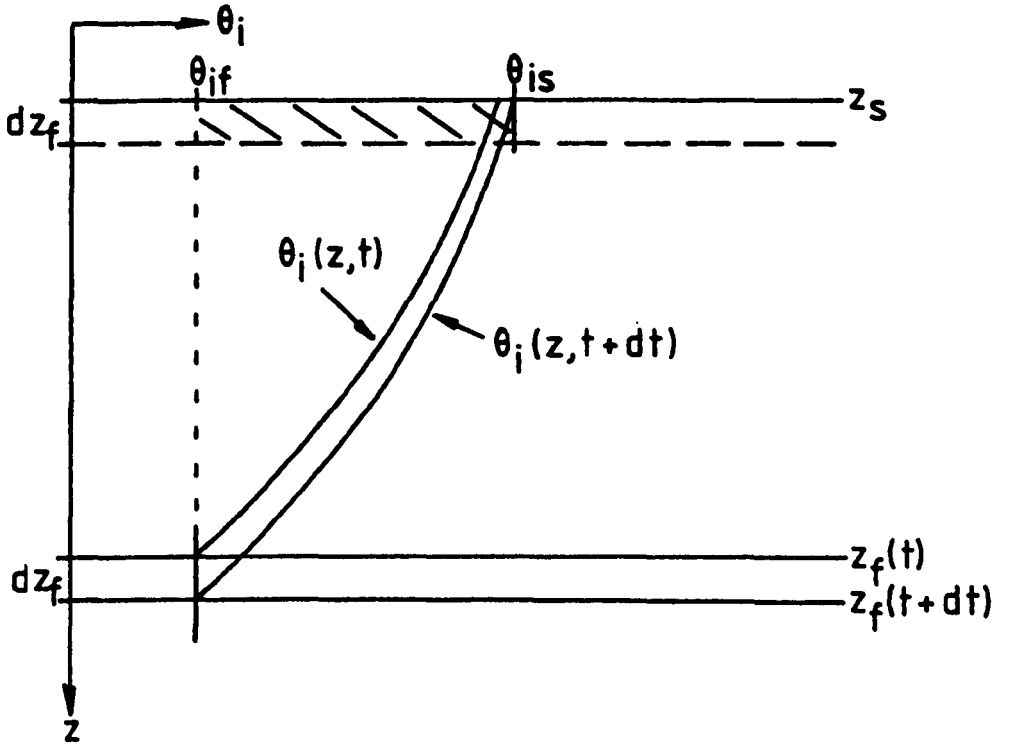

Figure 4.4 Change in the ice content profile in the frozen fringe in the time interval dt

CHAPTER 5

RESULTS OF THE COMPUTER PREDICTIONS

5.1 Introduction

At every stage during the development of the frost heave model, a considerable amount of computation was performed, much of which was described in Chapter 4. Of course, the predictions made with each update of the model inevitably superseded those at the previous stage. Therefore, having finalised the formulation of the model, simulations were carried out to assess its capabilities fully, and it is the results of these calculations which are reported in this chapter.

The main aim was to see how well the model performed in reproducing the behaviour observed in laboratory freezing experiments. To this end, a common set of boundary conditions, typical of those found in the laboratory, was applied in the majority of the simulations. Under these conditions, different aspects of the model were examined, with particular attention paid to the effect of variations in the overburden pressure. Thereafter, changes were made in the boundary conditions as part of a parametric investigation which sought to identify those variables having the greatest influence on the predicted heave.

In the next section, a detailed description of the computational

aspects of the simulations is given, including such information as the length of soil column modelled, the number of mesh points used, the size of time steps, and so on. This is followed by an overview of the results of the predictions, with examples of the typical behaviour across a range of overburden pressures. Section 5.4 examines more closely the effect of a low applied overburden, illustrating how the model copes with the disappearance of the frozen fringe. Finally, details of the parametric studies undertaken are included in Section 5.5.

It should be stated here that this chapter concentrates on simply reporting the results of the computer predictions and, as such, contains very little in the way of additional comment. The majority of the discussion on the outcome of the simulations is deferred until Chapter 6.

5.2 Details of the Simulations

In the previous chapter, the techniques used in the modelling of frost heave and ice lensing were described without reference to any specific freezing situation. Therefore, in this section, details of the actual physical problem modelled are provided along with the associated numerical data. First, though, some information on the computer program itself is presented.

The program was written in FORTRAN 77 and run on the University of Nottingham ICL 2900-series mainframe computer. A flow diagram

for the program is given in Figure 5.1, which highlights the basic steps performed by the program and the order in which they were executed. Depending on the boundary conditions (overburden, temperatures, etc.), one complete simulation, to a steady state condition, typically took around ten minutes of c.p.u. time. The entire program, approximately 450 lines in length (excluding comments), is reproduced in Appendix D.

All of the computations simulated the heave of a soil column, 150 mm in length, undergoing unidirectional freezing. Except where otherwise stated, the column was assumed initially to be at a uniform temperature of +4°C throughout. The surface was then cooled to -6°C whilst the temperature at the base of the sample was kept constant at +4°C. This size of soil column and the boundary temperatures were deliberately chosen to reflect the conditions found in a typical laboratory freezing test (see for example Jones and Dudek, 1979, Dudek, 1980).

For simplicity, the surface temperature was assumed to decrease linearly with time from +4 to -6°C, over a period of 10^5 seconds (around 28 hours). This rate of cooling is depicted by the solid line in Figure 5.2 and was chosen principally as a computational convenience. Clearly, other "cooling curves" are possible and are easily programmed or, as mentioned previously, the heat extraction rate rather than the temperature decrease could be specified.

The first calculation performed by the program is that of the temperature profile in the soil column, as the surface cools from

its initial temperature (subroutine COOLDOWN). This is done using a Crank-Nicolson finite difference scheme, for which the region was divided into 25 "elements", giving a mesh point every 6 mm along the 150 mm length of the column. The time step chosen for the calculation was 100 seconds, which was thought to be more than adequate for the prescribed cooling of the surface. Both the mesh size and time step could of course be varied as desired. The temperature profile is printed out as often as required. Typically, output was requested every 50 time steps, which is equivalent to a time period of approximately 1.4 hours.

Computation of the temperature profile continues until the moment when freezing begins at the surface of the soil sample. That is, when the temperature at the surface falls below zero sufficiently to allow frost penetration to occur, the current temperature profile in the column is automatically printed out, and control then passes to the main segment of the program to allow the calculation of the frost heave and ice lensing to commence.

The mathematical formulation of the frost heave model is such that it is necessary to prescribe initial non-zero values for the heave, H, and the freezing front position, z_f, in order to avoid numerical singularity problems (see also Gilpin, 1980). These starting values can be arbitrarily small, and are supplied as input to the program via the data file. For all the simulations described herein, a value of 0.1 mm was used for both quantities.

The initial time step for the freezing calculation is another of

the input data items and the optimum step size was found to be one second. This was the largest interval which did not produce an error in the computed value of the heave in the first time step and which was small enough to model the initial, highly transient behaviour adequately. As the calculation proceeds though, such a small time step is no longer needed and to reduce computation time, the step size is progressively increased. Based on experience, the time step was changed to 10 seconds after 10^4 seconds (2.8 hours) of freezing, and to 100 seconds after 10^5 seconds (27.8 hours).

Among the other data supplied to the program are the overburden, P, the saturated unfrozen hydraulic conductivity, k_o (see following sections), the temperature at the freezing front, T_f, and the initial value of the water pressure exponent, α. The freezing front temperature is assumed to be constant in the model and a value of -0.02°C was used in the simulations, as this was judged to be a reasonable measure of the freezing point depression. The full justification for this choice is given in Chapter 6.

As described in Chapter 4, the water pressure exponent is calculated by the model using the mass continuity equation across the frozen fringe (subroutine NEWALPHA). It was therefore thought that whatever initial value was chosen, it would not have a significant influence, since the model would adjust itself to the correct value as the computation proceeded. However, the calculation of α proved to be numerically unstable during the early stages of a simulation, due possibly to the initial rapid freezing which could cause the assumption of a slowly varying α to be violated. To

overcome this difficulty, α was kept constant for the first 2,500 seconds (around 40 minutes) of freezing. From then on, the exponent was successfully computed by the model, with the aid of a simple "averaging" scheme to smooth out any oscillations.

With α held fixed at the start of freezing, the choice of initial value became more important since a reasonable reproduction of the early behaviour was required. A range of values was therefore investigated and this led to $\alpha = 1000\ m^{-1}$ being used as the starting value in all the simulations. It should be emphasised that keeping α constant during the early part of the calculations did not affect the behaviour at later times, and was merely introduced to eliminate the initial numerical instability. The variation of α during the course of a simulation, and with respect to the overburden, is described in Section 5.5.

Having completed the initialisation of variables at the onset of freezing, the calculation of the frost heave and ice lensing proceeds in the manner detailed in Chapter 4 and illustrated in Figure 5.1. To summarise briefly, Equations (4.62) and (4.63) are solved first (subroutine RK) to give H and z_f at the next time step. These are then used in (4.12), (4.13) and (4.14) to yield T_s, u_s and u_f (provided that a frozen fringe exists. If not, control passes to subroutine NOFRINGE, from where the remainder of the calculation is conducted). The value of the water pressure exponent to be used at the next time step is found (subroutine NEWALPHA), followed by the maximum of the neutral stress in the frozen fringe (subroutine MAXSIGMA). All relevant information is printed out as frequently

as desired, according to the value assigned to the variable NPR in the data file. In other words, information is output every NPR time steps and typically NPR = 1000 was used.

If the maximum of the neutral stress is found to be greater than or equal to the overburden, a new ice lens is initiated. In this instance, the time and the position of the new lens are automatically printed out, along with the thickness of the previous lens. The location of the top of the frozen fringe, z_s, is then set equal to the position of the new lens.

Finally, the temperature profile in the unfrozen region is calculated (subroutine UNFROZEN), and this too is printed out every NPR time steps. Like the initial temperature profile calculation, a Crank-Nicolson finite difference scheme is employed, and, for convenience, the region was again divided into 25 elements. In this case however, the region and hence the mesh, contracts as frost penetration occurs, so that the position of each mesh point changes with each time step. Both the location and the temperature are therefore printed out for each point in the mesh.

Normally, a period of 2×10^6 seconds (approximately 556 hours) of freezing was simulated with each run of the program, by which time a steady state condition was usually achieved within the soil column. Of course, if necessary, the simulation could be allowed to continue beyond this time.

The numerical values used in the program for quantities such as

density, thermal diffusivity, latent heat of fusion etc. are all given in Appendix D. Details of other variables which were the subject of parametric investigations (e.g. hydraulic and thermal conductivities) are provided in the following sections.

5.3 General Behaviour

In this section, an overall view of the quality and magnitude of the predictions is presented with the aid of a number of figures illustrating the typical behaviour. For the most part, "standard" simulations are described, that is simulations performed with a chosen fixed set of values for certain parameters and boundary conditions. These were as follows:

Boundary temperatures: -6/+4°C (see Section 5.2)

Hydraulic conductivity function (Equation (4.5)): $k_o = 5 \times 10^{-9}$ ms^{-1}, $m = 7$

Thermal conductivities: $K_s = 4.0$, $K_f = 4.0$, $K_u = 3.0$ W m^{-1} °C^{-1}

The effect of variations in these conditions is discussed in Section 5.5.

To assess the overall capability of the model, predictions were obtained for a range of overburden pressures, and curves produced to aid analysis of the results. First, the heave is plotted against time for several different overburdens in Figure 5.3. The shape of these curves is as expected with the heave rate initially very high,

then decaying over time until a steady state (zero heave rate) is reached. In addition, the reduction in the predicted heave with increasing overburden is in accordance with experimental observation. This latter point is illustrated more clearly in Figure 5.4, which contains a plot of the total heave versus the overburden pressure. Here, "total heave" refers to the computed value of the heave at the moment when the heave rate drops below 0.01 mm per hour (2.78×10^{-9} ms^{-1}).

One aspect of the heaving mechanism which is not apparent in the curves of Figure 5.3 is the "cycling" of the heave rate and the frost penetration rate between successive ice lens formations. This phenomenon is depicted in Figure 5.5, in which heave rate is plotted against penetration rate, for the closing stages of a simulation. The plot begins at the point a_1, and between a_1 and b_2, the latest lens is growing and the frozen fringe is extending beneath it, whilst z_s remains constant. At b_2, a new lens is initiated and z_s accordingly jumps to a new value. This produces a sudden change (broken line) in the heave rate and the penetration rate to the point a_2. Between a_2 and b_3, z_s again remains constant as the new lens and the frozen fringe both grow. The cycle is repeated, with a decreasing mean penetration rate, until the penetration rate becomes negative at a_5. This indicates that the final or terminal lens has formed (initiated at b_5), since now the frozen fringe begins to decrease in thickness. Figure 5.5 shows that both the heave rate and the penetration rate eventually drop to zero, at which time steady state (constant heat flux) conditions are achieved.

This cyclic behaviour can be detected on a heave versus time curve when it is plotted to an enlarged scale (Figure 5.6). Here, the initiation of the last four lenses is shown for the same simulation as depicted in Figure 5.5.

Following the example of O'Neill and Miller (1980, 1985), the ability of the model to predict the location, thickness and time of initiation of each ice lens is demonstrated by Figure 5.7, in which a section of a freezing soil column is drawn to an enlarged vertical scale. The figure highlights the fact that the time and spacing between, and the thickness of successive lenses increases as freezing progresses. It should be noted that the temperature boundary conditions in this instance have been changed. The soil column was initially at a uniform temperature of +1°C, and the surface cooled (over a period of 27.8 hours) to -1°C, whilst the base was held at +1°C. These conditions were chosen partly to match more closely those of O'Neill and Miller (1980, 1985), and partly because they produce thicker and therefore more identifiable lenses for the purposes of illustration. Further observation of the effect of a change in boundary temperatures is included in Section 5.5.

A complete picture of the effect of freezing on a soil column is provided by Figure 5.8, which is an actual size (vertically) schematic view of a heaved soil sample, drawn from the results of a typical simulation. The model predicts that, as in most laboratory frost heave tests, the terminal lens accounts for the majority of the

heave of the soil column, a feature which is clearly evident in Figure 5.8.

5.4 Effect of Low Overburden Pressures

As indicated in Figures 5.3 and 5.4, the computations produced the expected increase in the heave of the soil column with decreasing applied overburden. The overall behaviour of each simulation was otherwise essentially the same, provided that the overburden was greater than approximately 25 kPa.

However, with an overburden pressure below this figure, a critical change in the frost heaving process was predicted by the model, namely the eventual disappearance of the frozen fringe. In Figure 5.9, a plot of the thickness of the frozen fringe at thermal equilibrium (steady state) versus the overburden is given, and this shows that the model forecasts the frozen fringe to be ultimately absent if the overburden is below about 25 kPa.

Whatever the overburden, Figure 5.5 demonstrated that frost penetration ceases and the freezing front retreats after initiation of the terminal ice lens. Under a low overburden, this reversal simply continues until the frozen fringe disappears completely. This phenomenon can be explained physically and details are included in Chapter 6. Indeed, the value of the overburden below which the frozen fringe eventually disappears can be calculated a priori as a

function of T_f, the freezing front temperature (see Chapter 6). At this point, it is sufficient to note that for T_f = -0.02°C, the formula predicts the "threshold" value to be 22.5 kPa. Figure 5.9 demonstrates that this is precisely the value produced by the model.

As explained in the previous chapter, a mechanism was introduced into the model to allow the heave to be calculated even in the absence of a frozen fringe. This involves solving a reduced system of equations once the fringe disappears. A measure of the success of this procedure is provided in Figure 5.10, which shows the heave against time for a simulation with zero applied load. In spite of the loss of the frozen fringe after around 44 hours, the curve remains smooth in accordance with observation of laboratory tests.

5.5 Results of Parametric Studies

This section describes the outcome of a number of parametric studies which were performed to examine the effect on the heave of variations in the "standard" conditions given in Section 5.3. First, though, the value of the exponent α in the water pressure profile approximation (Equation (4.56)) is discussed. Whilst this was not the subject of a parametric investigation, its behaviour is of interest and is included here for convenience.

It was explained in Section 5.2 that numerical considerations made it necessary to keep α constant during the early part of each simulation. Thereafter, α was computed at every time step as an integral

part of the modelling, and its value was found to vary throughout the course of a simulation. Between ice lens formations, α fluctuates cyclically in a similar manner to that depicted in Figure 5.5, with its value decreasing as the frozen fringe grows and abruptly increasing when a new lens is initiated. This behaviour continues during the ice lensing process, with a small but steady increase in the mean value of α over time. Then, after formation of the terminal lens when the freezing front begins to recede, α increases monotonically, eventually reaching a maximum when the freezing front becomes almost stationary. Although the system is close to thermal equilibrium at this stage, the value of α ultimately falls to zero upon reaching a true steady state some considerable time later (after more than 500 hours of freezing).

The exact time at which α attained its maximum value was not recorded by the program. However, for each simulation, the value of α was printed out along with other variables at the point when the heave rate dropped below 0.01 mm/hour, and it was found that this value was always within 10% of the maximum. The value of α thus obtained has been used to produce the curve of α versus overburden given in Figure 5.11.

The curve does not extend below an overburden of 25 kPa because in this region the frozen fringe disappears before α reaches a maximum and before the heave rate drops below 0.01 mm/hour. Initial comparison of Figure 5.11 with Figure 5.9 indicates that α increases as the thickness of the frozen fringe decreases, although the product

of the two in this instance increases with increasing overburden.

The first variation in the "standard" conditions to be reported here is a change in the freezing rate, that is the rate of cooling of the surface of the soil column. In Figure 5.2, the solid line shows the rate at which the surface was cooled in the majority of the simulations. In order to investigate the effect of a faster freezing rate, the surface of the soil was cooled from +4°C to -6°C over a period of 10^4 seconds rather than 10^5 seconds, represented by the broken line in Figure 5.2. The resulting heave and frost penetration are compared in Figures 5.12 and 5.13 with the previous solutions for an overburden of 25 kPa. These curves demonstrate that the model predicts precisely the behaviour expected, with the faster freezing producing inevitably more rapid frost penetration. This initially causes an increase in the heave rate, but in the longer term the ice lenses are narrower since they have less time to grow. The total heave is therefore lower than that due to the slower freezing.

Figure 5.14 illustrates the effect of a change in the boundary temperatures of the soil column. In both cases, the surface was cooled from the initial uniform temperature of the soil (+4 or +1°C) to the final sub-zero temperature (-6 or -1°C, respectively) over a period of 10^5 seconds (27.8 hours). It is perhaps most interesting to note that the heave due to the -1/+1°C boundary temperatures eventually exceeds that in the -6/+4°C case, which highlights the fact that a lower surface temperature does not necessarily imply a greater heave ultimately. The model again successfully reproduces

what happens in reality and further discussion is included in the next chapter.

The hydraulic conductivity function used in the computations was also the subject of a parametric study, and the results are given in Figure 5.15. Recalling the form of the function (Equation (4.5)),

$$k = k_o(1 - \frac{\theta_i}{\theta_o})^m$$

the constant k_o and the exponent m were varied and the total heave computed under a range of overburden pressures. Values of m=7 and m=9 were employed, following O'Neill and Miller (1980, 1985), accompanied by either $k_o = 5x10^{-9}$ or $k_o=1x10^{-9}$. Three of the four combinations of the two parameters are plotted in Figure 5.15, and the effect on the heave is clearly evident. The curves confirm the findings of other researchers who have isolated the hydraulic conductivity as being perhaps the most crucial parameter in frost heave modelling. Small variations in its representation or value can cause significant changes in the magnitude of numerical results. The subject is therefore covered in more detail in Chapter 6.

Finally, the effect of changes in the thermal conductivity values was investigated. However, no graphical results are presented for this study as the outcome was as expected and is largely predictable. For example, when the three conductivities were made equal (see Table 5.1), the heave-time curve for an overburden of 25 kPa was almost unchanged with an increase in the total heave of less than

3%, whilst the total frost penetration decreased by around 18%. These effects could be anticipated by examining the two energy balance equations in the model (4.58) and (4.59). K_s and K_f are equal, as they were in the "standard" simulations, so if the temperature gradients remain roughly the same, then no significant change would be expected in the heave. On the other hand, K_f and K_u are now equal whereas previously they were not, and (4.59) indicates that with this change the frost penetration rate would tend to decrease relative to the "standard" case.

THERMAL CONDUCTIVITIES ($Wm^{-1}\ °C^{-1}$)	TOTAL HEAVE (mm)	FROST PENETRATION (mm)
"Standard" values: $K_s = K_f = 4$ $K_u = 3$	56.7	80.5
Variant values: $K_s = K_f = K_u = 3$	58.3	66.0

Table 5.1 Effect on the Heave and Frost Penetration of a Change in the Thermal Conductivity Values (overburden = 25 kPa)

Any errors caused by inaccuracies in the thermal conductivities can therefore be readily quantified. More complex representations of the thermal conductivity are possible (see Chapter 6), but the assumption of a constant value in each region of the freezing soil is considered to be justified.

In this chapter, the results of computer predictions made with the frost heave model have been presented. Full details of the simulations performed have been given, and the computer program with associated numerical data is included in Appendix D. Discussion of the results, and the model in general, now follows in Chapter 6.

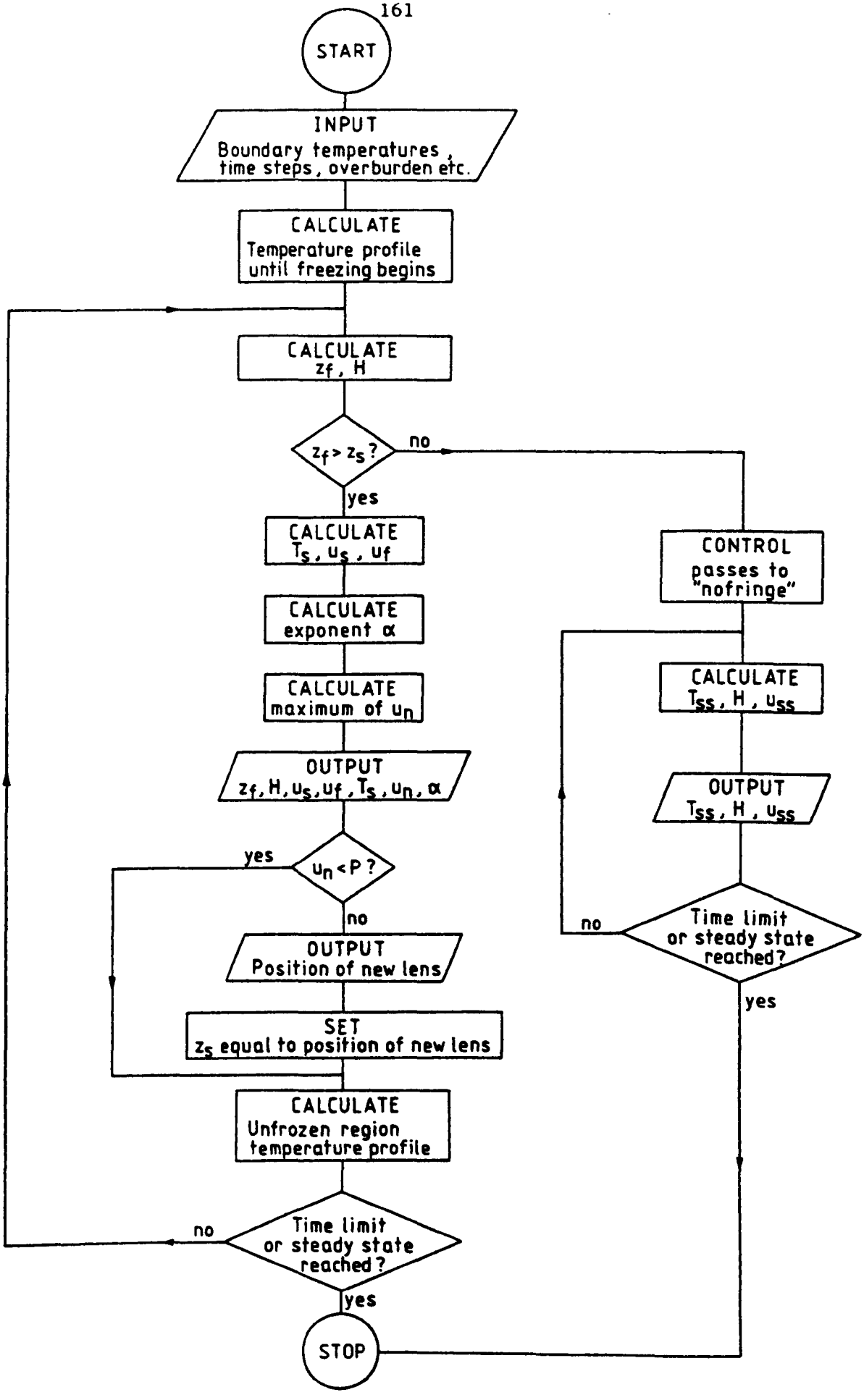

Figure 5.1 Flow diagram of computer program

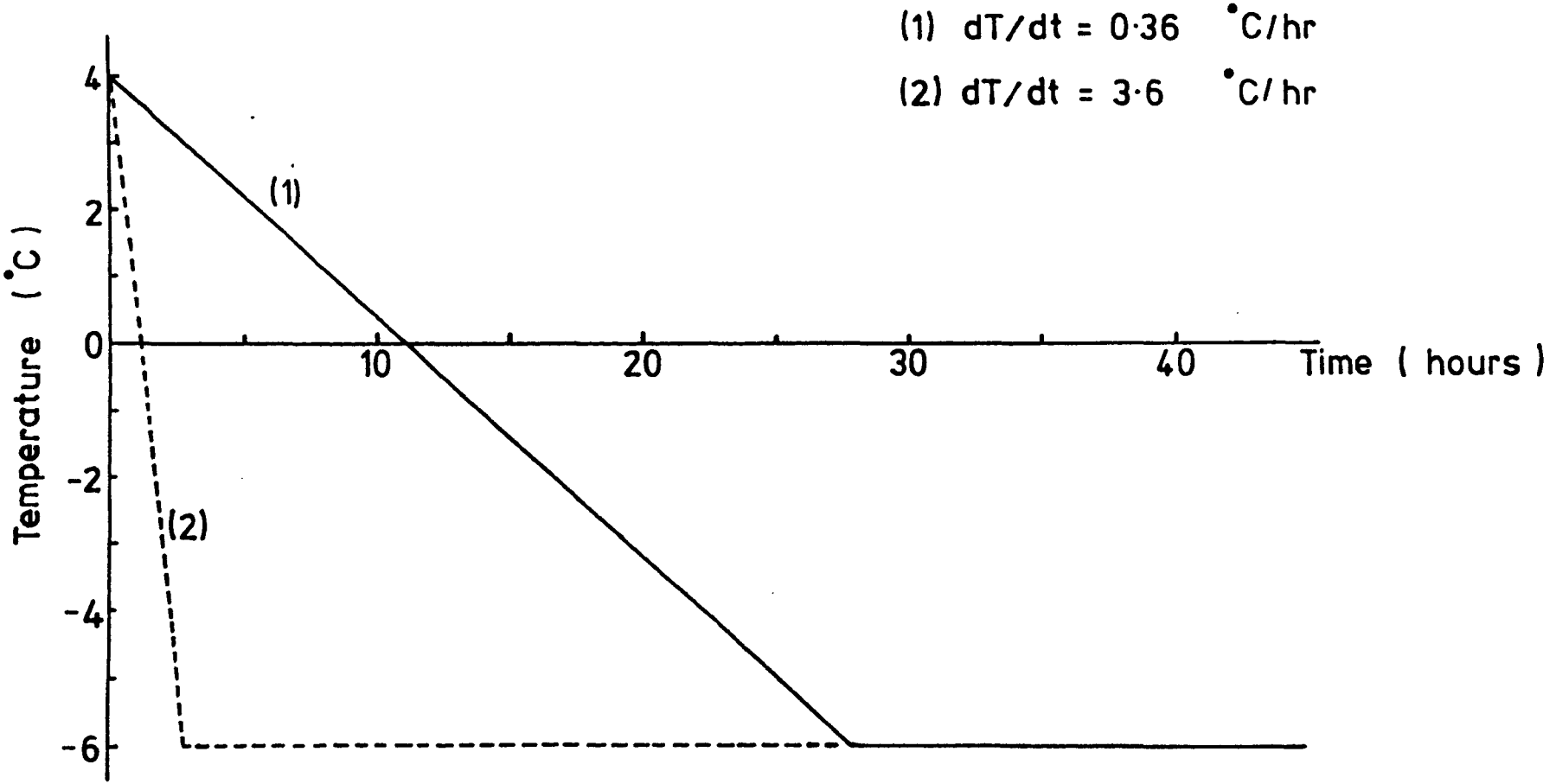

Figure 5.2 Rates of cooling of surface of soil column

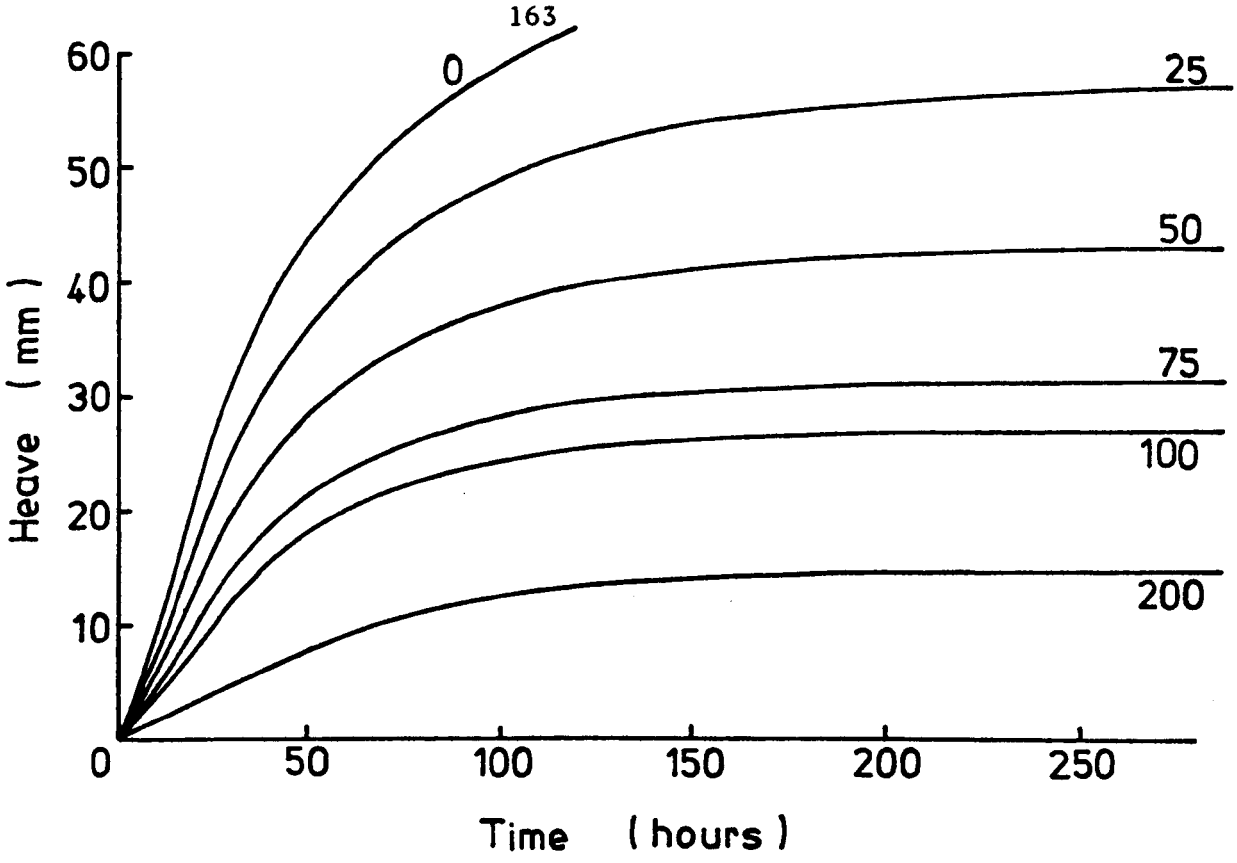

Figure 5.3 Heave versus time curves for different overburden pressures (values are in kPa)

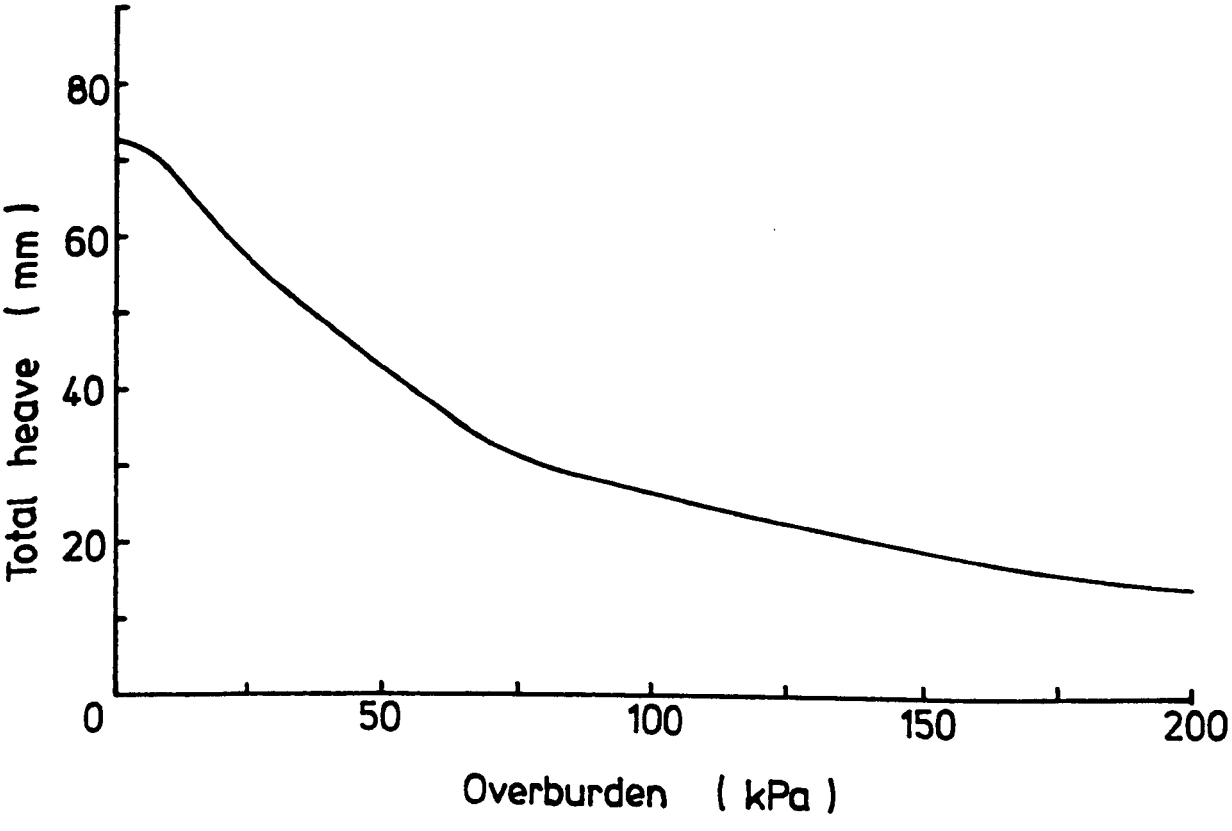

Figure 5.4 Total heave versus overburden

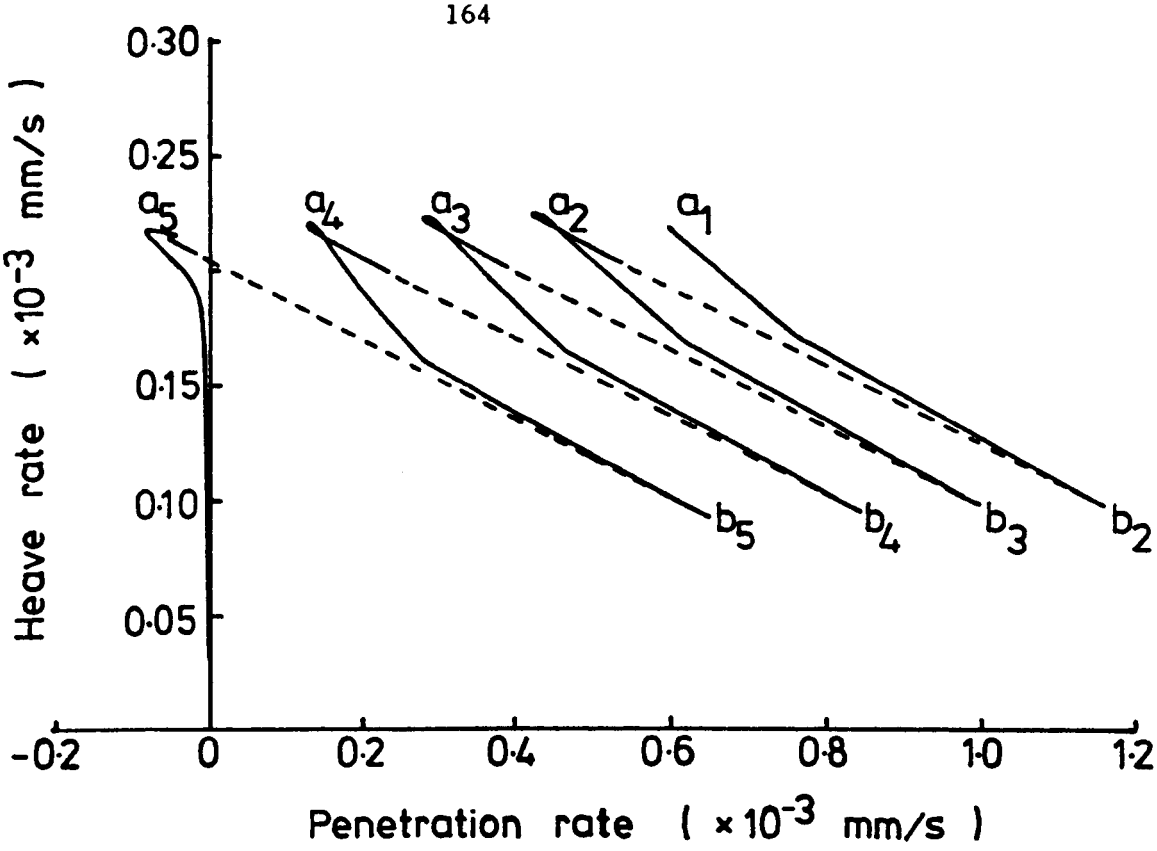

Figure 5.5 Heave rate versus frost penetration rate, for the closing stages of a simulation (overburden = 50 kPa)

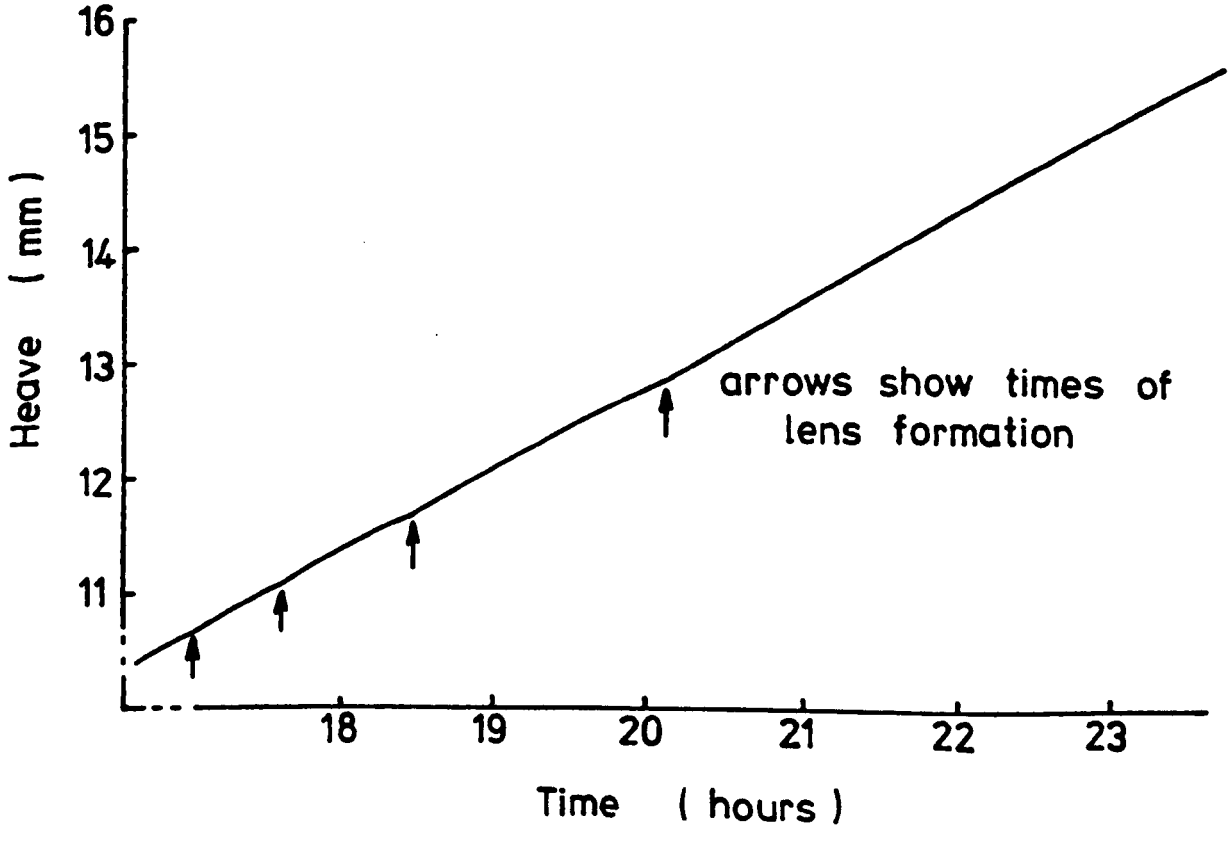

Figure 5.6 Heave against time showing the initiation of four ice lenses (overburden = 50 kPa)

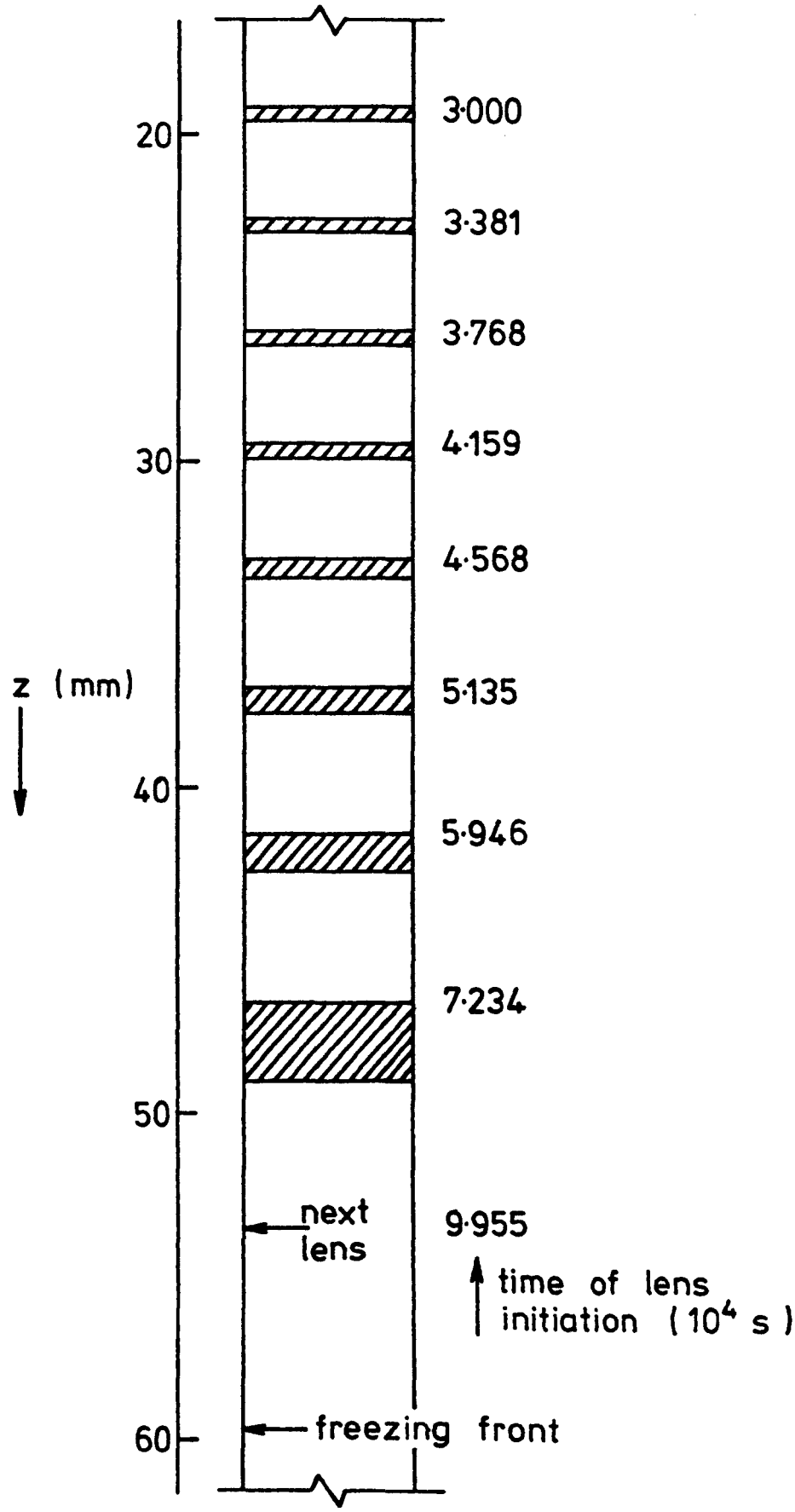

Figure 5.7 Location, thickness and time of initiation of ice lenses (hatched) in part of a freezing soil column (P = 25 kPa, T_c = -1°C, T_w = +1°C)

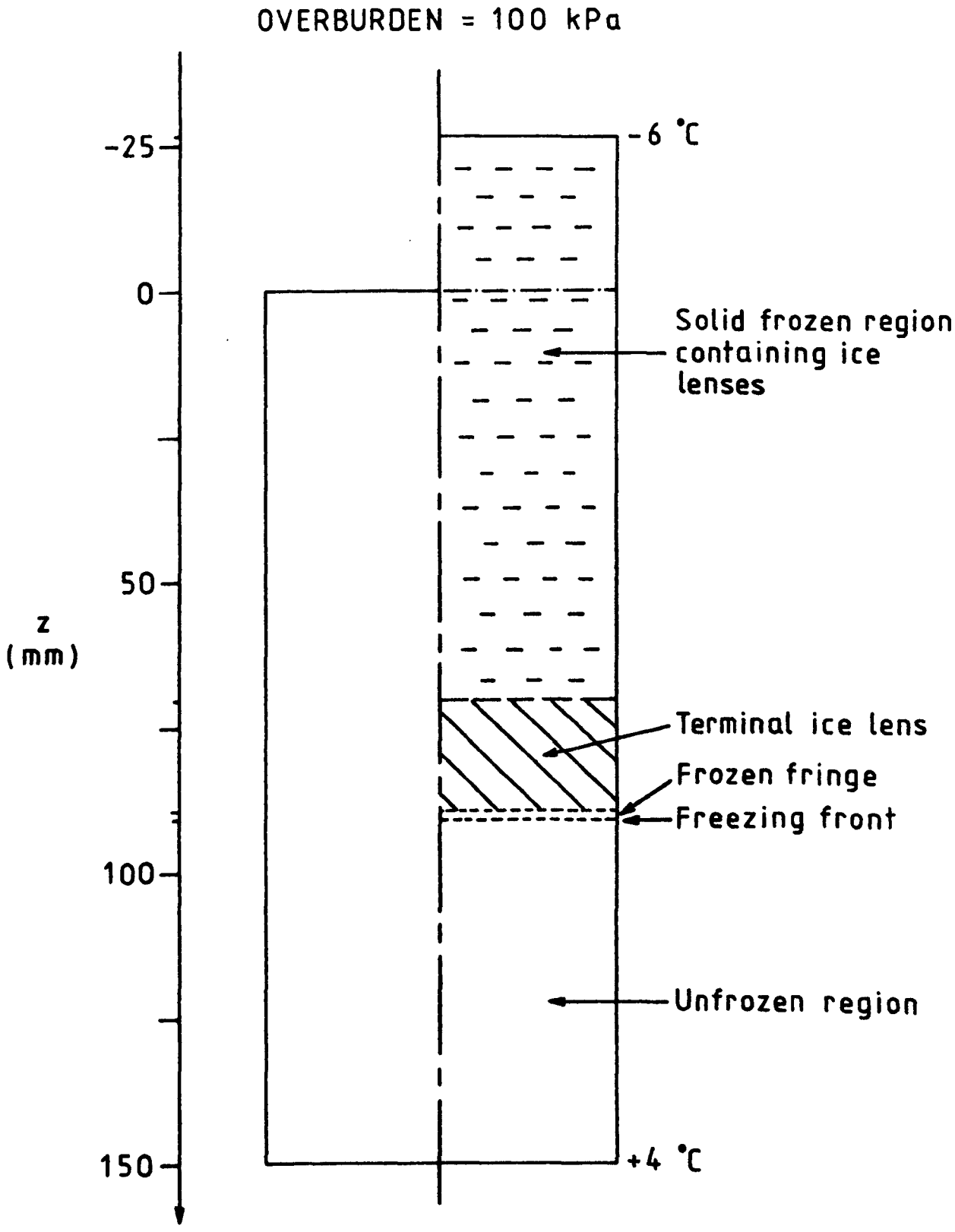

Figure 5.8 Schematic view of a heaved soil sample as predicted by the model (with exact vertical dimension)

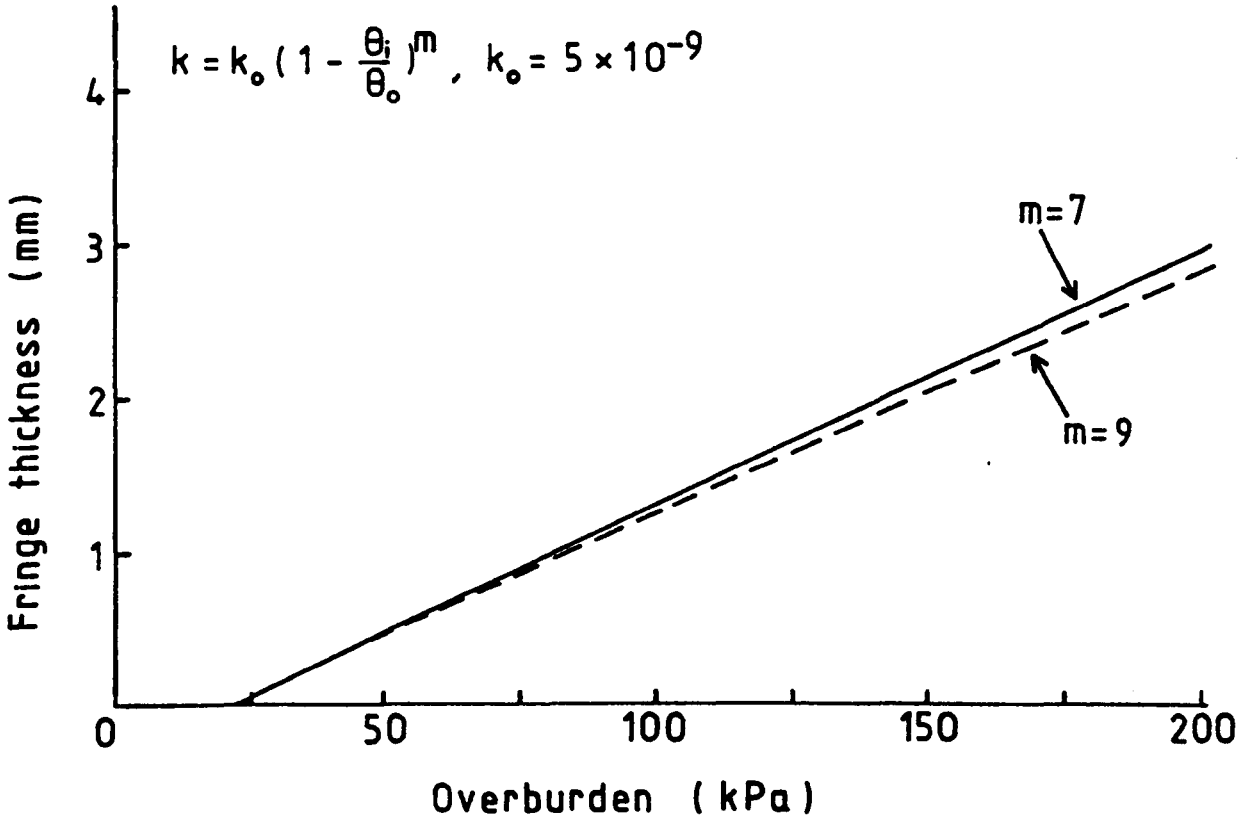

Figure 5.9 Thickness of the frozen fringe, at steady state conditions, versus overburden

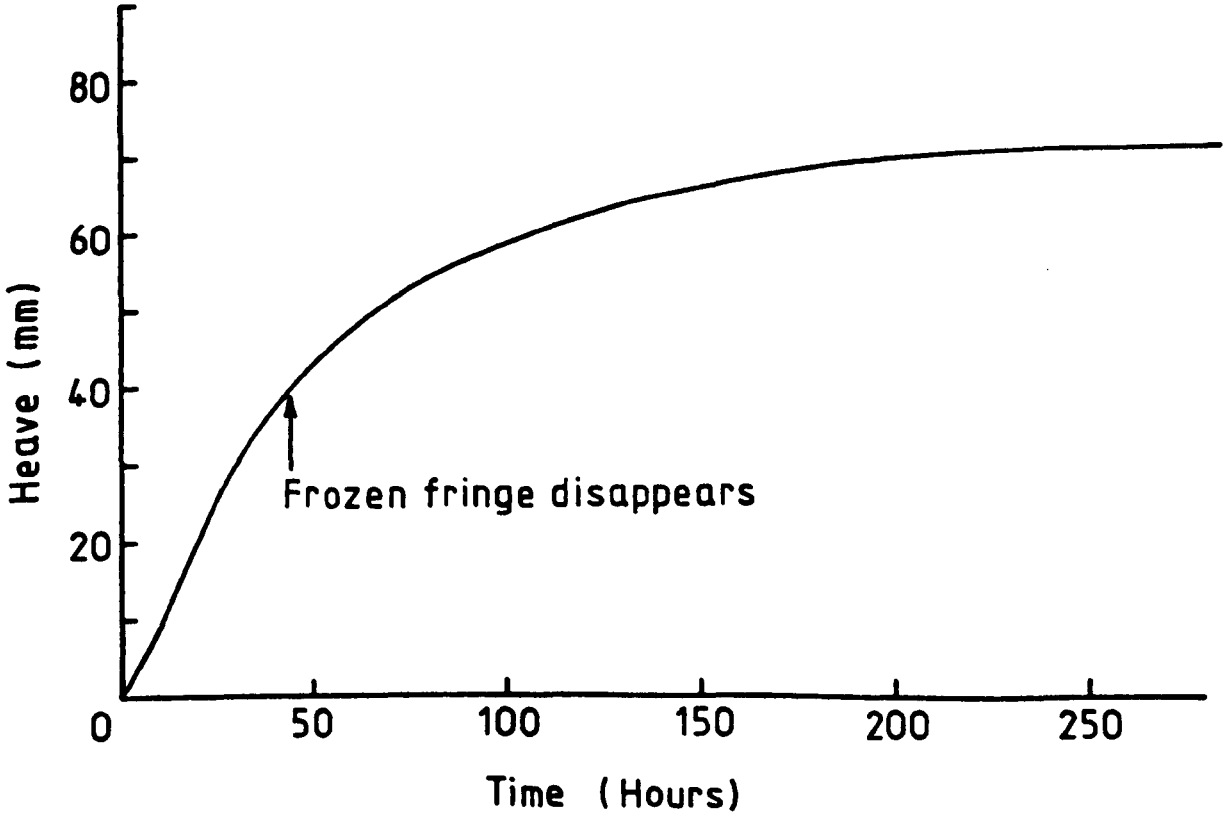

Figure 5.10 Heave versus time curve for zero overburden, showing the point when the frozen fringe disappears

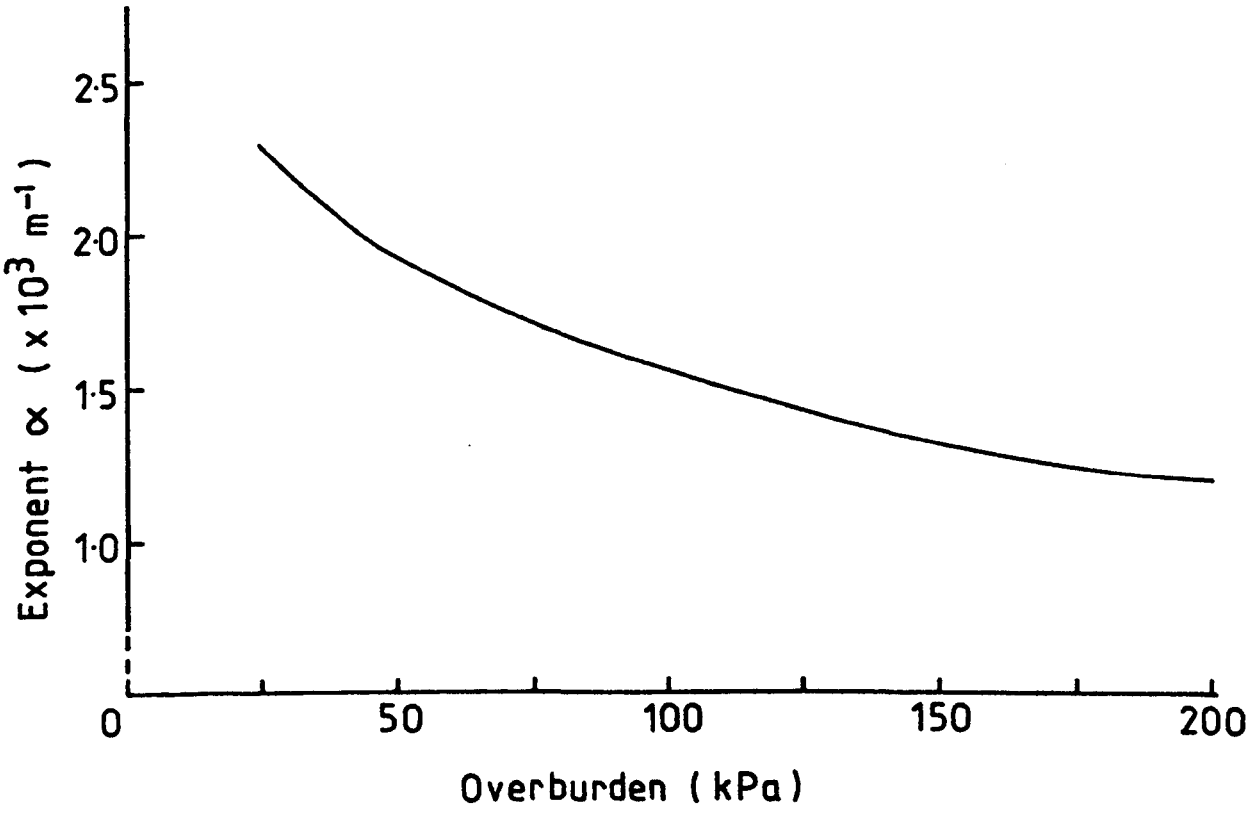

Figure 5.11 Water pressure exponent α against overburden, where the value of α is that at the time when the heave rate drops below 0.01 mm/hour

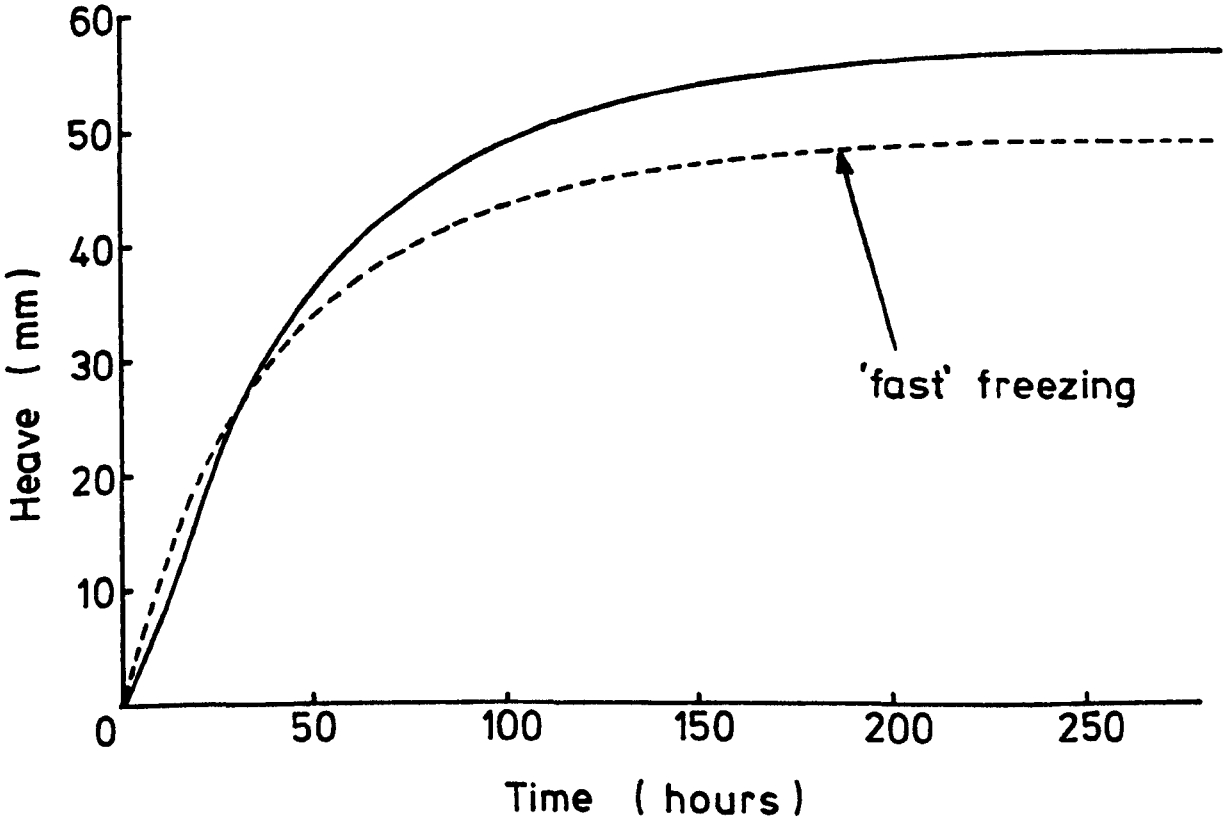

Figure 5.12 Heave versus time curves showing the effect of a faster freezing rate (overburden = 25 kPa)

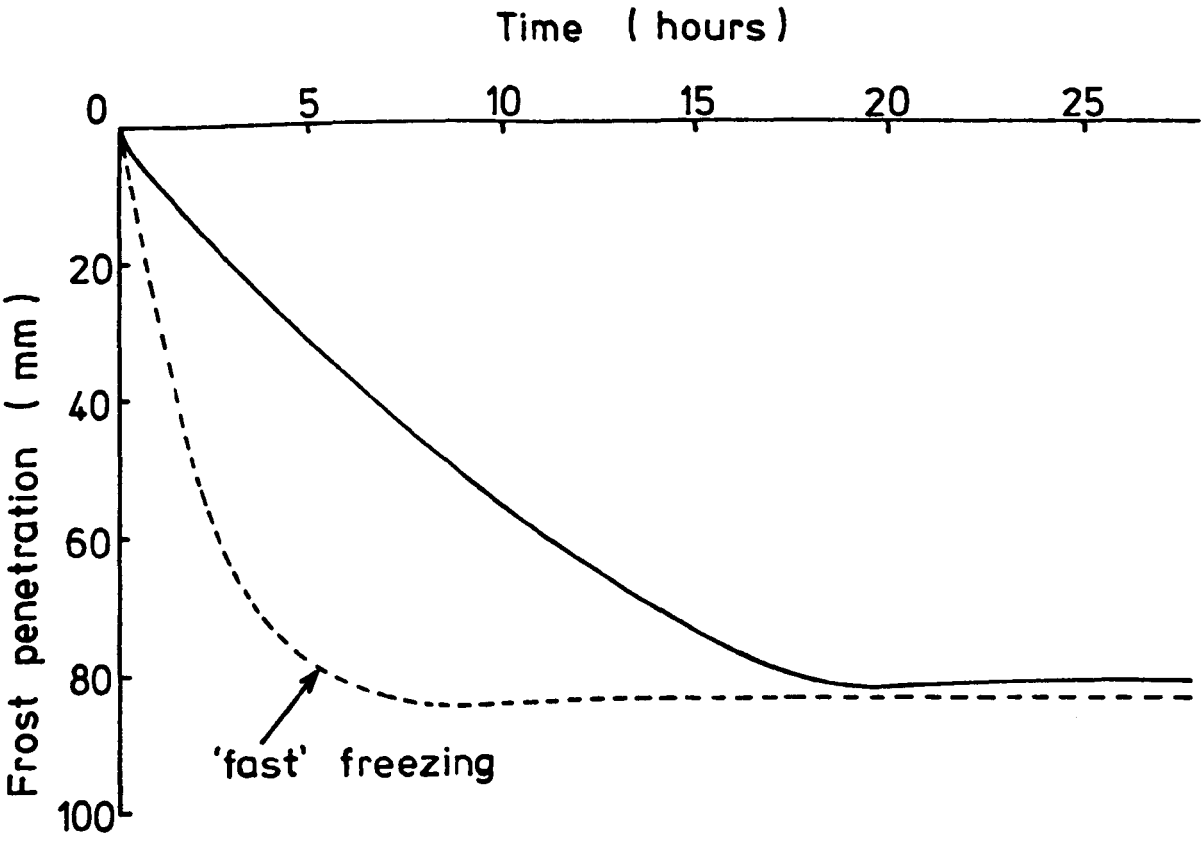

Figure 5.13 Effect of a faster freezing rate on the frost penetration (overburden = 25 kPa)

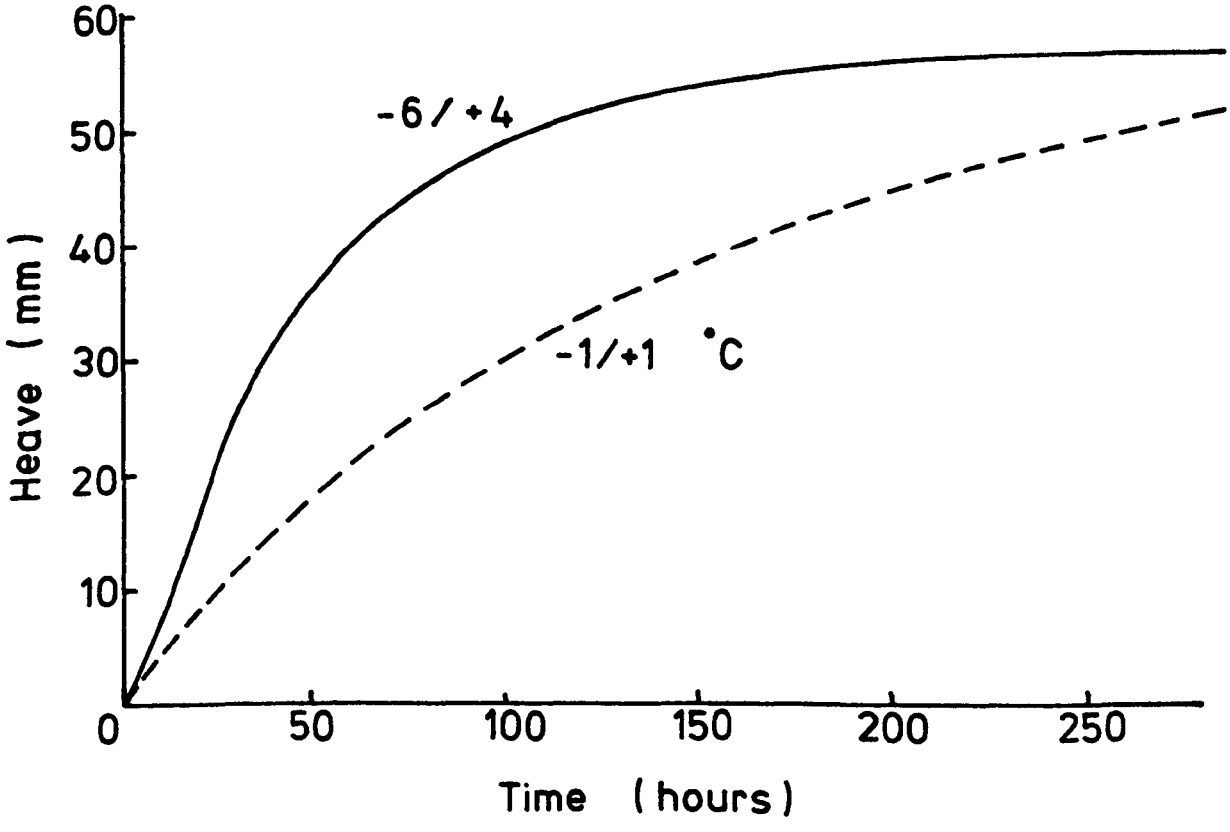

Figure 5.14 Comparison of heave versus time curves for samples frozen with different boundary temperatures (overburden = 25 kPa)

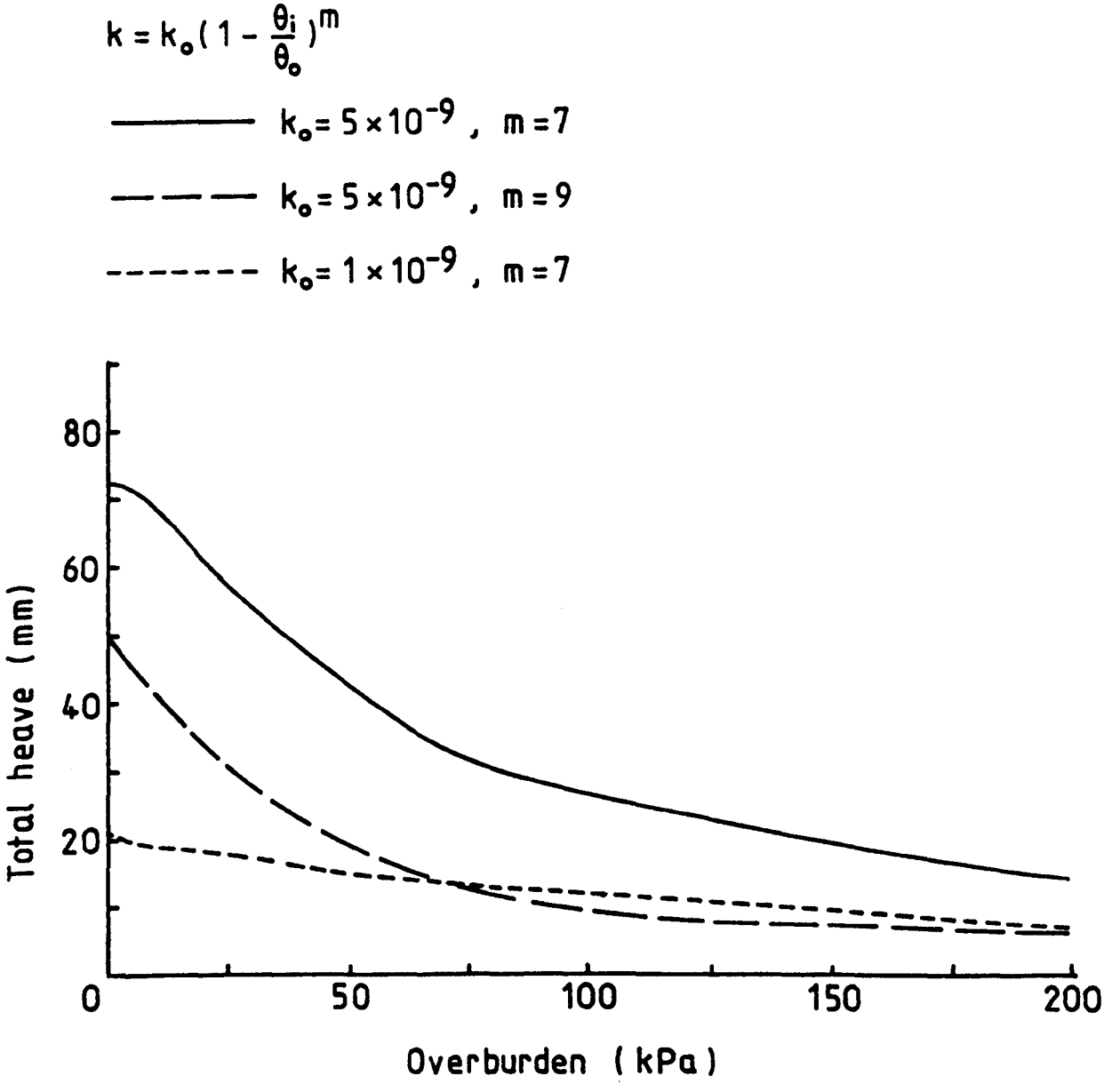

Figure 5.15 Curves of total heave against overburden due to variations in the hydraulic conductivity function

CHAPTER 6

DISCUSSION OF THE MATHEMATICAL MODEL

6.1 Introduction

This chapter contains a discussion of the frost heave model developed in this thesis, and includes an analysis of the results given in the previous chapter and a review of the model in the context of other published work. The first two sections concentrate on the computer simulations and offer evidence in support of the predicted behaviour. Sections 6.4 and 6.5 respectively assess the outcome of parametric investigations and the computational strengths of the model. Finally, the basis upon which the model is founded and the assumptions made therein are re-examined in Section 6.6.

6.2 Frost Heave and Ice Lensing

For a range of overburden pressures, the calculated heave versus time curves were given in Figure 5.3. In each case, for the first 30-50 hours of freezing, the curve is almost linear representing a near constant heave rate. After this period, the growth rate of the final ice lens, which was initiated some time earlier (see Table 6.1), begins to decrease until eventually heaving ceases as steady state conditions are attained in the soil column.

This is precisely the type of behaviour observed in laboratory freezing experiments on granular soils, as shown for example by Konrad and Morgenstern (1980) and McCabe and Kettle (1985). They respectively tested a silt and a sand/ground chalk mixture and, with samples similar in size to that chosen for the computations, the time periods over which steady conditions were achieved were close to the predicted values. Berg et al (1980) also produced an experimental curve like those in Figure 5.3, but over a longer time since their soil column was one metre in length, with the water level maintained 450 mm below the surface.

Several other researchers have traced only the linear portion of the heave versus time curve before terminating their experiments (e.g. Penner and Ueda, 1977 , Loch and Kay, 1978). Nevertheless, the computed time scales for this part of the heaving process again correspond well to those measured in the laboratory.

In general, the magnitude of the heaves reported in the literature are lower than the values calculated by the model, but it is difficult to draw any firm conclusions from this. The actual heave is strongly dependent on the particular soil tested, the temperature boundary conditions and the applied overburden. The soil modelled in the simulations, Attenborough silt, is highly frost-susceptible. For this soil, Thompson (1981) measured a heave of 31 mm for an unloaded specimen, but data were not available for other overburdens. However, Berg et al (1980) recorded around 60 mm of heave with a sample of Fairbanks silt, which has a similar grading curve to

Attenborough silt, with an overburden of 3.5 kPa.

The relationship between the predicted total heave and the overburden pressure was plotted in Figure 5.4 and is in agreement with observation, as demonstrated by McCabe and Kettle (1983). From their experiments on artificially blended granular materials, they concluded that frost heave is related to overburden by a hyperbolic curve that depends on the type of material.

McCabe and Kettle (1985) have also investigated the effects of different temperature boundary conditions and freezing rates on the frost heave. Using cold temperatures of -8 and -10°C, increases in the heave of up to 7 mm were obtained with "slow" freezing tests as compared with "rapid" freezing. Figure 5.12 illustrates that this behaviour is successfully reproduced by the mathematical model. In this particular case, "fast" freezing led to a reduction in the total heave of around 8 mm.

In another part of the same study, McCabe and Kettle showed through a series of five experiments that, all other things being equal, a lower surface temperature does not necessarily produce a greater overall heave. This provided evidence in support of the calculations depicted in Figure 5.14, which shows the results of two simulations with different temperarure boundary conditions. Effects such as these have given rise to the concept of an optimum heat extraction rate for a soil (Loch, 1979), the existence of which was confirmed by McCabe and Kettle.

One of the features of the ice lensing process which is clearly identified by the model is the cycling of the heave rate and penetration rate during successive lens formations (Figures 5.5 and 5.6). Although this phenomenon has not been reported in the experimental literature, this is hardly surprising. The resolution of typical heave-time curves, plotted with time scales such as those in Figure 5.3, is not sufficient to manifest the fluctuations visible in Figure 5.6. Moreover, readings in the laboratory are often taken at discrete intervals, rather than continuously, and would therefore be unlikely to detect the formation of individual ice lenses. The "cycling" has however been predicted by other mathematical models, notably those of Gilpin (1980) and Hopke (1980), and Miller (1984a) has indicated agreement with the form of Figure 5.6.

In Table 6.1, the computed time of formation of the final ice lens, and temperature at the base of the final lens when it is initiated, are given for a range of overburden pressures. In each case, the final lens is formed after approximately 20 hours of freezing, which is in close agreement with experiments on granular soils under comparable conditions (Konrad and Morgenstern, 1981, 1982b, Ishizaki and Nishio, 1985). Therefore, as demonstrated by Figures 5.3 and 5.8, the terminal lens accounts for the majority of the heave in the simulations, and this is also in accord with most laboratory frost heave tests (e.g. Konrad and Morgenstern, 1980, Akagawa et al, 1985).

OVERBURDEN (kPa)	TIME OF FORMATION OF FINAL ICE LENS (Hours)	TEMPERATURE AT BASE OF FINAL LENS WHEN FORMED (°C)
0	20.4	-0.080
5	18.8	-0.085
25	19.7	-0.106
50	20.1	-0.132
75	23.8	-0.158
100	19.6	-0.185
125	19.2	-0.213
150	22.1	-0.240
175	19.6	-0.266
200	19.7	-0.293

Table 6.1 Time and Temperature of Formation of the Final Ice Lens as Predicted by the Model

From Table 6.1, it can be seen that the temperature at the base of the final ice lens decreases with increasing overburden pressure, a trend which has been confirmed experimentally by Penner and Goodrich (1980) and Penner (1982). Such variation is in fact reflected throughout the lensing process and not just for the terminal lens. The temperature data in Table 6.1 have been plotted against the overburden in Figure 6.1, which reveals an exactly linear relationship between the two. Only Konrad and Morgenstern (1982b) have performed comparable measurements in this area with their studies of the formation of the terminal lens in samples of Devon silt. They obtained a linear relationship between lens temperature and overburden almost identical to that in Figure 6.1.

6.3 The Frozen Fringe and the Freezing Front

The penetration of the freezing front into the soil column during the course of a simulation was shown in Figure 5.13, for two different freezing conditions. The overall shape of these curves is similar to those produced in laboratory tests, as illustrated by Penner and Ueda (1978), Holden et al (1980) and Konrad and Morgenstern (1981). The model also predicts that the depth of frost penetration increases with increasing overburden, that is decreasing heave. That this must be the case can be inferred from consideration of the conditions existing at thermal equilibrium (steady state). Given fixed boundary temperatures, the heat flux through the soil column is constant, the temperature profile in each region is linear, heaving has ceased and the freezing front is stationary. Therefore, a column with an increased overburden, and hence a decrease in the total heave, must have a greater depth of frost penetration in order to maintain the steady thermal regime.

A plot of the calculated thickness of the frozen fringe at thermal equilibrium versus the overburden was given in Figure 5.9. A general increase in the fringe thickness with increasing overburden has been reported by Penner and Goodrich (1980), Penner (1982) and Konrad and Morgenstern (1982), although the linearity in Figure 5.9 has neither been confirmed nor contradicted. The eventual disappearance of the frozen fringe below around 25 kPa is discussed shortly.

It is apparent from Figure 5.5 that, after initiation of the final

ice lens, the rate of frost penetration becomes negative, that is the freezing front begins to retreat back towards the ice lens. This is accompanied by warming of the base of the final lens, which results in a decrease in the ice content and the suction there. Consequently, the heave rate decreases since growth of the lens is now retarded. This behaviour is explained with the aid of Figure 6.2.

After formation of the terminal lens, the soil continues to heave as steady state conditions are approached. In Figure 6.2, steady conditions are represented by a linear temperature profile throughout the soil column. This of course will only be true if the thermal conductivities in each region are the same. Nevertheless, the approximation is sufficient for the purposes of illustration. As further heaving occurs, the fixed boundary temperatures cause the freezing front to be "pulled upwards" in order to preserve the thermal balance. At the same time, the temperature at the base of the final lens increases.

By its nature, this process takes place at an ever decreasing rate, since the heave rate is decaying due to warming of the lens. Eventually, all movement stops when a true equilibrium state is reached. (Both the heave rate and penetration rate ultimately drop to zero in Figure 5.5).

Experimental evidence of these phenomena in granular soils has been provided by a number of researchers, in particular Penner and Goodrich

(1980), Konrad (1980), Penner (1982) and Ishizaki and Nishio (1985). Indeed, in formulating their segregation potential theory, Konrad and Morgenstern (1980) initially assumed that in a constant temperature freezing test the final ice lens is created when the freezing front becomes stationary. However, they later (1982a) conceded that the final lens must form before a stationary position is reached.

For relatively high overburden pressures, a frozen fringe remains after steady conditions have been attained in the soil column. Conversely, if the overburden applied to the soil is small or zero, the above description requires extension. After initiation of the terminal lens, the continuing frost heave may be so great as to cause the freezing front to retreat all the way back to the base of the lens. In other words, the frozen fringe can disappear completely, and this is precisely what is predicted by the mathematical model. As before, warming, but not melting, of the base of the ice lens then occurs until the heave rate eventually decays to zero.

As explained in Chapter 4, Section 4.10, an additional mechanism was included in the model to allow the simulations to continue in the absence of a frozen fringe, and an example of this was shown in Figure 5.10. Thus it appears that, under low overburden pressures, the secondary heaving model reduces in time to the primary model.

There is unfortunately very little discussion on this aspect in the literature. Konrad and Morgenstern (1980) stated that they expect the temperature at the base of the last ice lens to reach 0°C, for

zero overburden, which implies the absence of a fringe. They have also (1982b) photographed an unloaded sample of Devon silt which apparently does not contain a frozen fringe ahead of the final lens. Jones (1980), who was concerned with the frost heave of roads, suggested that an overburden pressure not significantly greater than zero contributes to a special case in which secondary heaving reduces to primary heaving. Finally, Gilpin (1980) predicted the disappearance of the frozen fringe with his model.

Certainly, the eventual loss of the frozen fringe under low overburden pressures is plausible. The retreat of the freezing front after formation of the terminal lens is a recognised occurrence and there is no reason to suppose that this must always cease before the fringe disappears completely.

The overburden below which a frozen fringe will be absent can in fact be calculated from an analysis of the Clapeyron equation at steady state conditions. This yields a formula for the "threshold" overburden as a function of the freezing front temperature, T_f. The form of the Clapeyron equation used throughout this thesis and derived in Appendix A is:

$$\frac{u_i}{\rho_i} - \frac{u_w}{\rho_w} = \frac{-LT}{T_o} \qquad \ldots (6.1)$$

When thermal equilibrium is reached, water flow ceases and $u_w \simeq 0$, so that at the base of the ice lens:

$$u_i = P = -\rho_i \frac{LT_s}{T_o} \qquad \ldots (6.2)$$

For a frozen fringe to exist in the soil, the ice lens temperature, T_s must be less than T_f. Therefore, the overburden necessary to sustain a frozen fringe at steady state is given by:

$$p > \frac{-\rho_i L T_f}{T_o} \qquad \ldots (6.3)$$

In the simulations, T_f was chosen to be -0.02°C, and hence from (6.3) the minimum overburden is 22.5 kPa. This is indeed the value obtained in the computations, as illustrated in Figure 5.9.

The choice of freezing front temperature, or freezing point depression, is thus an important one and estimates are normally based on information related to the particle size distribution of the soil. Recalling the Laplace surface tension equation:

$$u_i - u_w = \frac{2\sigma_{iw}}{r_{iw}} \qquad \ldots (6.4)$$

assuming the ice pressure at the freezing front is zero, (6.4) can be combined with (6.1) to produce an expression for the freezing front temperature, as follows:

$$T_f = \frac{-2\sigma_{iw}}{r_{iw}} \frac{T_o}{\rho_w L} \qquad \ldots (6.5)$$

Clearly, T_f depends on the radius of the ice/water interface, r_{iw} (see Figure 2.2), and methods of determining this from particle size distribution curves have been described by Sutherland and Gaskin (1973). For the current model, the following procedure was adopted:

the relationship between the soil particle radius, R and r_{iw} was taken to be $R/r_{iw} = 6.46$, based on an arrangement of close-packed spheres. Typically, particle radius is approximated by $R = 0.5\ (D_{50})$ and the grading curve for Attenborough silt given by Thompson (1981) yields $D_{50} = 0.03$ mm $= 3 \times 10^{-5}$ m. This leads to $r_{iw} = 2.32 \times 10^{-6}$m and, from (6.5), $T_f = -0.02°C$. This value for the freezing front temperature is unchanged (to two decimal places) if $R/r_{iw} = 5.6$, as recommended by Everett and Haynes (1965).

In contrast, Gilpin (1980) used for his model:

$$T_f = \frac{-4\sigma_{iw}}{R} \frac{T_o}{\rho_w L} \qquad \ldots (6.6)$$

which, when compared with (6.5), implies $R/r_{iw} = 2$. Gilpin performed simulations for values of R between 0.5 and 4.0×10^{-6} m, resulting in a range of T_f from -0.22 to -0.03°C. For the case $R = 2 \times 10^{-6}$ m, $T_f = -0.054°C$ and with an overburden pressure of 50 kPa, Gilpin predicted the disappearance of the frozen fringe which would be expected from Equation (6.3).

The value of -0.02°C used in the calculations for the freezing point depression appears to be reasonable, although there is evidently some debate as to how T_f should be determined. It would therefore be of benefit to investigate the effect of variations in T_f on the computed heave.

6.4 Analysis of the Key Parameters

A description of the variation in the water pressure profile exponent α (Equation (4.56)), both during the course of a simulation and with respect to the overburden, was provided in Section 5.5 and Figure 5.11. It is however difficult to draw from this any specific conclusions regarding the particular shape of the profile since its form also depends on the pressures at the top and bottom of the frozen fringe, u_s and u_f, and on the fringe thickness $(z_f - z_s)$, all of which are unknowns determined by the model.

Nevertheless, the extent of the agreement between the computer predictions and experimental observation is sufficient to support the use of the exponential approximation. The main advantage of this approach is that it affords greater flexibility by allowing the precise form of the water pressure profile to be computed by the model. This is achieved by satisfaction of mass continuity across the frozen fringe. Moreover, it removes the need to impose additional assumptions, such as continuity of water pressure gradient at the freezing front (cf. Holden, 1983). With the exception of the initial stages of a simulation (see Section 5.2), the calculation of α is numerically stable and convergence of the iteration scheme is normally achieved in one or two iterations. The exponential profile is mentioned again in Section 6.6.

The main items of soil data required by the model are the hydraulic conductivity in the frozen fringe, the ice content (or unfrozen water

content) as a function of the suction parameter ψ, and the thermal conductivity of the freezing soil. Of these, the thermal conductivity presents the least difficulty from a modelling point of view.

As explained in Chapter 5, the thermal conductivity was taken to be constant in each of the three regions (solid frozen, frozen fringe, unfrozen) of the soil. A similar strategy was adopted by Gilpin (1980), O'Neill and Miller (1980) and Konrad and Morgenstern (1984), reflecting the view that frost heave modelling is relatively insensitive to inaccuracies in the thermal conductivity. More accurate representations are possible and indeed could be easily included in the model. One example is the method of De Vries (1963), used by Harlan (1973), Taylor and Luthin (1976) and Hopke (1980), among others. Another alternative, chosen by O'Neill and Miller (1985), employs an effective conductivity in the frozen zone and a geometric mean formula in the frozen fringe. However, for present purposes, constant values in each region are thought to be adequate and, as shown by the simple parametric study discussed in Section 5.5, any errors are largely quantifiable.

As a result of the findings of Koopmans and Miller (1966), ice content as a function of ψ (the soil freezing characteristic) is determined readily from suction-moisture content data (the soil water characteristic) for the soil, and the latter can be measured accurately in the laboratory. In spite of this, experience during the development of the model (Chapter 4) highlighted the need for reliable data in this area. When investigating the heave under a range of overburden pressures,

the representation given by O'Neill and Miller (1980) was found to be anomalous. It appears likely that they too had problems with this because they later (O'Neill and Miller, 1985) adopted a "more realistic" soil freezing characteristic (see Figure 3.2). For the simulations described in the previous chapter, an approximation was made to soil water data for Attenborough silt (Thompson, 1981), as illustrated in Figure 4.1.

Without doubt, the most important input parameter in the mathematical formulation is the hydraulic conductivity in the frozen fringe, usually expressed as a function of unfrozen water or ice content. The difficulty arises because predictions of heave are highly sensitive to variations in its representation, and yet its measurement challenges the limits of current laboratory techniques. The requirement for accurate hydraulic conductivity data in frost heave modelling has been established by a number of researchers, as indicated in the review of mathematical models in Section 2.10. The sensitivity of the present model was demonstrated in Figure 5.15.

For convenience and in the absence of more appropriate data, Equation (4.5) was used to describe hydraulic conductivity as a function of ice content, following O'Neill and Miller (1980, 1985). For Attenborough silt, the only information available on hydraulic properties was the saturated unfrozen permeability, k_o, which is 10^{-8} ms^{-1}, according to Jones and Lomas (1983). This is slightly higher than the value assumed in the majority of the calculations, namely $k_o = 5 \times 10^{-9}$ ms^{-1}.

Attempts to measure water migration and hydraulic conductivity in

frozen soils at different temperatures have been made by Burt and Williams (1976), Perfect and Williams (1980) and Horiguchi and Miller (1980, 1983). Therefore, "the art of making direct measurements of hydraulic conductivity functions for frozen soils is developing slowly" (Horiguchi and Miller, 1983). Nonetheless, strict verification of the frost heave model will demand accurate data for this crucial parameter. Fortunately, for unidirectional freezing of an initially ice-free soil column, the hysteresis observed by Horiguchi and Miller need not be accounted for, except perhaps when the freezing front retreats after formation of the terminal ice lens.

6.5 Computational Aspects

As pointed out by Holden (1983), solution of the full partial differential equations for mass and energy in the frozen fringe is difficult and computationally expensive. This is chiefly because the fringe is a relatively narrow region across which large gradients exist, particularly in the water pressure. Consequently, a very small mesh size and a correspondingly small time step are necessary to model adequately the activity in the fringe. The problem is further aggravated by the need to iterate, since the equations are nonlinear.

Therefore a major advantage of the quasi-static approach is that it provides a considerable saving in computing effort without any serious loss in the predictive capability of the model. This is achieved by reducing the numerical problem to that of a straightforward temperature

calculation and the solution of two ordinary differential equations. During the early stages of a simulation, a small time step is required to accommodate the rapid freezing and the initiation of many very thin lenses. This is true also of the finite element solution of O'Neill and Miller (1980, 1985). However, because of the simplicity of the present approach, the computational penalty paid for this initial repetitive calculation is very small compared with that of O'Neill and Miller. The model then uses a time step appropriate for the movement of the freezing front.

The results presented in the previous chapter illustrate that the model is able to predict the frost heave of a soil column under any overburden pressure, and the computations remain stable throughout. This again is in contrast to O'Neill and Miller (1985), who reported that their simulations tended to become unstable during the "terminal stage of heave". This apparently did not occur under relatively high overburdens, but "the lower the value of P, the more likely were stability problems". It seems certain that these numerical difficulties were associated with the shrinking and eventual disappearance of the frozen fringe after formation of the final ice lens. As suggested by O'Neill (1983), the physics built into the model was evidently not adequate to cope with this behaviour.

Finally, O'Neill and Miller (1985) included in their program a routine to improve the accuracy of the calculation of lens initiation times. This operated in the following way: when the maximum of the neutral stress exceeded the overburden during any one time step, the last time

step was shortened and recalculated. This process was then repeated iteratively until the moment when u_n exceeded P was located precisely. After the initiation of each new lens, the time step was reset. In order to test its effectiveness, an attempt was made to incorporate a similar procedure into the current model. This was successful, but it was found to have negligible effect on the number and thickness of ice lenses and the overall heave. As the improvements were thus relatively minor, the extra computing effort was not thought to be warranted.

6.6 Summary of the Basis of the Model

The model for frost heave described in this thesis is founded upon Miller's theory for secondary heaving, in which the rigid ice assumption plays a key role. The quasi-static approach then makes a number of simplifications regarding temperature and water pressure, based on a knowledge of the conditions existing in a column of freezing soil.

The primary components of Miller's theory can be summarised as follows:

(1) The Clapeyron equation, describing the thermodynamics of the pore system.

(2) Concepts relating the different phases of the pore constituents, verified by experiment. These support the

use of the Laplace surface tension equation, Darcy's law for water flux and the soil freezing characteristic.

(3) A criterion for the initiation of ice lenses derived from pore stress partitioning.

In the strict thermodynamic sense, the Clapeyron equation is only applicable to equilibrium conditions. However, a number of researchers have confirmed its validity for predicting the conditions beneath a growing ice lens, in spite of the non-equilibrium environment (Penner and Goodrich, 1980, Konrad and Morgenstern, 1980, Yoneyama et al, 1983). It may be that although globally the system is not in equilibrium, in the region of a soil pore equilibrium may be maintained locally. Measurements have also shown, and it is now widely accepted, that Darcy's law can be applied to water flow through partially frozen soils (see for example, Horiguchi and Miller, 1980).

Ultimately, solution of the equations of the model is made possible by the rigid ice assumption, wherein ice forms on pre-existing ice and thus grows through the soil pores to form one solid body. This implies that ice in the frozen fringe is rigidly connected to lens ice, and both move toward the cold boundary during heave. In order therefore to accommodate the stationary soil matrix, this motion involves a process of microscopic regelation. That is, as the ice migrates, melting takes place on the warm side of soil grains and refreezing on the cold side.

The concepts of rigid ice and regelation are thus of fundamental

importance to the theory. Although strict proof of the existence of these mechanisms has yet to be found, the circumstantial evidence in their favour is strong (Miller, 1984b, Römkens and Miller, 1973), and alternative assumptions seem implausible (O'Neill and Miller, 1985).

Motivated by the slow nature of the freezing process, the quasi-static apprach uses approximating profiles for temperature and water pressure, to simplify the mathematical formulation of the theory and the subsequent computation. A linear temperature profile is assumed in the region above the base of the warmest ice lens and in the frozen fringe. The former is supported by the experimental observations of, for example, Jame and Norum (1976) and Fukuda et al (1980), and has also been adopted by Gilpin (1980) and O'Neill and Miller (1980, 1985). The assumption of a linear profile in the fringe is a stronger one but Konrad and Morgenstern (1980) concur with this. Moreover, O'Neill and Miller (1980, 1985) computed the temperature distribution in the fringe from the full partial differential equations and gave an example in which the temperature profile is almost linear.

From a knowledge of the behaviour of the soil water suction, the water pressure profile in the frozen fringe is assumed to have an exponential form. This is in agreement with Miller's (1977, 1978) own description of the conditions in the fringe and adequately represents the profile visualised by most other researchers.

The model is formulated by applying conservation of mass and energy

at the boundaries of the frozen fringe. In addition, the precise form of the water pressure profile is established by imposing mass continuity across the fringe. The basic equations are reduced to a pair of ordinary differential equations, which are solved by a standard numerical procedure. The model retains the ability to predict the time, position and thickness of each ice lens.

Finally, the comments of O'Neill and Miller (1985) regarding the "completeness" of the model are echoed. Clearly, it is possible to obtain a set of equations for which solutions exist for the quantities of interest. However, it may be that certain interactions which take place on a microscopic level should also be included in the model. For example, regelation is a complex process involving the recirculation of water and heat on a microscopic scale. Whether such processes are implicitly modelled in the macroscopic equations, or whether they should be quantified explicitly is not clear. The general form and magnitude of computer predictions suggests that these effects, if absent, may be small but may nevertheless represent "corrections" to the macroscopic model.

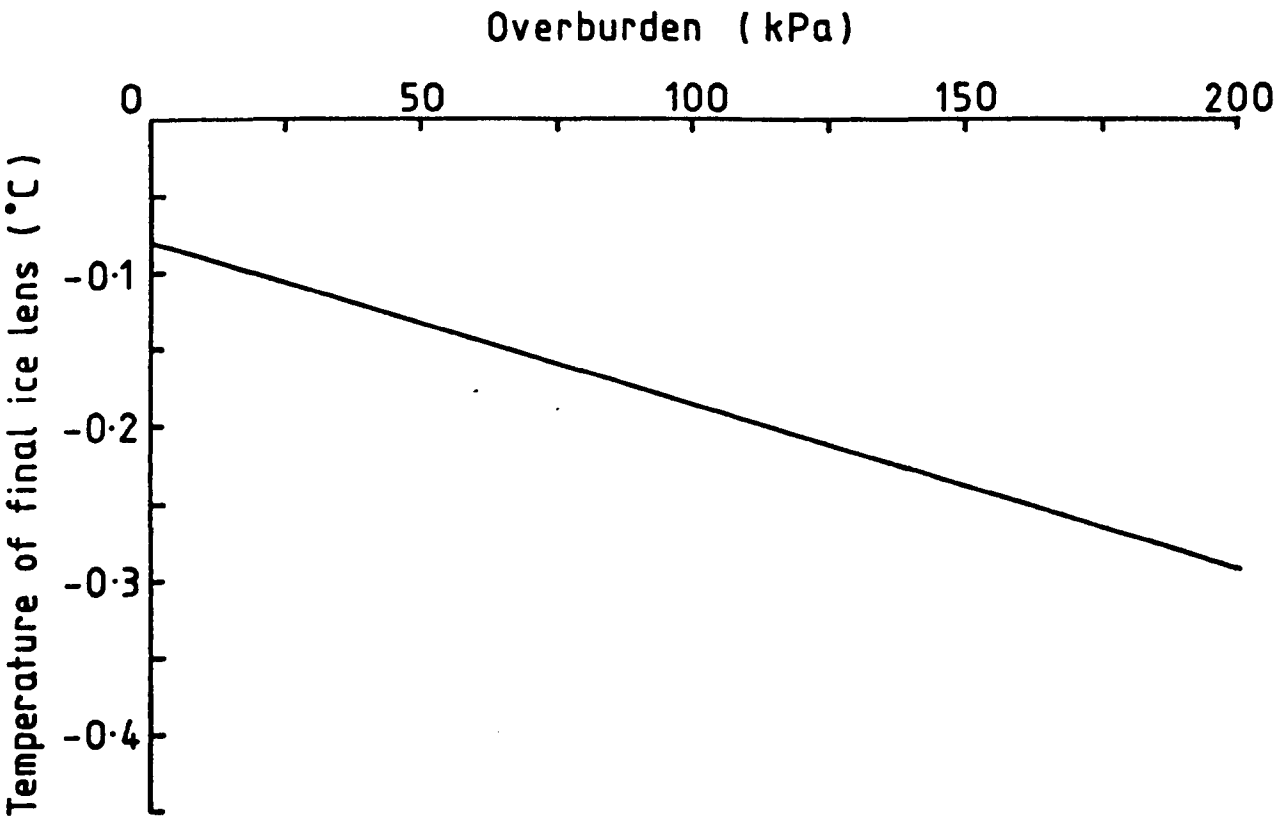

Figure 6.1 Temperature at the base of the final ice lens when it is initiated versus overburden

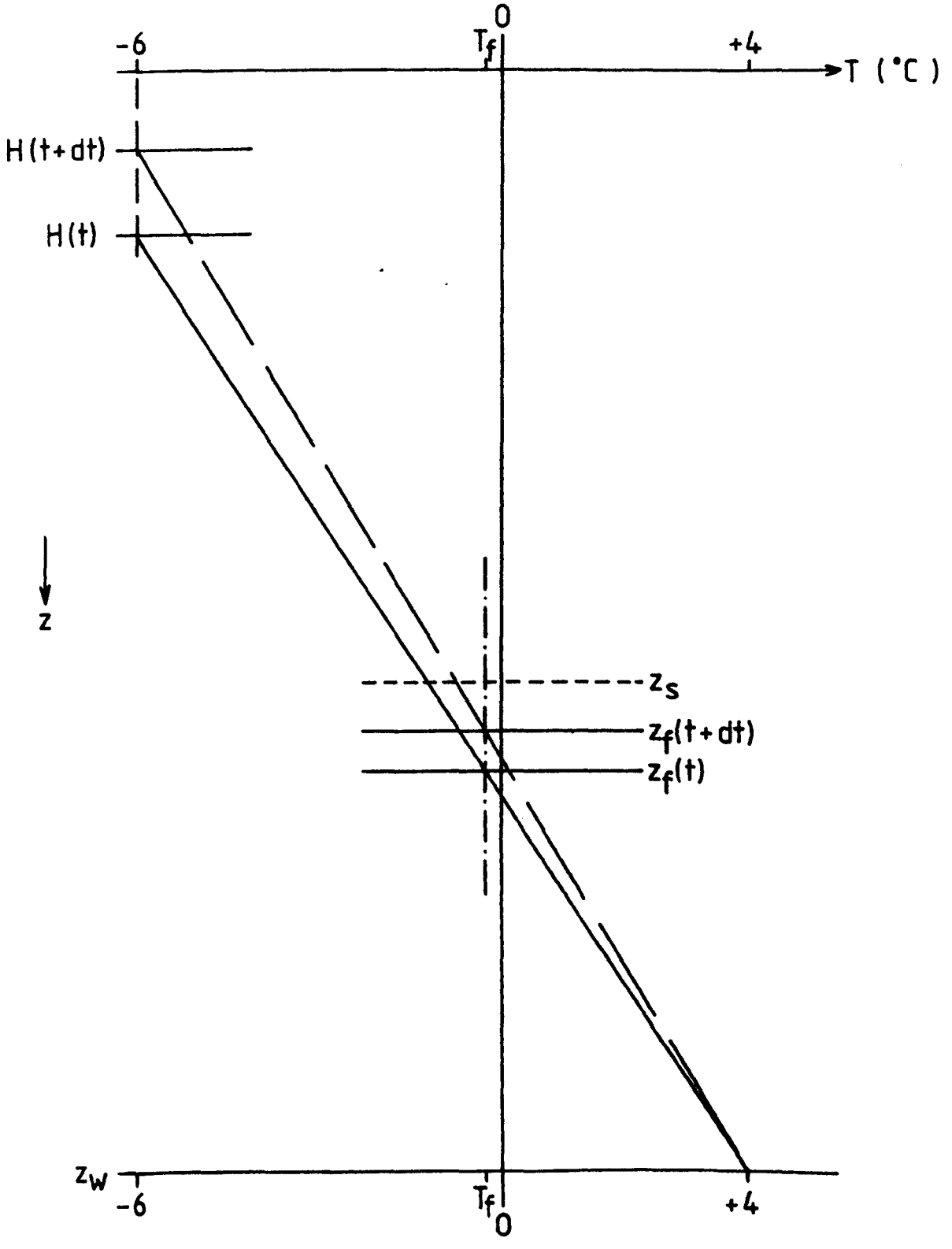

Figure 6.2 Schematic diagram depicting the retreat of the freezing front and the warming of the base of the final lens, as steady conditions are approached in the soil column

CHAPTER 7

CONCLUSIONS AND RECOMMENDATIONS

7.1 Summary of the Model

In this thesis, a mathematical model for frost heave and ice lensing has been developed, based on the theory of secondary heaving proposed by Miller (1972, 1977, 1978). Miller's theory was chosen as the foundation for the model following a critical review of research into frost heave and, in particular, the state of the art in mathematical modelling.

The main aim was to simplify the mathematical formulation, and the subsequent computation, whilst retaining the capability to predict the observed phenomena. This has been achieved by using a quasi-static approach to the solution of the governing equations, as suggested by Holden (1983).

The results of computations simulating the unidirectional freezing of a finite column of soil have demonstrated that the model performs well under a range of boundary conditions. For any applied overburden pressure (including zero), predictions of frost heave and ice lensing can be made and the simulations continue to steady state conditions. In addition, under relatively low overburdens, the model not only predicts the disappearance of the frozen fringe after formation of

the terminal lens, but also contains a mechanism for calculating the heave after this has occurred. Thus, both primary and secondary heaving are modelled. The numerical problems experienced by O'Neill and Miller (1985) during the final stages of heaving have therefore been avoided.

The results of the calculations are in agreement with laboratory freezing tests in both form and magnitude, and the model responds to changes in the boundary conditions in accordance with observation.

Moreover, parametric studies can be performed readily, particularly as the computer program is comparatively inexpensive to run. These investigations have shown that the frost heave model is most sensitive to variations in the hydraulic conductivity, which confirms the findings of other researchers. The importance of accurate input data for the soil freezing characteristic has also been highlighted, whilst the influence of the thermal conductivity has been found to be relatively small.

A major drawback of the model remains that it requires reliable data for certain critical parameters, notably the hydraulic conductivity in the frozen fringe, for which experimental determination is difficult. It may eventually be possible to simplify the representation of such parameters in the model, thereby reducing the need for detailed measurements. However, before this can happen, strict verification of the model is necessary which requires

development of laboratory techniques at the limits of current expertise.

Against this, the model has much to commend it in that it has a number of advantages over models employing a more complex approach. The quasi-static assumption permits formulation of the physical problem in terms of straightforward mathematics which, in turn, reduces considerably the programming effort required. As mentioned previously, experience with running the computer program has shown it to be economical, numerically stable and highly robust.

The results of the simulations provide further evidence in support of Miller's theory and confirm the validity of the quasi-static approach. The development of the model has also yielded other benefits, particularly in identifying the key areas in frost heave modelling. Successive stages in the evolution of the model focussed attention on different aspects of the idealisation, and therefore provided valuable insight into the heaving process. It is felt that this experience will improve understanding of both the secondary heave theory and the mechanics of frost heave as a whole.

7.2 Recommendations for Future Work

Having produced a model for frost heave and ice lensing which requires relatively little computing capacity, the next stage in the development would be to implement the program on a microcomputer.

This would meet the need identified by Baker et al (1987), the aim being to provide a rapid estimate of frost heave in quasi-one-dimensional situations.

Some generalisation of the program would be necessary in this case to widen its applicability. This would chiefly involve enlarging the input data file to include quantities such as the height of the soil column to be analysed, the mesh size and time steps to be used, the soil material data and so on. It may also be possible to make further simplifications according to the requirements of a particular problem. For example, an initial temperature profile could be assumed in the soil column at the onset of freezing, rather than calculating the profile during the cooling down period. These changes represent modifications only to the computer code, and not the mathematical model, and would therefore be accommodated easily.

In accordance with Miller's theory, the model applies only to saturated, solute-free, granular materials, and generalisation of the theory to three phases (unfrozen water, ice and air) is necessary before the heave of unsaturated soils can be modelled. However, in certain circumstances, the model may be useful for design purposes in providing a conservative (upper bound) estimate of the heave of unsaturated, compressible materials.

Finally, with the increasing use of artificial ground freezing techniques, there is a growing need for a theory of frost heave

applicable in two or three dimensions, from which to construct appropriate mathematical models. Such a theory must include stress analysis, coupled heat and moisture transfer and compressibility, and will therefore demand far more sophisticated soil mechanics than is contained in the one-dimensional theory. Thus, although significant progress has been made in frost heave modelling, as exemplified by the work described in this thesis, considerable challenges remain for future researchers.

APPENDIX A

DERIVATION OF THE CLAUSIUS-CLAPEYRON EQUATION

The following derivation is relatively simple and not entirely rigorous, but is considered to be sufficient for present purposes. A more complete derivation is provided by Loch (1978).

Edlefsen and Anderson (1943) define the absolute free energy, f, of a material to be:

$$f = e + uV - Ts \qquad \ldots (A.1)$$

where: e = internal energy

u = pressure

V = specific volume

T = absolute temperature

s = entropy

and: f is equivalent to the Gibbs free energy, g, used by Gold (1957) (Section 2.3). For two phases to coexist in equilibrium, their absolute free energies must be the same. Therefore, using the suffices i and w for ice and water:

$$f_i = f_w \qquad \ldots (A.2)$$

Furthermore, when any change occurs in the system, the two free

energies must change by an equal amount, that is:

$$df_i = df_w \qquad \ldots (A.3)$$

As no useful work is done, this implies:

$$V_i\, du_i - s_i\, dT = V_w\, du_w - s_w\, dT \qquad \ldots (A.4)$$

where the temperature change is the same in both phases.

Rearranging (A.4):

$$V_i\, du_i - V_w\, du_w = (s_i - s_w)\, dT \qquad \ldots (A.5)$$

Now: $(s_i - s_w) = \frac{-L}{T}$

where: L = latent heat of fusion, so that (A.5) can be written:

$$V_i\, du_i - V_w\, du_w = \frac{-L\,dT}{T} \qquad \ldots (A.6)$$

If the changes are assumed to be from a reference state $u_i = 0$, $u_w = 0$ (gauge pressures), $T = T_o$ (273.15 K), then:

$$du_i = u_i, \quad du_w = u_w, \quad dT = T - T_o = -\Delta T$$

where: ΔT is the freezing point depression.

Equation (A.6) then becomes:

$$V_i\, u_i - V_w\, u_w = \frac{L\Delta T}{T_o} \qquad \ldots (A.7)$$

where it is assumed:

$$\frac{\Delta T}{T} \simeq \frac{\Delta T}{T_o}$$

An alternative expression of (A.7) is:

$$\frac{u_i}{\rho_i} - \frac{u_w}{\rho_w} = \frac{-LT}{T_o} \qquad \ldots (A.8)$$

where now: T = freezing temperature in °C

Equation (A.8) is the form of the Clausius-Clapeyron equation used throughout this thesis.

APPENDIX B

FORMULATION OF CONSERVATION EQUATIONS TO MODEL HEAT AND MASS TRANSFER IN FREEZING SOIL

Consider a fixed region R containing solid particles, water, air and possibly ice. The following assumptions are made:

1. The material within the region is homogeneous;

2. Heat transfer by movement of gases and vapours within the region is negligible;

3. Free convection is negligible;

4. Water in the material pores has the same properties as bulk water except that it freezes at a lower temperature;

5. Energy losses due to evaporation are negligible.

For the mass conservation equation, the rate at which mass is transported into R is equated to the rate of mass increase in R.

The rate at which mass is transported into R is given by:

$$- \int_S \underset{\sim}{q} \cdot \underset{\sim}{n} \, dS \qquad \ldots (B.1)$$

where: $\underset{\sim}{q}$ = rate of mass transport

$\underset{\sim}{n}$ = outward normal to surface S of region R

dS = surface element

The rate at which mass is increased in R

$$= \frac{\partial}{\partial t} \int_R (\rho_w \theta_w + \rho_i \theta_i)\, dV \qquad \ldots (B.2)$$

where: θ_w, θ_i = volumetric water and ice contents

ρ_w, ρ_i = densities of water and ice

dV = volume element

Equating (B.1) and (B.2) and use of the Divergence Theorem yields:

$$\int_R [\frac{\partial}{\partial t} (\rho_w \theta_w + \rho_i \theta_i) + \text{div } \underset{\sim}{q}]\, dV = 0 \qquad \ldots (B.3)$$

This holds for any region R, hence:

$$\frac{\partial}{\partial t} (\rho_w \theta_w + \rho_i \theta_i) + \text{div } \underset{\sim}{q} = 0 \qquad \ldots (B.4)$$

Now: $\underset{\sim}{q} = \rho_w \underset{\sim}{v}$

where: $\underset{\sim}{v}$ = water flux vector

and assuming Darcy's Law applies to water flux within the region, that is:

$$\underset{\sim}{v} = -k \text{ grad } \phi \qquad \ldots (B.5)$$

where: k = hydraulic conductivity and

ϕ = total head

then (B.4) becomes:

$$\rho_w \frac{\partial \theta_w}{\partial t} + \rho_i \frac{\partial \theta_i}{\partial t} = \rho_w \text{ div } (k \text{ grad } \phi) \qquad \ldots \text{ (B.6)}$$

assuming densities remain constant. Rewriting (B.6) gives:

$$\frac{\partial \theta_w}{\partial t} + \frac{\rho_i}{\rho_w} \frac{\partial \theta_i}{\partial t} = \text{div } (k \text{ grad } \phi) \qquad \ldots \text{ (B.7)}$$

The energy equation is obtained by equating the rate at which energy increases in R to the rate of flow of energy by conduction and convection into R. The rate at which heat is conducted into R is:

$$- \int_S \underset{\sim}{Q} \cdot \underset{\sim}{n} \, dS \qquad \ldots \text{ (B.8)}$$

where: $\underset{\sim}{Q}$ = heat flux vector

The rate of convection of heat into R is:

$$- \int_S C_w T \underset{\sim}{v} \cdot \underset{\sim}{n} \, dS \qquad \ldots \text{ (B.9)}$$

where: T = temperature

C_w = volumetric specific heat capacity of water

Within R, the heat energy may change due to the heat capacity of the

material or as a result of phase change. Thus, the rate at which heat energy increases in R is:

$$\frac{\partial}{\partial t} \int_R (CT - \rho_i L\theta_i)\, dV \qquad \ldots (B.10)$$

where: C = volumetric specific heat capacity of the soil

L = latent heat of fusion of water

Equating (B.8) and (B.9) with (B.10) and using the Divergence Theorem gives:

$$\int_R \left[\frac{\partial}{\partial t} (CT - \rho_i L\theta_i) + \text{div } (\underset{\sim}{Q} + C_w T \underset{\sim}{v}) \right] dV = 0 \qquad \ldots (B.11)$$

and this holds for all regions R. Hence:

$$\frac{\partial}{\partial t} (CT - \rho_i L\theta_i) + \text{div } (\underset{\sim}{Q} + C_w T \underset{\sim}{v}) = 0 \qquad \ldots (B.12)$$

Fourier's Law of heat conduction states that:

$$\underset{\sim}{Q} = -K \text{ grad } T \qquad \ldots (B.13)$$

where: K = thermal conductivity

and substitution of this into (B.12) yields:

$$\frac{\partial}{\partial t} (CT - \rho_i L\theta_i) + \text{div } (-K \text{ grad } T) + \text{div } (C_w T \underset{\sim}{v}) = 0 \qquad \ldots (B.14)$$

If both heat and mass transfer occur in one dimension, then Equations (B.7) and (B.14) reduce to:

$$\frac{\partial \theta_w}{\partial t} + \frac{\rho_i}{\rho_w} \frac{\partial \theta_i}{\partial t} = \frac{\partial}{\partial z} \left(k \frac{\partial \phi}{\partial z} \right) \quad \ldots \text{(B.15)}$$

and:

$$C \frac{\partial T}{\partial t} - \rho_i L \frac{\partial \theta_i}{\partial t} = \frac{\partial}{\partial z} \left(K \frac{\partial T}{\partial z} \right) - C_w \frac{\partial}{\partial z} (T v_z) \quad \ldots \text{(B.16)}$$

assuming heat capacities and densities remain constant.

APPENDIX C

COMPUTING THE TEMPERATURE PROFILE AHEAD OF THE FREEZING FRONT

The finite difference formulation for computing the temperature profile in the unfrozen region is described below. The method uses Crank-Nicolson finite differences, based on a convected mesh. A formula for the temperature gradient just ahead of the freezing front is also derived.

Let the equation of the freezing front be given by:

$$z_f(t) = \varepsilon(t) \qquad \ldots (C.1)$$

so that, at the j^{th} time step:

$$z_f = \varepsilon_j \qquad \ldots (C.2)$$

The finite difference mesh is defined by:

$$\delta z_j = \frac{z_w - \varepsilon_j}{n}, \quad \delta z_{j+1} = \frac{z_w - \varepsilon_{j+1}}{n} \text{ etc.} \qquad \ldots (C.3)$$

where: n = number of "elements" into which region is divided.

Hence, the total number of mesh points is (n+1).

The temperature at a point $z = \varepsilon_j + i\delta z_j$ is denoted by $T_{i,j}$. Now,

during the small time interval δt, the velocity of the freezing front is assumed to remain constant, so that:

$$\epsilon_{j+1} = \epsilon_j + \dot{\epsilon}_j \delta t \qquad \ldots (C.4)$$

where: $\dot{\epsilon}_j$ = the speed of the front.

The distance travelled by the mesh point with temperature $T_{i,j}$ in time δt is:

$$\delta z = (\epsilon_{j+1} + i\delta z_{j+1}) - (\epsilon_j + i\delta z_j) \qquad \ldots (C.5)$$

which, with (C.3) and (C.4) yields:

$$\delta z = \left(\frac{n-i}{n}\right) \dot{\epsilon}_j \delta t \qquad \ldots (C.6)$$

Therefore, in the limit, the velocity of this point is:

$$\frac{dz}{dt} = \left(\frac{n-i}{n}\right) \dot{\epsilon}_j \qquad \ldots (C.7)$$

Since the temperature $T = T(z(t),t)$, the total time derivative is:

$$\frac{dT}{dt} = \frac{\partial T}{\partial z}\frac{dz}{dt} + \frac{\partial T}{\partial t} \qquad \ldots (C.8)$$

The one-dimensional heat equation is:

$$\frac{\partial T}{\partial t} = \mu \frac{\partial^2 T}{\partial z^2} \qquad \ldots (C.9)$$

Thus, substituting for $\partial T/\partial t$, and dz/dt from (C.7), into (C.8) gives:

$$\frac{dT}{dt} = \frac{\partial T}{\partial z}\left(\frac{n-i}{n}\right)\dot{\epsilon}_j + \mu\frac{\partial^2 T}{\partial z^2} \qquad \ldots (C.10)$$

To obtain the numerical solution for the temperature, Crank-Nicolson finite difference approximations for the derivatives are used, as follows:

$$\frac{dT}{dt} = \frac{T_{i,j+1} - T_{i,j}}{\delta t} \qquad \ldots (C.11)$$

$$\frac{\partial T}{\partial z} = \tfrac{1}{2}\left[\frac{T_{i+1,j+1} - T_{i-1,j+1}}{2\delta z_{j+1}} + \frac{T_{i+1,j} - T_{i-1,j}}{2\delta z_j}\right] \qquad \ldots (C.12)$$

$$\frac{\partial^2 T}{\partial z^2} = \tfrac{1}{2}\left[\frac{T_{i+1,j+1} - 2T_{i,j+1} + T_{i-1,j+1}}{(\delta z_{j+1})^2}\right.$$

$$\left. + \frac{T_{i+1,j} - 2T_{i,j} + T_{i-1,j}}{(\delta z_j)^2}\right] \qquad \ldots (C.13)$$

Substitution of (C.11) to (C.13) into (C.10), along with (C.3) yields:

$$T_{i-1,j+1}\left[\frac{(n-i)\,\dot{\epsilon}_j}{4(z_w-\epsilon_{j+1})} - \frac{\mu n^2}{2(z_w-\epsilon_{j+1})^2}\right]$$

$$+ T_{i,j+1}\left[\frac{1}{\delta t} + \frac{\mu n^2}{(z_w-\epsilon_{j+1})^2}\right]$$

$$- T_{i+1,j+1}\left[\frac{(n-i)\dot{\epsilon}_j}{4(z_w-\epsilon_{j+1})} + \frac{\mu n^2}{2(z_w-\epsilon_{j+1})^2}\right] \qquad \text{(continued)}$$

$$= T_{i-1,j}\left[\frac{\mu n^2}{2(z_w-\varepsilon_j)^2} - \frac{(n-i)\,\dot{\varepsilon}_j}{4(z_w-\varepsilon_j)}\right]$$

$$+ T_{i,j}\left[\frac{1}{\delta t} - \frac{\mu n^2}{(z_w-\varepsilon_j)^2}\right]$$

$$+ T_{i+1,j}\left[\frac{(n-i)\,\dot{\varepsilon}_j}{4(z_w-\varepsilon_j)} + \frac{\mu n^2}{2(z_w-\varepsilon_j)^2}\right] \qquad \ldots \text{(C.14)}$$

(C.14) represents a system of equations which can be written:

$$bT_{1,j+1} - c_1T_{2,j+1} = d_1 - a_1T_{0,j+1}$$

$$a_2T_{1,j+1} + b\,T_{2,j+1} - c_2T_{3,j+1} = d_2$$

$$a_3T_{2,j+1} + b\,T_{3,j+1} - c_3T_{4,j+1} = d_3$$

$$\vdots$$

$$a_{n-1}\,T_{n-2,j+1} + b\,T_{n-1,j+1} = d_{n-1} + c_{n-1}\,T_{n,j+1}$$

$$\ldots \text{(C.15)}$$

or, in matrix form:

$$\underset{\sim}{A}\,\underset{\sim}{T}_{j+1} = \underset{\sim}{B} \qquad \ldots \text{(C.16)}$$

where: $\underset{\sim}{A}$ is a tri-diagonal matrix

$\underset{\sim}{B}$ is a vector of "known" quantities

$\underset{\sim}{T}_{j+1}$ is the vector of unknown temperatures at the next time step

$$a_i = \frac{(n-i)\,\dot{\varepsilon}_j}{4(z_w-\varepsilon_{j+1})} - \frac{\mu n^2}{2(z_w-\varepsilon_{j+1})^2}$$

$$b = \frac{1}{\delta t} + \frac{\mu n^2}{(z_w-\varepsilon_{j+1})^2}$$

$$c_i = \frac{(n-i)\,\dot{\varepsilon}_j}{4(z_w-\varepsilon_{j+1})} + \frac{\mu n^2}{2(z_w-\varepsilon_{j+1})^2} \qquad \ldots \text{(C.17)}$$

and: $$d_i = T_{i-1,j}\left[\frac{\mu n^2}{2(z_w-\varepsilon_j)^2} - \frac{(n-i)\,\dot{\varepsilon}_j}{4(z_w-\varepsilon_j)}\right]$$

$$+ T_{i,j}\left[\frac{1}{\delta t} - \frac{\mu n^2}{(z_w-\varepsilon_j)^2}\right]$$

$$+ T_{i+1,j}\left[\frac{(n-i)\,\dot{\varepsilon}_j}{4(z_w-\varepsilon_j)} + \frac{\mu n^2}{2(z_w-\varepsilon_j)^2}\right]$$

for $i = 1, 2, \ldots, (n-1)$.

The system (C.15) is solved by the standard technique of Gaussian Elimination. The first equation is used to eliminate $T_{1,j+1}$ from the second, leaving an equation in the two unknowns $T_{2,j+1}$ and $T_{3,j+1}$. This is then used to eliminate $T_{2,j+1}$ from the third equation, and so on. This process eventually yields a value for $T_{n-1,j+1}$ from the last equation, and the remaining unknown temperatures are obtained by successive back substitution. (Note that $T_{o,j+1}$ and $T_{n,j+1}$ are known since these are the freezing front and warm boundary temperature, respectively).

The procedure for computing the temperature profile in the unfrozen

region is then as follows: from the initial (or previous) temperature profile, the new position of the freezing front, ε_{j+1}, and hence its speed, $\dot{\varepsilon}_j$, is calculated via the energy balance equation at the freezing front; this allows the equations (C.15) to be solved, thus providing the temperature profile at the next time step; from this new profile, the temperature gradient just ahead of the freezing front is evaluated (see below), in order to calculate the new position of the freezing front; the procedure is then repeated.

The temperature gradient at the freezing front is computed by fitting a parabola through the first three mesh points, which, at the j^{th} time step, are (z_f,T_f), $(z_f+\delta z_j,T_{1,j})$ and $(z_f+2\delta z_j,T_{2,j})$. The parabola is given by:

$$T = k_1(z-z_f)^2 + k_2(z-z_f) + k_3 \qquad \ldots (C.18)$$

or, since $T = T_f$ at $z = z_f$,

$$T = k_1(z-z_f)^2 + k_2(z-z_f) + T_f \qquad \ldots (C.19)$$

Clearly, from (C.19):

$$\left.\frac{\partial T}{\partial z}\right|_{z_f} = k_2 \qquad \ldots (C.20)$$

Now, substituting the two other points given above into (C.19) leads to the simultaneous equations:

$$T_{1,j} = k_1 \delta z_j^2 + k_2 \delta z_j + T_f$$

$$T_{2,j} = 4k_1 \delta z_j^2 + 2k_2 \delta z_j + T_f \qquad \ldots \text{(C.21)}$$

Solving these for k_2 yields:

$$k_2 = \left.\frac{\partial T}{\partial z}\right|_{z_f} = \frac{4T_{1,j} - T_{2,j} - 3T_f}{2\delta z_j} \qquad \ldots \text{(C.22)}$$

According to Beck (1977), the error in this approximation is of order δz_j^2. The temperature gradient just ahead of the freezing front, as calculated by (C.22) is used in the energy balance equation at the freezing front (see Chapter 4).

APPENDIX D

THE COMPUTER PROGRAM AND NUMERICAL DATA

D.1 Numerical Data

Below is a list of the numerical values used for the physical quantities in the computer program. The list includes only those values which remained unchanged throughout all the simulations. Those quantities, such as hydraulic conductivity, which were subject to variation (e.g. in parametric studies) are given in Chapter 5.

Density of unfrozen water,	$\rho_w = 1000$ kg m^{-3}
Density of ice,	$\rho_i = 917$ kg m^{-3}
Density of frozen soil matrix,	$\rho_s = 2000$ kg m^{-3}
Latent heat of fusion of water,	$L = 3.35 \times 10^5$ J kg^{-1}
Volumetric specific heat capacity of saturated unfrozen soil,	$C = 2.8 \times 10^6$ J $m^{-3} °C^{-1}$
Thermal diffusivity of saturated unfrozen soil,	$\mu = 1.07 \times 10^{-6}$ m^2 s^{-1}
Absolute freezing temperature of water at atmospheric pressure,	$T_o = 273.15$ K
Freezing front temperature,	$T_f = -0.02$ °C

Ice/water interfacial energy, $\sigma_{iw} = 0.0331\ Nm^{-1}$

Porosity of the soil, $\theta_o = 0.4$

Acceleration due to gravity, $g = 9.81\ m\ s^{-2}$

D.2 The Computer Program

In the computer program, the calculation of frost heave and ice lensing is performed in terms of non-dimensionalised variables for length, time, temperature, pressure and thermal conductivity. The non-dimensionalisation is carried out as follows:

Length, $z' = \frac{z}{\bar{z}}$, where: $\bar{z} = 10^{-3}$ m;

Time, $t' = \frac{t}{\bar{t}}$, where: $\bar{t} = 10^2$s;

Temperature, $T' = \frac{T}{\bar{T}}$, where: $\bar{T} = 10°C$;

Pressure, $u' = \frac{u}{P}$, where: P = overburden;

Thermal conductivity, $K' = \frac{K}{\bar{K}}$, where: $\bar{K} = 3\ W\ m^{-1}\ °C^{-1}$

The primed quantities are the non-dimensional variables.

A copy of the computer program, written in FORTRAN 77, is given in the following pages. The program contains regular comments, particularly at the beginning of each subroutine, to aid understanding.

```
JOB(JOBNAME=:NUET.ETXDP0AB,STARTCLASS=4,OCPTIME=1000)
FORTRAN77
----
      PROGRAM FIXEDOVERBDN
C**********************************************************************
C** This program performs the simulation of the freezing of a soil   **
C** sample. The surface of the sample, initially at TA, is cooled    **
C** at a rate defined in the COOLDOWN routine. COOLDOWN also         **
C** calculates the temperature profile in the sample as cooling      **
C** proceeds. Freezing begins when the surface temperature, T0,      **
C** falls below zero. N.B. Temperatures, time, lengths and pressures **
C** are all non-dimensionalised quantities in this program. Some     **
C** important variable names are:                                    **
C**      ZS - Position of lensing/ice segregation front              **
C**      ZF - Position of freezing/penetration front                 **
C**      US, TS - Water pressure and temperature at ZS               **
C**      UF, TF - Water pressure and temperature at ZF               **
C**      T - Time      DT - Time step      H - Heave                 **
C**      OB - Overburden pressure                                    **
C**      TIS, TIF - Ice content at ZS and ZF                         **
C**      HKS, HKF - Permeability at ZS and ZF                        **
C**      HK0 - Saturated unfrozen permeability                       **
C** N.B. This version includes the soil self-weight which is         **
C**       important at low overburden pressures and necessary when   **
C**       simulating heave under zero overburden. Pressures are now  **
C**       non-dimensionalised with respect to some chosen value PND. **
C**********************************************************************
      DIMENSION TIN(26),TOUT(26)
      COMMON ZS,ZF,ZFS,ZM,US,TS,TF,TA,T0,T,F,G,H,SIGMA,DT,DTDZ,HK0,
     ?TIS,HKS,TIF,HKF,A2,B2,A3,B3,C1,B4,E1,UF,OB,ALPHA,PND
C** Height of sample (ZB) in mm and number of spatial **
C** steps for temperature calculations                **
      ZB=150.0
      NST=25
C** Pressure non-dimensionalised w.r.t. PND (Pa) **
      PND=1.0E3
C** Read in OB, HK0 and TF for this particular run, **
C** also initial value of ALPHA, the parameter in   **
C** the water pressure profile approximation         **
      READ(5,*)OB,HK0,TF,ALPHA
C** Call subroutine to begin cooling procedure and print **
C** the temperature profile at the onset of freezing      **
      CALL COOLDOWN(TIN,NST+1,NST,100)
      WRITE(6,96)
      DO 1 I=1,NST+1
      ZPT=(I-1)*ZB/NST
      WRITE(6,97)ZPT,TIN(I)
 1    CONTINUE
C** Read in initial values (variables given above) **
      READ(5,*)ZS,ZF,H,T,DT,NTS,NPR
C** NTS=Number of time steps to be executed once freezing commences **
C** NPR=Frequency of printout i.e. print every NPR steps            **
      TA=0.4
      T0=TIN(1)
      H0=H
      WRITE(6,100)
      WRITE(6,101)T,H,ZS,ZF
      WRITE(6,102)DT,NTS
      WRITE(6,103)OB,HK0,ALPHA
      WRITE(6,104)
```

```
      KPR=0
      JPR=0
C** Initial values for ice content and hydraulic conductivity **
C** at the base of the ice lens and at the freezing front     **
      TIS=0.3444
      HKS=5.0E-15
      TIF=THETA(0.0,TF)
      HKF=HK0
      SUM=0.0
      COUNT=0.0
      ALPHA0=ALPHA
      IFLAG=0
C** Begin freezing calculation proper **
      DO 6 I=1,NTS
      KPR=KPR+1
      JPR=JPR+1
      ZF0=ZF
C** DTDZ=dT/dZ at Z=Zf+ (i.e. temp. gradient at freezing front) **
      DZJ=(ZB-ZF)/NST
      DTDZ=(4.0*TIN(2)-TIN(3)-3.0*TIN(1))/(2.0*DZJ)
C** Call subroutine to calculate H and ZF at next time step. This **
C** enables subsequent calculation of UF, US and TS, plus ice     **
C** content and hydraulic conductivity at ZS and ZF               **
 8    CALL RK
C** However, if frozen fringe disappears, we need to solve the  **
C** reduced system of equations. The following IF..THEN enables **
C** a statement to be written when this situation occurs and    **
C** control to be transferred for solution of the new system    **
      IF(ZF.LE.ZS) THEN
            AVE=SUM/COUNT
            WRITE(6,92)SUM,COUNT,AVE
            WRITE(6,94)
            WRITE(6,110)T,H,ZF,US,TS,SIGMA,ZM,T0,UF,F,G,ALPHA
            CALL NOFRINGE
      END IF
      CALL RHS(H,ZF,T)
      TS=(G-B2)/A2
      US=(A3*TS)+B3
      UF=(G-E1*US-B4)/C1
      TIS=THETA(US,TS)
      HKS=HK0*((1.0-TIS/0.4)**7.0)
      TIF=THETA(UF,TF)
      HKF=HK0*((1.0-TIF/0.4)**7.0)
C** Call subroutine to calculate new value of ALPHA, the parameter **
C** in the exponential water pressure profile approximation. ALPHA **
C** is held constant initially until calculation settles down.     **
C** Then a "smoothed" value of ALPHA is used as input for the      **
C** calculation at the next time step                              **
      IF(T.GT.25.0) THEN
            CALL NEWALPHA
            ALPHA1=ALPHA
            ALPHA2=(ALPHA0+ALPHA1)/2.0
            ALPHA=(ALPHA0+ALPHA2)/2.0
            ALPHA0=ALPHA
            SUM=SUM+ALPHA
            COUNT=COUNT+1.0
      END IF
C** Call subroutine to find the maximum value, SIGMA, of the neutral **
C** stress and its position, ZM, in the frozen fringe              **
      CALL MAXSIGMA
```

```
C** Introduce new variable PRESS to define ice pressure at base **
C** of latest ice lens ( = overburden + self-weight )           **
      PRESS=(OB+8.9958*H+19.62*ZS)/PND
C** Printout results every NPR time steps **
      IF(KPR.LT.NPR) GOTO 2
      KPR=0
      WRITE(6,95)TIS,HKS,TS,US,UF,HKF
      WRITE(6,110)T,H,ZF,US,TS,SIGMA,ZM,T0,UF,F,G,ALPHA
C** If SIGMA is greater than or equal to PRESS, a new lens is   **
C** formed. A message is printed and ZS is adjusted accordingly **
 2    IF(SIGMA.LT.PRESS) GOTO 3
      WRITE(6,95)TIS,HKS,TS,US,UF,HKF
      DH=H-H0
      WRITE(6,120)ZM,T,DH
      ZS=ZM
      H0=H
C** Calculate temperature profile in unfrozen region and **
C** printout this profile every NPR time steps           **
 3    CALL UNFROZEN(TIN,NST+1,NST,ZF0,ZF,TF,DT,TOUT)
      IF(JPR.LT.NPR)GOTO 5
      JPR=0
      WRITE(6,98)
      DO 4 L=1,NST+1
      ZPT=ZF+((ZB-ZF)*(L-1)/NST)
      WRITE(6,99)ZPT,TOUT(L)
 4    CONTINUE
C** Surface temp. continues to decrease until it reaches -6 deg. C **
 5    T0=T0-0.001*DT
      IF(T0.LE.-0.6)T0=-0.6
C** Change time step length as calculation progresses **
      IF(T.GT.100.099) DT=0.1
      IF(T.GT.1000.09) DT=1.0
C** Condition to print message when the heave rate becomes **
C** very small i.e. less than 0.01 mm/hour = 2.78E-9 m/s   **
      IF(G.LT.2.78E-4.AND.IFLAG.EQ.0.AND.T.GT.25.0) THEN
            WRITE(6,90)
            WRITE(6,110)T,H,ZF,US,TS,SIGMA,ZM,T0,UF,F,G,ALPHA
            IFLAG=1
      END IF
      DO 6 K=1,NST+1
      TIN(K)=TOUT(K)
 6    CONTINUE
C** Calculate the average value of parameter ALPHA **
      AVE=SUM/COUNT
      WRITE(6,92)SUM,COUNT,AVE
 90   FORMAT(1H0,'*** HEAVE RATE LESS THAN 0.01 mm/hour',
     ?' *** VALUES AT THIS POINT ARE:')
 92   FORMAT(1H0,'TOTAL=',F12.2,'/',F8.1,' = ',F5.2)
 94   FORMAT(1H0,'*** FROZEN FRINGE HAS DISAPPEARED - "NOFRINGE"',
     ?' ROUTINE CALLED *** LATEST VALUES ARE:')
 95   FORMAT(8X,'ICE CONTENT=',F6.4,', PERMEABILITY=',E10.4,
     ?', TS=',F8.5,', US=',E11.4,', UF=',E11.4,', HKF=',E10.4)
 96   FORMAT(1H0,'TEMPERATURE PROFILE AT ONSET OF FREEZING:')
 97   FORMAT(4X,'Z=',F5.1,4X,'TEMP.=',F6.3)
 98   FORMAT(6X,'TEMPERATURE PROFILE IN UNFROZEN REGION IS:')
 99   FORMAT(4X,'Z=',F7.3,4X,'TEMP.=',F6.3)
 100  FORMAT(1H0,'INITIAL CONDITIONS ARE ')
 101  FORMAT(1H0,'AT TIME ',F10.3,'  H=',F6.3,'  ZS=',F6.3,' ZF=',F6.3)
 102  FORMAT(1H0,'USING TIME STEP ',F8.4,' FOR ',I6,' STEPS.')
 103  FORMAT(1H0,'OVERBURDEN =',E10.3,'   k(0)=',E10.3,'   ALPHA=',F5.2)
```

```
 104  FORMAT(1H0,'  TIME',7X,'H',6X,'ZF',6X,'US',6X,'TS',
     ?7X,'SIGMA    ZM',6X,'T0',6X,'UF',7X,'F',7X,'G')
 110  FORMAT(1X,F10.3,10F8.3,'       ALPHA=',F5.2)
 120  FORMAT(1H0,'NEW LENS AT ZS= ',F10.3,'  AT TIME  ',F10.4,
     ?'  OLD LENS THICKNESS = ',F10.5)
      STOP
      END

      SUBROUTINE COOLDOWN(TNEW,NDM,N,M)
C**********************************************************************
C** This routine calculates the temperature distribution in the      **
C** sample as it is cooled from its initial temperature TG by        **
C** application of a specified temperature gradient at the surface.  **
C** The calculation is done by solving the 1-D heat conduction       **
C** equation using an implicit (Crank-Nicolson) finite difference    **
C** scheme. The array TOLD contains the temperature distribution     **
C** prior to a decrement in the surface temperature TNEW(1). The new **
C** profile is then calculated and stored in the array TNEW. A       **
C** return is made to the main program once the surface becomes cold **
C** enough to initiate freezing.                                     **
C**********************************************************************
      DIMENSION TNEW(NDM),TOLD(26),RHS(26),CA(26),CK(26)
      DATA OK,OT,OL,BK,SP/3.0,100.0,0.001,1.0,2.8E6/
C** Initial ground temp.,time step and length step **
      TG=0.4
      TST=100.0/M
      ZST=150.0/N

      BETA=(OK*OT/(OL*OL))*(BK/SP)
      AA=(BETA/2.0)*TST/(ZST*ZST)
      BB=-1.0-(2.0*AA)
      CC=(2.0*AA)-1.0
      DD=-AA
C** Initial temperature distribution **
      DO 10 I=1,N+1
      TOLD(I)=TG
 10   CONTINUE
C** Bottom boundary condition - temperature fixed at TG **
      TNEW(N+1)=TG
      KOUNT=1
      KPRINT=0
C** Specified surface temperature gradient **
 15   TNEW(1)=TG-(0.001*KOUNT*TST)

      RHS(2)=(DD*(TOLD(3)+TOLD(1)))+(CC*TOLD(2))-(AA*TNEW(1))
      DO 20 J=3,N-1
      RHS(J)=(DD*(TOLD(J+1)+TOLD(J-1)))+(CC*TOLD(J))
 20   CONTINUE
      RHS(N)=(DD*(TOLD(N+1)+TOLD(N-1)))+(CC*TOLD(N))-(AA*TNEW(N+1))

      CA(2)=BB
      CK(2)=RHS(2)
      DO 30 K=3,N
      CA(K)=BB-(AA*AA)/CA(K-1)
      CK(K)=RHS(K)-(AA*CK(K-1))/CA(K-1)
 30   CONTINUE
C** Calculate new temperature distribution and printout this **
C** every 50 time steps                                      **
      TNEW(N)=CK(N)/CA(N)
      DO 40 L=N-1,2,-1
```

```
      TNEW(L)=(CK(L)-AA*TNEW(L+1))/CA(L)
 40   CONTINUE
      KPRINT=KPRINT+1
      IF(KPRINT.LT.50)GOTO 46
      KPRINT=0
      TIMENOW=KOUNT*TST
      WRITE(6,300)TIMENOW
      DO 45 J=1,N+1
      ZPT=ZST*(J-1)
      WRITE(6,310)ZPT,TNEW(J)
 45   CONTINUE
C**  Condition to return to main program when surface temperature **
C**  becomes cold enough for frost penetration to occur           **
 46   IF(TNEW(1).LE.-0.01)GOTO 55

      DO 50 I=1,N
      TOLD(I)=TNEW(I)
 50   CONTINUE
      KOUNT=KOUNT+1
      GOTO 15

 300  FORMAT(6X,'AT TIME ',F8.1,' , TEMPERATURE DISTRIBUTION IS:')
 310  FORMAT(4X,'Z=',F5.1,4X,'TEMP.=',F6.2)

 55   RETURN
      END


      SUBROUTINE UNFROZEN(TNOW,LP,NN,EJ,EJ1,TFF,TDT,TUNEW)
C*********************************************************************
C** Once freezing has begun, this routine calculates the temperature **
C** distribution in the unfrozen region, i.e. between ZF (EJ1) and   **
C** ZB. It solves the 1-D heat equation using a Crank-Nicolson       **
C** finite difference scheme with a contracting (or possibly         **
C** expanding) mesh. The important temperature gradient at the       **
C** freezing front (dT/dz at Zf+) is evaluated in the main program.  **
C** The old distribution TUOLD is supplied via the array parameter   **
C** TNOW. The new distribution is written into array TUNEW.          **
C*********************************************************************
      REAL TNOW(LP),TUNEW(LP),TUOLD(26),AA(26),CC(26),MU(26),LA(26),
     ?A0(26),C0(26),DD(26)
      DATA OK,OT,OL,BK,SP/3.0,100.0,0.001,1.0,2.8E6/
C** Height of sample and bottom boundary temperature **
      ZB=150.0
      TG=0.4
      ZJ=ZB-EJ
      ZJ1=ZB-EJ1
      BETA=(OK*OT/(OL*OL))*(BK/SP)
C** EDOT=Speed of the freezing front, i.e.                 **
C**          (New position-Old position)/Time interval    **
      EDOT=(EJ1-EJ)/TDT

      DO 210 J=1,NN+1
      TUOLD(J)=TNOW(J)
 210  CONTINUE
C** Bottom boundary condition **
      TUNEW(NN+1)=TG

      BN1=BETA*NN*NN/(ZJ*ZJ)
      BN2=BETA*NN*NN/(ZJ1*ZJ1)
```

```
      B0=(1.0/TDT)-BN1
      BB=(1.0/TDT)+BN2
      DO 215 I=2,NN
      AA(I)=(((NN+1-I)*EDOT)/(4.0*ZJ1))-(BN2/2.0)
      CC(I)=(((NN+1-I)*EDOT)/(4.0*ZJ1))+(BN2/2.0)
      A0(I)=(BN1/2.0)-(((NN+1-I)*EDOT)/(4.0*ZJ))
      C0(I)=(BN1/2.0)+(((NN+1-I)*EDOT)/(4.0*ZJ))
 215  CONTINUE
C** Freezing front temperature **
      TUNEW(1)=TFF

      DD(2)=A0(2)*TUOLD(1)+B0*TUOLD(2)+C0(2)*TUOLD(3)-AA(2)*TUNEW(1)
      DO 220 I=3,NN-1
      DD(I)=A0(I)*TUOLD(I-1)+B0*TUOLD(I)+C0(I)*TUOLD(I+1)
 220  CONTINUE
      DD(NN)=A0(NN)*TUOLD(NN-1)+B0*TUOLD(NN)+C0(NN)*TUOLD(NN+1)+
     ?CC(NN)*TUNEW(NN+1)
C** Now calculate new temperature profile in unfrozen region **
      LA(2)=BB
      MU(2)=DD(2)
      DO 225 J=3,NN
      LA(J)=BB+(AA(J)*CC(J-1))/LA(J-1)
      MU(J)=DD(J)-(AA(J)*MU(J-1))/LA(J-1)
 225  CONTINUE
      TUNEW(NN)=MU(NN)/LA(NN)
      DO 230 J=NN-1,2,-1
      TUNEW(J)=(MU(J)+CC(J)*TUNEW(J+1))/LA(J)
 230  CONTINUE
C** Main program contains write statement for these results **
      RETURN
      END



      SUBROUTINE RK
C*************************************************************************
C** This routine contains the standard fourth order Runge-Kutta       **
C** scheme which is used to solve the coupled O.D.E.'s                **
C**         dZf/dt = F,     dH/dt = G.                                 **
C*************************************************************************
      REAL K1,K2,K3,K4,L1,L2,L3,L4
      COMMON ZS,ZF,ZFS,ZM,US,TS,TF,TA,T0,T,F,G,H,SIGMA,DT,DTDZ,HK0,
     ?TIS,HKS,TIF,HKF,A2,B2,A3,B3,C1,B4,E1,UF,OB,ALPHA,PND
      CALL RHS(H,ZF,T)
      K1=DT*F
      L1=DT*G
      ZZ=ZF+0.5*K1
      HH=H+0.5*L1
      TT=T+0.5*DT
      CALL RHS(HH,ZZ,TT)
      K2=DT*F
      L2=DT*G
      ZZ=ZF+0.5*K2
      HH=H+0.5*L2
      CALL RHS(HH,ZZ,TT)
      K3=DT*F
      L3=DT*G
      ZZ=ZF+K3
      HH=H+L3
      T=T+DT
```

```
      CALL RHS(HH,ZZ,T)
      K4=DT*F
      L4=DT*G
      ZF=ZF+(K1+2*(K2+K3)+K4)/6
      H=H+(L1+2*(L2+L3)+L4)/6
      RETURN
      END

      SUBROUTINE RHS(HH,ZZ,TT)
C*****************************************************************************
C** This routine calculates the right-hand sides of the two O.D.E.'s **
C**       dZf/dt = F,        dH/dt = G.                                      **
C** The variables arise from the full set of five equations, viz.           **
C**           dZf/dt = A1*TS + B1,                                          **
C**           dH/dt = A2*TS + B2,                                           **
C**             US = A3*TS + B3,                                            **
C**           dH/dt = E1*US + C1*UF + B4,                                   **
C**       and dH/dt = E2*US + C2*UF + E3*dZf/dt + B5.                       **
C*****************************************************************************
      COMMON ZS,ZF,ZFS,ZM,US,TS,TF,TA,T0,T,F,G,H,SIGMA,DT,DTDZ,HK0,
     ?TIS,HKS,TIF,HKF,A2,B2,A3,B3,C1,B4,E1,UF,OB,ALPHA,PND
C** Non-dimensionalised thermal conductivities **
C**       FK=Kf, SK=Ks and UK=Ku                **
      FK=4.0/3.0
      SK=4.0/3.0
      UK=1.0

      ZW=150.0
      EE=1.0/(ZZ-ZS)
      C=1.0/(ZW-ZZ)
      A1=FK*EE
      B2=SK/(ZS+HH)
      A2=9.7658*(A1+B2)/(1.0-TIS)
      B3=TF*A1
      B2=-9.7658*(B3+T0*B2)/(1.0-TIS)
      B1=9.7658*(B3-UK*DTDZ)/TIF
      A1=-9.7658*A1/TIF
      A3=1.226432E7/PND
      B3=1.0905*(OB+8.9958*HH+19.62*ZS)/PND
      EY=EXP(-ALPHA*(ZZ-ZS))
      EZ=1.0/(1.0-EY)
      E1=-1.111634E4*PND*HKS*ALPHA*EZ/(1.0-TIS)
      C1=-E1
      B4=-1.0905E5*HKS/(1.0-TIS)
      E2=1.111634E4*HKF*PND*ALPHA*EY*EZ/TIF
      C2=-E2-(1.111634E4*PND*HK0*C/TIF)
      B5=1.0905E5*(HKF-HK0)/TIF
      E3=0.0905

      G1=E1*(A2*B3-A3*B2)
      G2=A2*(1.0-C1/C2)
      G3=A2*B5*C1/C2
      G4=E2*(A3*B2-A2*B3)*C1/C2
      G5=(E2*A3+E3*A1)*C1/C2
      G6=E3*(A1*B2-A2*B1)*C1/C2
      G=(G1+A2*B4-G3+G4+G6)/(G2-E1*A3+G5)
      F=A1*(G-B2)/A2+B1

      RETURN
      END
```

```
      SUBROUTINE MAXSIGMA
C**********************************************************************
C** This routine finds the position (ZM) and the value (SIGMA) of    **
C** the maximum of the neutral stress in the frozen fringe. A simple **
C** search method is used, as follows: the fringe is divided into    **
C** ten step-lengths (DZ) and, starting at ZS, the neutral stress    **
C** (defined by the function SIG) is evaluated at successive points  **
C** (z0=ZS, z1=z0+DZ, z2=z1+DZ etc.) until SIG(zR+1) < SIG(zR). The  **
C** maximum is then known to lie in (zR-1, zR+1), length 2DZ. The    **
C** method is then repeated using a smaller step length (DZ/10)     **
C** until ZM is located to the required accuracy.                    **
C**********************************************************************
      COMMON ZS,ZF,ZFS,ZM,US,TS,TF,TA,T0,T,F,G,H,SIGMA,DT,DTDZ,HK0,
     ?TIS,HKS,TIF,HKF,A2,B2,A3,B3,C1,B4,E1,UF,OB,ALPHA,PND

      ZFS=ZF-ZS
      DZ=ZFS*0.1
      Z0=ZS
 200  Z1=Z0+DZ
      Z2=Z1+DZ
      S1=SIG(Z1)
      S2=SIG(Z2)
      IF(S2.GE.S1) THEN
            IF(Z2.GE.ZF) THEN
                  ZM=ZF
                  SIGMA=S2
                  RETURN
            END IF
            Z0=Z1
            GOTO 200
      END IF
      IF(DZ.LT.5.0E-3) THEN
            ZM=Z0
            SIGMA=SIG(ZM)
            RETURN
      END IF
      DZ=DZ*0.1
      GOTO 200
      END


      FUNCTION SIG(ZZ)
C**********************************************************************
C** Evaluates the neutral stress SIG at the level ZZ within the      **
C** frozen fringe. CHI is the "stress partition factor", UW and UI    **
C** are water and ice pressures respectively. UW is approximated by  **
C** an exponential function (see comments in SUBROUTINE NEWALPHA)    **
C**********************************************************************
      COMMON ZS,ZF,ZFS,ZM,US,TS,TF,TA,T0,T,F,G,H,SIGMA,DT,DTDZ,HK0,
     ?TIS,HKS,TIF,HKF,A2,B2,A3,B3,C1,B4,E1,UF,OB,ALPHA,PND
      ZW=150.0
      ZFZ=(ZF-ZZ)/ZFS
      EZ=EXP(-ALPHA*ZFS)
      ACONST=(UF-US*EZ)/(1.0-EZ)
      BCONST=(US-UF)/(1.0-EZ)
      UW=ACONST+BCONST*EXP(-ALPHA*(ZZ-ZS))
      TZ=ZFZ*TS+(ZZ-ZS)*TF/ZFS
      PSI=(-2.5076E-3*PND*UW)-3.3977E5*TZ
```

```
      UI=UW+33.1*PSI/PND
      THI=THETA(UW,TZ)
      CHI=(1.0-THI/0.4)**1.5
      SIG=CHI*UW+(1.0-CHI)*UI
      RETURN
      END

      SUBROUTINE NEWALPHA
C*************************************************************************
C** Calculates the new value of ALPHA, the parameter in the water      **
C** pressure approximation, viz. UW = A + B*EXP(-ALPHA*(Z-ZS)). The     **
C** new value is found using the old value in the "overall" mass       **
C** continuity equation:                                               **
C**                     dH/dt = a*UF + b*dZf/dt + c                    **
C*************************************************************************
      COMMON ZS,ZF,ZFS,ZM,US,TS,TF,TA,T0,T,F,G,H,SIGMA,DT,DTDZ,HK0,
     ?TIS,HKS,TIF,HKF,A2,B2,A3,B3,C1,B4,E1,UF,OB,ALPHA,PND
      DATA OT,OL,PW,PI,AG/100.0,0.001,1000.0,917.0,9.81/
      ALPHAZ=ALPHA
      ZW=150.0
      PWG=PW*AG
      USF=US-UF
      W=1.0/(ZW-ZF)
      W1=PND*UF*W/OL
      WA=HK0*(W1+PWG)/HKS
      W2=(OL/OT)*(PWG/HKS)
      WB=W2*(1.0-PI/PW)*TIS*F
 500  EX=1.0-EXP(-ALPHA*(ZF-ZS))
      WC=(OL*EX)/(PND*USF)
      WW=(1.0-TIS)*(WA-WB)
      ALPHA=WC*(WW-PWG)
      IF(ABS(ALPHA-ALPHAZ).LT.0.001) RETURN
      ALPHAZ=ALPHA
      GOTO 500
      END

      FUNCTION THETA(UX,TX)
C*************************************************************************
C** Calculates the ice content THETA as a function of the parameter    **
C** PSI. The function used here is based on two straight line fits     **
C** to suction/moisture content data for Attenborough Silt.            **
C*************************************************************************
      COMMON ZS,ZF,ZFS,ZM,US,TS,TF,TA,T0,T,F,G,H,SIGMA,DT,DTDZ,HK0,
     ?TIS,HKS,TIF,HKF,A2,B2,A3,B3,C1,B4,E1,UF,OB,ALPHA,PND
      PSI=(-2.5076E-3*PND*UX)-3.3977E5*TX
      IF(PSI.LT.55.0) THEN
            THETA=0.001
      ELSE IF(PSI.GE.4.25E4)THEN
            THETA=0.0198*(ALOG10(PSI)+3.0)+0.19
      ELSE
            THETA=0.1179*(ALOG10(PSI)+3.0)-0.5583
      END IF
      RETURN
      END

      SUBROUTINE NOFRINGE
C*************************************************************************
C** Control is transferred to here if and when the frozen fringe       **
C** disappears ( for overburden values P < -Pi.L.Tf/273.15 ). We now    **
C** need to solve the reduced system of four equations ( energy,       **
```

```
C** mass, Clapeyron, Darcy ) in the four unknowns H, UF, TF ( no      **
C** longer fixed ) and V ( water flux ). By elimination, this system **
C** can be reduced to the non-linear O.D.E.                           **
C**              dH/dt = F(H).                                       **
C** The function F(H) is evaluated in FUNCTION FN(HZ) below, and      **
C** SUBROUTINE RK2 solves the above equation using the standard       **
C** fourth order Runge-Kutta formula. Some important variable names: **
C**          H - Heave          G - Heave rate                       **
C**          UFF, TFF - Water pressure and temperature at base of ice **
C**                     lens ( =ZF=ZS )                             **
C**********************************************************************
      COMMON ZS,ZF,ZFS,ZM,US,TS,TF,TA,T0,T,F,G,H,SIGMA,DT,DTDZ,HK0,
     ?TIS,HKS,TIF,HKF,A2,B2,A3,B3,C1,B4,E1,UF,OB,ALPHA,PND
      COMMON/SHARE/ZFF,TFF
      ZFF=ZF
      MPR=100
      LPR=0
      IFLAG=0
      WRITE(6,402)
 400  LPR=LPR+1
C** Change time step length as calculation proceeds **
      IF(T.GT.100.099) DT=0.1
      IF(T.GT.1000.09) DT=1.0
      CALL RK2
      G=FN(H)
      UFF=(A3*TFF)+B3
C** Printout values every MPR time steps **
      IF(LPR.LT.MPR) GOTO 401
      LPR=0
      WRITE(6,403)T,H,UFF,TFF,G
C** Print message when heave rate becomes very small **
 401  IF(G.LT.2.78E-4.AND.IFLAG.EQ.0) THEN
           WRITE(6,404)
           WRITE(6,403)T,H,UFF,TFF,G
           IFLAG=1
      END IF
C** Stop program after a certain time ( x100 seconds) **
      IF(T.GT.20000.0) THEN
           WRITE(6,403)T,H,UFF,TFF,G
           WRITE(6,405)
           STOP
      END IF
      GOTO 400
 402  FORMAT(1H0,'    TIME',4X,'HEAVE',5X,'UW',7X,'T',7X,'G')
 403  FORMAT(1X,F10.3,4F8.3)
 404  FORMAT(1H0,' *** HEAVE RATE LESS THAN 0.01 mm/hour',
     ?' *** VALUES AT THIS POINT ARE:')
 405  FORMAT(1H0,'** TIME OUT - PROGRAM STOPPED **')
      RETURN
      END

      SUBROUTINE RK2
      REAL J1,J2,J3,J4
      COMMON ZS,ZF,ZFS,ZM,US,TS,TF,TA,T0,T,F,G,H,SIGMA,DT,DTDZ,HK0,
     ?TIS,HKS,TIF,HKF,A2,B2,A3,B3,C1,B4,E1,UF,OB,ALPHA,PND
      J1=DT*FN(H)
      H1=H+0.5*J1
      J2=DT*FN(H1)
      H1=H+0.5*J2
      J3=DT*FN(H1)
```

```
      H1=H+J3
      T=T+DT
      J4=DT*FN(H1)
      H=H+(J1+2.0*(J2+J3)+J4)/6.0
      RETURN
      END

      FUNCTION FN(HZ)
      COMMON ZS,ZF,ZFS,ZM,US,TS,TF,TA,T0,T,F,G,H,SIGMA,DT,DTDZ,HK0,
     ?TIS,HKS,TIF,HKF,A2,B2,A3,B3,C1,B4,E1,UF,OB,ALPHA,PND
      COMMON/SHARE/ZFF,TFF
      DATA OK,OT,OL,TB/3.0,100.0,0.001,10.0/
      DATA PW,PI,PS,AG,AL,TK/1000.0,917.0,2000.0,9.81,3.35E5,273.15/
      ZB=150.0
      FK=4.0/3.0
      UK=1.0

      R=1.0/(ZB-ZFF)
      Q1=1.0/(ZFF+HZ)
      Q2=(OK/OL)*(UK*R+FK*Q1)
      Q3=PW*AL*AL*HK0*R/(AG*TK*OL)
      Q4=(TB*OK/OL)*(UK*TA*R+FK*T0*Q1)
      Q5=(OB/OL+PI*AG*HZ+PS*AG*ZS)*R/(PI*AG)
      Q6=PW*AL*HK0*(Q5+1.0)

      QQ=TB*(Q2+Q3)
      TFF=(Q4-Q6)/QQ
      P1=-PW*HK0*OT/(PI*AG*OL*OL)
      P2=OB+(PI*AG*OL*HZ)+(PS*AG*OL*ZS)+(PI*AL*TB*TFF/TK)

      FN=P1*(P2*R/PI+OL*AG)
      RETURN
C** First line of data is : OB, HK0, TF, ALPHA          **
C** Second line of data is : ZS, ZF, H, T, DT, NTS, NPR **
      END
++++
ADF
0.0  5.0E-9  -0.002  1.0
0.0  0.1  0.1  0.1  0.01  38000  1000
++++
AOF(NAME=/SPOOL&200)
EXEC(PROGRAM=FIXEDOVERBDN)
EJ
****
```

REFERENCES

Aguirre-Puente, J. and M. Frémond (1976) Frost propagation in wet porous media. Lecture Notes in Mathematics 503, Springer Verlag, 137-147.

Aguirre-Puente, J., M. Frémond and J. M. Menot (1977) Gel dans les milieux poreux: perméabilité variable et mouvements d'eau dans la partie à température négative. Proc. Int. Symp. on Frost Action in Soils, Lulea, 1, 5-28.

Akagawa, S., Y. Yamamoto and S. Hashimoto (1985) Frost heave characteristics and scale effect of stationary frost heave. Proc. Fourth Int. Symp. on Ground Freezing, Sapporo, 1, 137-143.

Anderson, D. M. and N. R. Morgenstern (1973) Physics, chemistry and mechanics of frozen ground: a review. Second Int. Conf. on Permafrost, North American Contribution, Nat. Acad. Sci., 257-288.

Baker, T. H. W., H. L. Jessberger, B. D. Kay and N. Maeno (1987) Ground freezing '85 - a summary. Cold Regions Science and Technology, 13, 301-306.

Beck, A. P. (1977) Numerical solution of Stefan problems. B.Sc. thesis, University of Nottingham.

Berg, R. L. (1984) Status of numerical models for heat and mass transfer in frost-susceptible soils. Fourth Int. Conf. on Permafrost (1983), Final Proceedings, National Academy Press, 67-71.

Berg, R., J. Ingersoll and G. Guymon (1980) Frost heave in an instrumented soil column. Cold Regions Science and Technology, 3, 211-221.

Beskow, G. (1935) Soil freezing and frost heaving with special application to roads and railroads. Swedish Geol. Soc., 26th Year Book No. 3 (Series C, No. 375) (translated and published by Northwestern University, Evanston, Illinois, 1947).

Bishop, A. W. (1955) The principle of effective stress. Lecture delivered in Oslo, reprinted in Teknisk Ukeblad, 39, 859-863 (1959).

Bresler, E., D. Russo and R. D. Miller (1978) Rapid estimate of unsaturated hydraulic conductivity function. Soil Science Society of America Journal, 42, 170-172.

British Standards Institution (1986) BS 812 Testing Aggregates Pt. 124: Method for determination of frost heave. (Document 86/10382 - Draft for public comment), BSI, London.

Burt, T. P. and P. J. Williams (1976) Hydraulic conductivity in frozen soils. Earth Surface Processes, 1, 349-360.

Carslaw, H. S. and J. C. Jaeger (1959) Conduction of heat in solids. Clarendon Press, Oxford.

Chamberlain, E. J. (1981) Frost susceptibility of soil: a review of index tests. USA CRREL Monograph 81-2, Hanover, N.H.

Croney, D. and J. C. Jacobs (1967) The frost susceptibility of soils and road materials. Road Research Laboratory Report, LR90, Crowthorne.

Department of Transport (1976) Specification for road and bridge works, HMSO, London.

Department of Transport (1986) Specification for highway works, HMSO, London.

De Vries, D. A., (1963) Thermal properties of soils. In Physics of Plant Environment, ed. W. R. Van Wijk, North Holland, Amsterdam.

Dirksen, C. and R. D. Miller (1966). Closed system freezing of unsaturated soil. Soil Science Society of America Proc., 30, 168-173.

Dudek, S. J-M. (1980) The experimental and theoretical prediction of frost heave in granular materials. Ph.D. thesis, University of Nottingham, U.K.

Edlefsen, N. E. and A. B. C. Anderson (1943) Thermodynamics of soil moisture. Hilgardia, 15, 31-298.

Everett, D. H. (1961) The thermodynamics of frost damage to porous solids. Transactions of the Faraday Society, 57, 1541-1551.

Everett, D. H. and J. M. Haynes (1965) Capillary properties of some model pore systems with special reference to frost damage. RILEM Bulletin, Paris, New Series, 27, 31-38.

Frémond, M. (1974) Variational formulation of the Stefan problem - coupled Stefan problem - frost propagation in porous media. Computational Methods in Nonlinear Mechanics, ed. J. T. Oden, Austin, U.S.A., 341-349.

Fukuda, M., A. Orhun and J. N. Luthin (1980) Experimental studies of coupled heat and moisture transfer in soils during freezing. Cold Regions Science and Technology, 3, 223-232.

Fukuda, M. and S. Nakagawa (1985) Numerical analysis of frost heaving based upon the coupled heat and water flow model. Proc. Fourth Int. Symp. on Ground Freezing, Sapporo, Japan, 1, 109-117.

Gardner, W. R. (1958) Some steady state solutions of the unsaturated moisture flow equation with application to evaporation from a water table. Soil Science, 85, 228-232.

Gilpin, R. R. (1980) A model for the prediction of ice lensing and frost heave in soils. Water Resources Research, 16, 918-930.

Gold, L. W. (1957) A possible force mechanism associated with the freezing of water in porous materials. Highway Research Board, Bulletin 168, 65-73.

Guymon, G. L. and J. N. Luthin (1974) A coupled heat and moisture transport model for arctic soils. Water Resources Research, 10, 995-1001.

Guymon, G. L., T. V. Hromadka II and R. L. Berg (1980) A one-dimensional frost heave model based upon simulation of simultaneous heat and water flux. Cold Regions Science and Technology, 3, 253-262.

Guymon, G. L., R. L. Berg, T. C. Johnson and T. V. Hromadka II (1981) Results from a mathematical model of frost heave. Transportation Research Record, 809, 2-6.

Guymon, G. L., R. L. Berg and T. V. Hromadka II (1983). Field tests of a frost heave model. Proc. Fourth. Int. Conf. on Permafrost, Fairbanks, Alaska, 409-414.

Harlan, R. L. (1973) Analysis of coupled heat-fluid transport in partially frozen soil. Water Resources Research, 9, 1314-1323.

Hill, D. and N. R. Morgenstern (1977) Influence of load and heat extraction on moisture transfer in freezing soils. Proc. Int. Symp. on Frost Action in Soils, Lulea, 1, 76-91.

Hoekstra, P. (1966) Moisture movement in soils under temperature gradients with the cold-side temperature below freezing. Water Resources Research, 2, 241-250.

Hoekstra, P. (1969) Water movement and freezing pressures. Soil Science Society of America Proc., 33, 512-518.

Hoekstra, P., E. Chamberlain and T. Frate (1965). Frost heaving pressures. Highway Research Record 101, 28-38.

Holden, J. T. (1979) On the equations of heat and moisture flow during soil freezing-discussion. Can. Geotech. J., 16, 830-831.

Holden, J. T. (1983) Approximate solutions for Miller's theory of secondary heave. Proc. Fourth Int. Conf. on Permafrost, Fairbanks, Alaska, 498-503.

Holden, J. T., R. H. Jones and S. J-M. Dudek (1980) Heat and mass flow associated with a freezing front. Second Int. Symp. on Ground Freezing, Trondheim, Preprints 502-514. (Also Engineering Geology, 18, (1981), 153-164).

Holden, J. T., D. Piper and R. H. Jones (1985) Some developments of a rigid-ice model of frost heave. Proc. Fourth Int. Symp. on Ground Freezing, Sapporo, 1, 93-99.

Hopke, S. W. (1980) A model for frost heave including overburden. Cold Regions Science and Technology, 3, 111-127.

Horiguchi, K. and R. D. Miller (1980) Experimental studies with frozen soil in an "ice sandwich" permeameter. Cold Regions Science and Technology, 3, 177-183.

Horiguchi, K. and R. D. Miller (1983) Hydraulic conductivity functions of frozen materials. Proc. Fourth Int. Conf. on Permafrost, Fairbanks, Alaska, 504-508.

Ishizaki, T. and N. Nishio (1985) Experimental study of final ice lens growth in partially frozen saturated soil. Proc. Fourth Int. Symp. on Ground Freezing, Sapporo, 1, 71-78.

Jame, Y. W. and D. I. Norum (1976) Heat and mass transfer in freezing unsaturated soil in a closed system. Proc. Second Conf. on Soil Water Problems in Cold Regions, Edmonton, 46-62.

Jones, R. H. (1980) Frost heave of roads. Q. J. Eng. Geology, 13, 77-86.

Jones, R. H. (1980) Developments and applications of frost susceptibility testing. Second Int. Symp. on Ground Freezing, Trondheim, Preprints 748-759. (Also Engineering Geology, 18, (1981), 269-280).

Jones, R. H. (1987) Frost susceptibility: a case history of specification development. UNBAC Symposium, University of Nottingham, U.K.

Jones, R. H. and S. J-M. Dudek (1979) Comparison of the precise freezing cell with other facilities for frost heave testing. Transportation Research Record, 705, 63-71.

Jones, R. H. and K. J. Lomas (1983) The frost susceptibility of granular materials. Proc. Fourth Int. Conf. on Permafrost, Fairbanks, Alaska, 554-559.

Kay, B. D. (1985) Remarks made during the closing session of the Fourth Int. Symp. on Ground Freezing, Sapporo, Japan (see also Baker et al, 1987).

Konrad, J-M. (1980) Frost heave mechanics. Ph.D thesis, Dept. of Civil Engineering, University of Alberta, Canada.

Konrad, J-M. and N. R. Morgenstern (1980) A mechanistic theory of ice lens formation in fine-grained soils. Can. Geotech. J., 17, 473-486.

Konrad, J-M. and N. R. Morgenstern (1981) The segregation potential of a freezing soil. Can. Geotech. J., 18, 482-491.

Konrad, J-M. and N. R. Morgenstern (1982a) Prediction of frost heave in the laboratory during transient freezing. Can. Geotech. J., 19, 250-259.

Konrad, J-M. and N. R. Morgenstern (1982b) Effects of applied pressure on freezing soils. Can. Geotech. J., 19, 494-505.

Konrad, J-M. and N. R. Morgenstern (1984) Frost heave prediction of chilled pipelines buried in unfrozen soils. Can. Geotech. J., 21, 100-115.

Koopmans, R. W. R. and R. D. Miller (1966) Soil freezing and soil water characteristic curves. Soil Science Society of America Proc., 30, 680-685.

Loch, J. P. G. (1978) Thermodynamic equilibrium between ice and water in porous media. Soil Science, 126, 77-80.

Loch, J. P. G. (1979) Influence of heat extraction rate on ice segregation rate of soils. Frost i Jord, 20, 19-30.

Loch, J. P. G. (1980) Frost action in soils: State of the art. Second Int. Symp. on Ground Freezing, Trondheim, Preprints, 581-596. (Also Engineering Geology, 18, (1981), 213-224).

Loch, J. P. G. and R. D. Miller (1975) Tests of the concept of secondary frost heaving. Soil Science Society of America Proc., 39, 1036-1041.

Loch, J. P. G. and B. D. Kay (1978) Water redistribution in partially frozen, saturated silt under several temperature gradients and overburden loads. Soil Science Society of America Journal, 42, 400-406.

Lunardini, V. J. (1981) Heat transfer in cold climates. Van Nostrand Reinhold, New York, 731 pp.

McCabe, E. Y. and R. J. Kettle (1983) The influence of surcharge loads on frost susceptibility. Proc. Fourth Int. Conf. on Permafrost, Fairbanks, Alaska, 816-820.

McCabe, E. Y. and R. J. Kettle (1985) Thermal aspects of frost action. Proc. Fourth Int. Symp. on Ground Freezing, Sapporo, 1, 47-54.

Menot, J. M. (1978) Equations of frost propagation in unsaturated porous media. Proc. First Int. Symp. on Ground Freezing, Bochum. (Also Engineering Geology, 13, (1979), 101-109).

Miller, R. D. (1970) Ice sandwich: Functional semipermeable membrane. Science, 169, 584-585.

Miller, R. D. (1972) Freezing and heaving of saturated and unsaturated soils. Highway Research Record, 393, 1-11.

Miller, R. D. (1977) Lens initiation in secondary heaving. Proc. Int. Symp. on Frost Action in Soils, Lulea, 2, 68-74.

Miller, R. D. (1978) Frost heaving in non-colloidal soils. Proc. Third Int. Conf. on Permafrost, Edmonton, National Research Council of Canada, 1, 707-713.

Miller, R. D. (1980) The adsorbed film controversy. Cold Regions Science and Technology, 3, 83-86.

Miller, R. D. (1984a) Private communication.

Miller, R. D. (1984b) Thermally induced regelation: a qualitative discussion. Fourth Int. Conf. on Permafrost (1983), Final Proceedings, National Academy Press, 61-63.

Miller, R. D., J. P. G. Loch and E. Bresler (1975) Transport of water and heat in a frozen permeameter. Soil Science Society of America Proc., 39, 1029-1036.

Miller, R. D. and E. E. Koslow (1980) Computation of rate of heave versus load under quasi-steady state. Cold Regions Science and Technology, 3, 243-251.

Murray, W. D. and F. Landis (1959) Numerical and machine solutions of transient heat conduction problems involving melting or freezing. J. Heat Transfer, Trans. ASME(c), 81, 106-112.

National Research Council (1984) Ice segregation and frost heaving. Report of Ad Hoc Study Group on Ice Segregation and Frost Heaving, National Research Council, National Academy Press, Washington.

O'Neill, K. (1983) The physics of mathematical frost heave models: a review. Cold Regions Science and Technology, 6, 275-291.

O'Neill, K. and R. D. Miller (1980) Numerical solutions for a rigid ice model of secondary frost heave. Second Int. Symp. on Ground Freezing, Trondheim, Preprints, 656-669. (Also CRREL Report 82-13 (1982), Hanover, N.H.).

O'Neill, K. and R. D. Miller (1985) Exploration of a rigid ice model of frost heave. Water Resources Research, 21, no. 3, 281-296.

Penner, E. (1957) Soil moisture tension and ice segregation. Highway Research Board, Bulletin 168, 50-64.

Penner, E. (1959) The mechanism of frost heaving in soils. Highway Research Board, Bulletin 225, 1-22.

Penner, E. (1966) Frost heaving in soils. First Int. Conf. on Permafrost Proceedings, Nat. Acad. Sci., Washington D.C., 197-202.

Penner, E. (1967) Heaving pressure in soils during unidirectional freezing. Can. Geotech. J., 4, 398-408.

Penner, E. (1982) Aspects of ice lens formation. Proc. Third Int. Symp. on Ground Freezing, Hanover, 239-245.

Penner, E. and T. Ueda (1977) The dependence of frost heaving on load application. Proc. Int. Symp. on Frost Action in Soils, Lulea, 1, 92-101.

Penner, E. and T. Ueda (1978) A soil frost susceptibility test and a basis for interpreting heaving rates. Proc. Third Int. Conf. on Permafrost, Edmonton, National Research Council of Canada, 1, 721-727.

Penner, E. and L. E. Goodrich (1980) Location of segregated ice in frost susceptible soil. Second Int. Symp. on Ground Freezing, Trondheim, Preprints 626-639.

Perfect, E. and P. J. Williams (1980) Thermally induced water migration in frozen soils. Cold Regions Science and Technology, 3, 101-109.

Piper, D. and J. T. Holden (1984) Some results from a mathematical model predicting ice lensing and frost heave. Proc. Symposium on relating theory to practice in artificial ground freezing, University of Nottingham, U.K.

Roe, P. G. and D. C. Webster (1984) Specification for the TRRL frost heave test. TRRL, SR 829, Crowthorne, Berkshire.

Römkens, M. J. M. and R. D. Miller (1973) Migration of mineral particles in ice with a temperature gradient. J. Colloid and Interface Sci., 42, 103-111.

Schofield, R. K. (1935) The pF of the water in soil. Trans. 3rd Int. Cong. Soil Science, 2, 37-48.

Sheppard, M. I., B. D. Kay and J. P. G. Loch (1978) Development and testing of a computer model for heat and mass flow in freezing soils. Proc. Third Int. Conf. on Permafrost, Edmonton, National Research Council of Canada, 1, 75-81.

Sill, R. C. and A. S. Skapski (1956) Method for the determination of surface tension of solids from their melting points in thin wedges. Journal of Chemical Physics, 24, 4, 644-651.

Sutherland, H. B. and P. N. Gaskin (1973) Pore water and heaving pressures developed in partially frozen soils. Second Int. Conf. Permafrost, North American Contribution, Nat. Acad. Sci., 409-419.

Taber, S. (1929) Frost heaving. J. Geology, 37, 428-461.

Taber, S. (1930) The mechanics of frost heaving. J. Geology, 38, 303-317.

Takagi, S. (1977) Segregation freezing temperature as the cause of suction force. Proc. Int. Symp. on Frost Action in Soils, Lulea, 1, 59-66.

Takagi, S. (1980a) The adsorption force theory of frost heaving. Cold Regions Science and Technology, 3, 57-81.

Takagi, S. (1980b) Summary of the adsorption force theory of frost heaving. Cold Regions Science and Technology, 3, 233-235.

Takashi, T., H. Yamamoto, T. Ohrai and M. Masuda (1978) Effect of penetration rate of freezing and confining stress on the frost heave ratio of soil. Proc. Third Int. Conf. on Permafrost, Edmonton, National Research Council of Canada, 1, 736-742.

Taylor, G. S. and J. N. Luthin (1976) Numeric results of coupled heat-mass flow during freezing and thawing. Proc. Second Conf. on Soil Water Problems in Cold Regions, Edmonton, 155-172.

Taylor, G. S. and J. N. Luthin (1978) A model for coupled heat and moisture transfer during soil freezing. Can. Geotech. J., 15, 548-555.

Terzaghi, K. (1936) The shearing resistance of saturated soils and the angle between the planes of shear. Proc. First Int. Conf. Soil Mechanics, 1, 54-56.

Thompson, J. D. (1981) Subgrade effects on the frost heave of roads. Ph.D thesis, University of Nottingham, U.K.

Williams, P. J. (1967) Properties and behaviour of freezing soils. Norwegian Geotechnical Institute, Publication no. 72, Oslo.

Williams, P. J. (1979) Pipelines and permafrost: physical geography and development in the circumpolar north. Topics in Applied Geography, Longman, London.

Williams, P. J. and T. P. Burt (1974) Measurement of hydraulic conductivity of frozen soils. Can. Geotech. J., 11, 647-650.

Yoneyama, K., T. Ishizaki and N. Nishio (1983) Water redistribution measurements in partially frozen soil by X-ray technique. Proc. Fourth Int. Conf. on Permafrost, Fairbanks, Alaska, 1445-1450.